1993

Fatigue strength of welded attachments with large eccentricity

John E. Tarquinio
Lehigh University

AUTHOR:

Tarquino, John

TITLE:

Fatigue Strength of Welded Attachments with Large Eccentricity

DATE: October 10, 1993

FATIGUE STRENGTH OF WELDED ATTACHMENTS WITH LARGE ECCENTRICITY

by

John Tarquinio

A Thesis

Presented to the Graduate and Research Committee

of Lehigh University

in Candidacy for the Degree of

Master of Science

in

Civil Engineering

Lehigh University

27 August 1993

This thesis is accepted and approved in partial fulfillment of the requirements for the Master of Science

August 26, 1993
Date

Thesis Advisor

Chairperson of Department

Acknowlegements

This work was accomplished with the support of the U.S. Navy (CD-NSWC) under contract N00167-02-K-0042 entitled "Producibility: Foundation Integration with Double-Hull." The work was conducted at the Engineering Research Center for Advanced for Large Structural Systems (ATLSS) at Lehigh University. The Principal Investigator of the project was Dr. Robert Dexter and Dr. Ben Yen was the thesis supervisor.

Special thanks go to Dr. Robert Dexter who provided encouragement and support that helped a great deal in producing this thesis. He expressed a true interest in my education with regard to the subject presented here as well as beyond the scope of this report. Sincere thanks also go to Dr. Ben Yen for is support and care expressed for my time at Lehigh and my future career.

The author appreciates the direction and advice offered by Mr. David McAfee of David Taylor Research Center, Carderock. The input of all of the employees of Vibtech, Inc. was of great value. In addition, many others contributed to the production of this thesis. Bob Dales, Mike Beaky and Steve Leonard provided daily technical support and advice in the laboratory. John Hoffner produced the test fixtures needed and Dave Schnalzer did the welding. Mark Kaczinski, Ed Tomlinson and Russ Longenbach setup and maintained the computer control and data acquistion systems. Additional laboratory technical support was provided by Todd Anthony and Larry Heffner. George Kober, Chih-Ping "Frank" Fan and Ken Gilvary provided much needed assistance in the daily preparation and

monitoring of the tests as well as reduction of the data collected. Professor Emeritus George Irwin provided thoughtful comments. Frank Stokes and J.William Jahn provided administrative support. The figures were prepared by Jack Gera. Photographs were provided by Richard Sopko.

TABLE OF CONTENTS

LIST OF TABLES

LIST OF FIGURES

ABSTRACT

Fatigue experiments were conducted on full-scale mockups of one cell of the uni-directional, advanced double-hull with a variety of foundation attachment configurations with large eccentricities to support structure. These foundation attachments were subjected to axial and bending loading to characterize their fatigue resistance. The influence of reversal loading was also investigated for these uniaxially stressed details. In addition, the influence of an in-plane stress applied in phase with a axial stress was investigated (biaxial loading). It was found that the fatigue strength of the various configurations and eccentricities could be correlated using the hot-spot stress concept and the AASHTO Category C fatigue design curve. A number of definitions of hot-spot stress were evaluated. It was determined that the hot-spot stress range as determined by a 3 mm strain gage placed at the point of highest strain along the weld length and positioned perpendicular to the weld about 5 mm from the weld toe adequately correlated the fatigue strength of the various details. Stress concentration factors were developed relating nominal stress to the hot-spot stress for use in design.

KEY WORDS: ship design, double hull, fatigue, weld, hot-spot, multiaxial loading

1.0 INTRODUCTION

1.1 Foundation Attachment Details for the Advanced Double-Hull

The U.S. Navy is developing an advanced (unidirectional) double-hull ship design proposed for the next generation of surface combatants. The advanced double hull is two unstiffened shells with continuous web plates or girders fillet welded to the shells [2,3,4]. This advanced double-hull is contrasted with a conventional stiffened-panel hull in Figure 1.1. The double-hull design provides several advantages relative to a stiffened-panel design, e.g.:

1. the resistance to penetration by missile is greater than a single hull of the same weight,

2. the redundancy of the double hull provides better tolerance to damage from grounding, collision, or fatigue cracking, and;

3. the structure is significantly simplified by eliminating the transverse frames between bulkheads, the longitudinal stiffeners between girders, and the thousands of brackets and chocks associated with these members.

The simplification of the structure reduces the cost of fabrication and reduces the number of fatigue critical details at the intersections of these members.

Attachments to the hull or strength deck are among the most fatigue critical weld details with respect to the hull girder primary bending stress. Foundation attachments are particularly critical because the machinery or equipment may exert large inertial forces on the attachment elements, i.e. the foundation attachments are subjected to multiaxial fatigue loading. Foundations are the structures attaching machinery and equipment to the hull or deck of a ship. An example of a typical foundation in a military ship is shown

in Figure 1.2. Due to the critical nature of these details and their loading, foundations in military ships have typically been designed to spread the forces over at least two frames and stiffeners as shown in Figure 1.2. Traditional detailing rules are used to assure adequate fatigue resistance. An explicit consideration of the fatigue resistance of the attachment details would be a more general approach.

Foundations have been developed for conventional hulls to support small equipment and machinery in the range 0.1 to 700 kg. In recent years, foundations have evolved to improve producibility and thus save weight. These light foundation structures are typically simple truss panels consisting primarily of angle shapes as shown in Figure 1.2. This foundation design is to be adapted to the advanced double hull. However, because there are no fatigue design criteria to optimize, restrictions are imposed that are not required. The present Military Standards governing fabrication [1] put several constraints on the design which make it much more expensive. For example, the Mil-Std requires that the foundation elements land precisely over the internal girders with an eccentricity of less than one plate thickness. Pads may be required where the angle sections land on the hull plate. Furthermore, backup structure inside the cells may be required.

In many cases, however, the regular inertial loading on these foundations due to seaway motion is very small. In some cases, the angle sections which comprise the foundation frame are oversized with respect to fatigue because the size of the angles is governed by other considerations such as vibration or shock loading. In these cases, some of the

above requirements may be unnecessary. It would greatly reduce fabrication costs if:

1. the backup structure was not required (additional welded attachments may actually increase the probability of cracking);
2. the space between the hulls was not obstructed with backup structure (inhibiting automated construction and the use of the space for distributed systems);
3. the transverse spacing of the elements of the foundation structure did not have to correspond to the girder spacing, and;
4. the as-built location of the girders did not have to be determined precisely and the alignment did not have to be verified by inspection.

1.2 Fatigue Assessment of Foundations with Large Eccentricity

Eliminating backup structure and increasing eccentricity allowances for foundation design would greatly increase producibility, save weight, and reduce costs. However, the fatigue strength of these eccentric attachment details may be a potential problem.

The fatigue strength of these details can be considered in terms of the two loading directions (although there may be some interactions), i.e.: 1) with respect to the primary hull-girder bending stresses and, 2) with respect to forces in the attachments. The fatigue strength of a given attachment detail with respect to the primary hull-girder bending stresses is well characterized by previous experiments and can be predicted, using nominal stress range, as Category E or E' details. However, the fatigue strength with respect to forces in the attachments decreases rapidly as the eccentricity increases. Eccentric or misaligned details without backup structure can create intense distortion in the thin hull or deck plate. The plate bending stress in the gap region between the girder and the foundation angle may be as large as 15 times the nominal axial stress in the angle, i.e. the stress concentration factor (SCF) is as great as 15. However, if the loading in the

foundation elements is such that the even the concentrated stress ranges are small, such an eccentric or misaligned detail may be justified.

A similar problem of fatigue due to distortion has been investigated in bridges [5]. Secondary members such as diaphragms and cross-bracing induce out-of-plane distortion in beam webs. When the distortion is concentrated in small gaps, cracking typically occurs. However, existing bridge design rules do not provide guidance for determining the stress in the secondary member nor the stress local to the distortion. The extent of the bridge design guidance is to require definite load paths for all out-of-plane forces. In effect, this requires that all transverse elements be fully welded to the flanges to eliminate gaps. This requirement is similar to the rules of the Mil Std, which preclude the use of a detail with excessive eccentricity. However, it is inefficient to require precise alignment and/or backup structure if the stress ranges in the attachment are very low. Because of the potentially big economic incentive, this misaligned detail may be used. Therefore, a practical fatigue assessment method is required for the reliable application of this misaligned attachment detail.

The standard S-N curve approach to fatigue assessment is based on nominal stress in the member rather than the stress local to the weld detail. The S-N curves for various categories of details are determined from full-scale tests. In these nominal-stress based S-N curves, the effect of the local stress concentration is reflected in the fatigue detail category. In other words, the design equation, which states that the applied stress ranges

must be less than the resistance at a certain number of cycles, reflects the effect of local stress concentration in the resistance side of the design equation. However, the foundation attachment with large eccentricity is much worse than the most severe detail category (i.e. Category E' in the AASHTO bridge design code or Eurocode Category 40). There is no precedent for this detail. Because of the large and highly variable SCF, a unique category would be required for each foundation attachment configuration. The testing to develop a unique S-N curve would have to be carried out for each possible configuration. It would be more practical to have a fatigue design approach based on the concentrated stresses near the weld which would take into account the SCF.

One "local" approach which has been tried is to base the fatigue design on the local stress at the weld toe where the cracking originates. This is the stress quantity that is most relevant to the early growth of the fatigue crack. This approach shifts the effect of the stress concentration from the resistance side of the equation to the applied loading side of the equation. All the resistance curves should then consolidate to a single curve reflecting the intrinsic fatigue resistance of the material. Unfortunately, the local weld toe stresses are impossible to quantify due to sensitivity to the local weld toe geometry which is highly variable. Therefore, this ideal theoretical approach is impractical. Indeed, attempts to use this approach for welded structures have led to disaster [34].

A more practical fatigue design method based on local stresses has been developed for tubular joints in offshore structures [6,7,8]. The method, called the "hot-spot stress"

approach, is based on the stress in the plate normal to the weld axis at some small distance from the weld toe. The stress at this location is influenced by the global stress concentration but is not close enough to the weld to be influenced by the local stress concentration due to the weld toe. The S-N curve used with this approach is essentially the S-N curve for a transverse butt or fillet weld in a nominal membrane stress field. Thus, the statistical effects of the local weld toe geometry and microdefects which are impossible to quantify are included empirically in the resistance side of the design equation [6]. In the hot-spot approach, the global stress concentration due to the relative configuration of the members is reflected in the applied loading side of the design equation. Thus, this approach is intermediate between the extremes of the nominal stress approach and the true local stress approach.

Unfortunately, methods for measuring and evaluating hot-spot stress as well as the associated S-N curve vary depending on which code or recommendation is followed [10-14]. Various definitions for hot-spot stress are given in Table 2.1. The degree to which certain effects are reflected on either the resistance side or the applied load side of the design equation depends on the particular definition of hot-spot stress. A rational method of determining a hot-spot stress using reliable and appropriate modelling techniques and an appropriate S-N design curve need to be developed for foundations with varying configurations and eccentricity.

1.3 Objectives, Approach, and Scope

Extensive fatigue testing is required to develop a basis for designs that do not conform to traditional standards. The purpose of the study reported herein is the preliminary development of such a fatigue design basis for lightweight foundation attachments with no backup structure and large eccentricity. The approach used was to perform fatigue tests on full-scale mock-ups of one cell of the double hull with a variety of foundation attachment configurations. The fatigue behavior of the unloaded attachments with respect to primary hull-girder bending stress range is already well characterized [18,21]. Therefore, the focus of these tests was on characterizing the fatigue strength when axial and bending loads are applied to the foundation elements. Six experiments included in-phase loading of the hull plate in addition to the loading of the foundation elements to assess the fatigue strength due to biaxial loading. These biaxial experiments confirmed previous findings with regard to multiaxial loading which indicate that, in most cases, one mode of loading dominated the fatigue cracking process. Therefore, for design purposes, the loading in the secondary axis could be safely ignored.

It was found that the fatigue strength of the various configurations and eccentricities could be correlated using the hot-spot concept. The method applied was essentially the hot-spot method recommended in Chapter 10 in AWS D1.1 for tubular joints. The recommended hot-spot S-N curve in AWS D1.1 (called the X2 curve) is essentially the same as the AASHTO Category C S-N curve at over one million cycles. However, there are large differences in the slope and in the constant-amplitude fatigue limit (CAFL). The

Category C curve is the appropriate S-N curve for a butt joint with reinforcement subject to a uniform membrane stress (i.e., SCF = 1.0). Because of the link to the nominal stress S-N curve for a butt weld and because the slope and CAFL best represent the available data, the AASHTO Category C curve was chosen as the baseline S-N curve for the hot-spot approach in this study. The AASHTO Category C curve is essentially the same as the UK H&SE T curve which is widely used with the hot-spot stress range in the offshore industry outside the U.S. It is also the same as the Eurocode 90 S-N curve and several others. In fact, the approach could be applied equally well to any of these S-N curves. Through experimental measurement (i.e. strain gages) of local stress due to distortion of a detail with excessive eccentricity, a hot-spot stress can be determined for comparison to the C curve. A finite element modelling method has been developed so that details not tested may be analyzed for fatigue characteristics [39].

This fatigue assessment approach may also be useful for details in other types of welded structures with excessive misalignment or which otherwise exhibit distortion. For example, there may be similar situations in bridges where the strict ban on gap-type details is not warranted by the relatively light loading. In this case, the fatigue design criteria developed here could be used to achieve more economical bridge details.

The various fatigue design approaches are reviewed in greater detail in the following Chapter. In particular, the hot-spot method of fatigue assessment is reviewed and methods of defining hot-spot stress are examined. In Chapter 3, descriptions of test

specimens, test setup and procedures are covered. Chapter 4 discusses results of testing. Finally, Chapter 5 summarizes the conclusions and recommendations from this study.

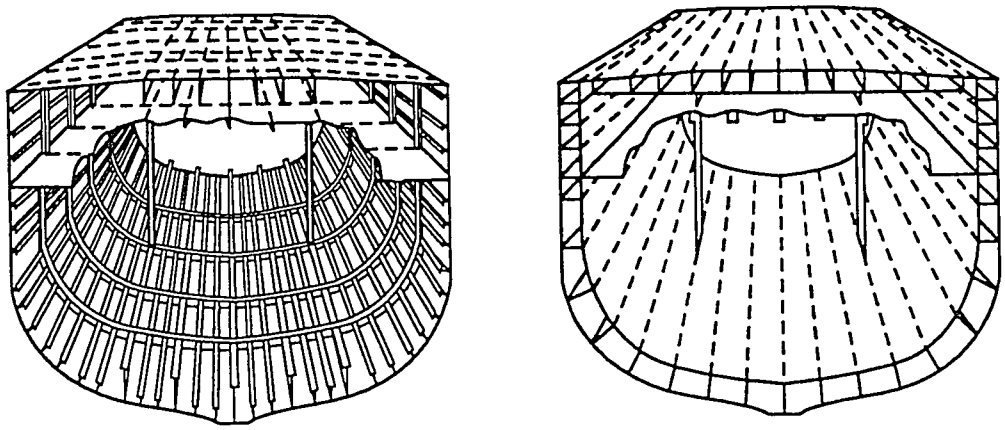

Figure 1.1 Comparison of conventional ship and advanced double-hull ship construction

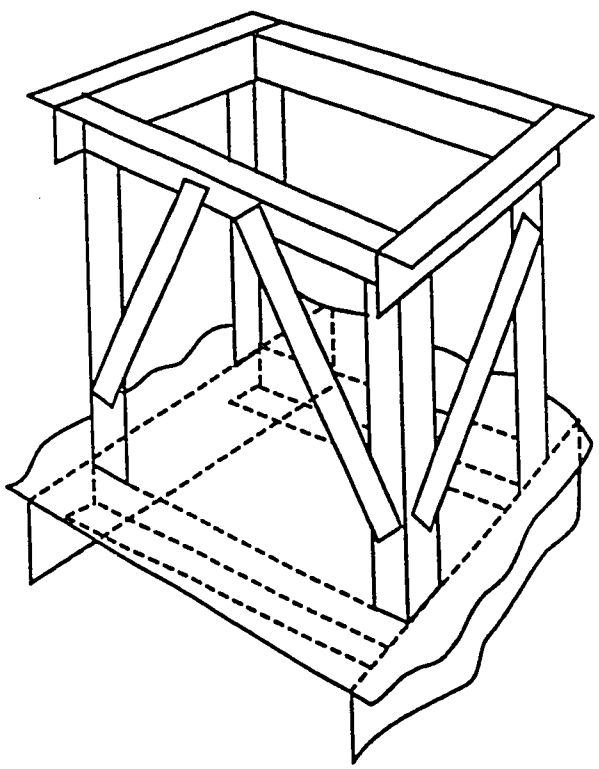

Figure 1.2 Typical foundation for light-weight equipment with backup structure

2.0 BACKGROUND

2.1 Fatigue Analysis

Various levels of stress analysis may be adopted as a basis for predicting fatigue life of welded structures. A global nominal stress remote from the weld may be used. This lumps variables such as geometric stress concentration factor, weld shape characteristics and local notch strain into one variable called the design "category". Examining the stress in slightly greater detail in the vicinity of the weld, a hot-spot stress analysis incorporates a geometric SCF but again local weld characteristics are incorporated into the design category. The local notch strain approach refines the strain field even further to incorporate weld effects. At the extreme is fracture mechanics which takes the stress analysis to the level of the crack itself. As the reference stress or strain nears the weld, the number of required modification factors decreases. However, the difficulty in determining an accurate stress state increases. There must be a compromise between the complexity of analysis and the ease and cost of acquiring adequate fatigue resistance data. Therefore, it is often preferable to use the nominal stress approach because the nominal stresses are easily quantifiable. However, the nominal stress approach is not universally applicable.

2.1.1 Nominal Stress

The nominal stress approach categorizes weld details according to fatigue resistance [17,18,19]. These categories have been developed through fatigue testing of particular details and characterized by the nominal stress remote from the weld. Difficult-to-

quantify and highly-variable factors such as weld discontinuities and stress concentrations due to weld geometry are indirectly taken into account because these factors also affect the full-scale test specimens and thus are reflected in the resistance curves. Fatigue resistance data, which exhibits large scatter, must be generated for each category. Such large variation requires a statistically significant number of duplicate tests. Tests generally consist of constant amplitude cyclic loading of a particular detail at a known nominal stress range. Results are typically presented using a log-log scale plot of nominal stress range versus number of cycles to failure (S-N). The lower 95% confidence level of a this S-N data is used to establish a fatigue resistance design curve (or S-N curve).

As shown in Figure 2.1, the nominal stress is the nominal axial force divided by the nominal gross cross-sectional area, the largest nominal bending stress at the location of possible cracking, or the superposition of these stresses. In general, nominal stress is calculated using simple elastic formulas. This makes for a straightforward design approach. However, global geometric effects usually cause a significant redistribution of the membrane stress across the member section. Examples of such effects are shown in Figure 2.2. These effects should be considered when the nominal stress approach is used. Therefore, for more complex structures a coarse finite element mesh analysis is sometimes used to determine nominal stresses [16].

Research has shown that stress range is the dominant stress variable influencing the behavior of welded details [17,18,21,22]. The existence of residual tensile stresses at the

weld toe makes the full stress range effective, regardless if some portion of the stress range is in compression. The residual stresses are generally in the range of yield. Therefore, an applied compression load still imposes a range of tensile stress in the vicinity of the weld. As would be expected given the state of residual stress at the weld, parameters such as minimum stress, maximum stress and stress ratio have an insignificant effect in fatigue design. Interestingly, the strength and type of steel have a negligible effect on the fatigue resistance of a particular detail for long life fatigue [18,19]. Likewise, the welding process generally does not have a significant effect on fatigue strength [23]. Thus, the design is greatly simplified since stress range and detail configuration are the only parameters to be considered in most cases.

However, developing adequate fatigue resistance design curves for the nominal stress approach can be expensive. Theoretically, a unique design curve is required for each type of detail including variations in loading and member sizes. Each of the design curves requires a statistically significant number of full-scale details for adequate definition. These full-scale fatigue tests are performed at a number of different stress ranges with constant-amplitude loading. The logarithm of stress range (S) versus number of cycles to failure (N) is generally plotted with S on the y-axis and N on the x-axis. Using log-normal statistics, a least squares determination of the 95% confidence limit is determined from this data to develop a lower bound curve referred to as an S-N design curve. In equation form, this is

$$N = C\,S^{-m} \qquad (2.1)$$

or $$\log(N) = \log(C) - m\log(S)$$

where:
- N = number of cycles to failure
- C = constant dependent on detail
- S = constant amplitude stress range
- m = inverse slope of the S-N curve.

Note that m is most commonly referred to as the slope of the S-N curve. However, given the convention of plotting the dependent value (N) on the abscissa, m is actually the inverse of the slope of the curve as plotted. Therefore, an increase in "slope" will result in an S-N curve that is less steep.

Design curves have been developed for many weld details which have been incorporated in design standards such as the American Association of State Highway and Transportation Officials (AASHTO) Standard Specifications for Highway Bridges [15]. The AASHTO curves are shown in Figure 2.3. These curves correspond to categories of details grouped together according to their relative fatigue strength. Categories are labeled A through E' in order of decreasing fatigue strength. There is also a category F for fillet, plug and slot welds loaded in shear in any direction. With the exception of the F curve, each of these curves has a slope of 3 which is typically the standard for welded structures. Also, a constant-amplitude fatigue limit (CAFL) is defined below which a detail effectively has an infinite fatigue life given constant-amplitude loading.

The AASHTO curves are essentially the same as those of the American Institute of Steel

Construction (AISC) Manual of Steel Construction [20] and the American Welding Society (AWS) Structural Welding Code D1.1 [10]. Other curves have been developed such as those of the Eurocode[12] which are the same as those proposed by the International Standards Organization (ISO) and recommended by the International Institute of Welding (IIW). There are 14 curves plus a shear design curve in the Eurocode which are categorized according to stress range in MPa at 2 million cycles. AASHTO curves were adjusted to agree with seven of the Eurocode curves [24], i.e. category A is Eurocode 160, category B is Eurocode 125, etc. There are also design curves recommended by the UK Health & Safety Executive (UK H&SE) which are the same as those published by the American Bureau of Shipbuilding (ABS) [13,25]. The Ships Structures Committee (SSC) recently recommended yet another family of curves [26].

It is hoped that eventually these various codes are standardized to reflect only one set of design curves for welded structures. However, regardless of which code or recommendation is used, all approach fatigue resistance design in the same manner. Complexities such as residual stress, weld profile, weld size and weld discontinuities are random phenomena which are avoided with the nominal stress design concept. Stress concentrations due to global geometry are accounted for by the establishment of different categories. This allows for an easy design procedure by eliminating difficult to determine variables. Therefore, the nominal stress approach is recommended where an applicable design category exists and a nominal stress can be easily determined. For instance, in a previous study, it was determined that, the AASHTO design curves can be used directly

for some weld details used in the primary structure of the advanced double-hull [21].

2.1.2 Hot Spot Stress

The hot-spot stress approach reduces the various fatigue resistance design curves of the nominal stress approach to a single baseline curve. This is done by using a stress near the weld toe, known as the hot-spot stress, as the design stress. The hot-spot stress accounts for the stress concentration effects due to geometry of the detail but still excludes weld effects such as profile and size. These variables are assumed to be absorbed in the scatter of data. The hot-spot stress is defined as the point at the weld toe where the strain range attains a maximum value. It is determined using strain gages, finite element analysis or empirical formulas. Similar to the nominal stress method, test data are typically presented using a log-log plot of hot-spot stress versus number of cycles to failure (S-N). Unfortunately, there are varying methods of establishing the hot-spot stress that need to be evaluated to determine the best approach to the hot-spot concept.

In defining hot-spot stress it is necessary to distinguish between two levels of stress at the weld toe. First is the geometric stress which is the stress due to global geometry. It is assumed the stress due to global geometry varies linearly approaching the weld. The second level of stress quantifies additional local stress risers such as weld profile and size. The stress gradient approaching the weld and the levels of stress analysis are shown in Figure 2.4. The hot-spot stress approach uses only the geometric stress in the design procedure excluding the local stress. The point along the weld toe at which the geometric

stress is maximum is known as the hot-spot stress. Plastic work at this hot spot can actually generate heat under rapid cyclic loading. Assuming that there are no gross flaws elsewhere along the weld toe, it is expected that cracking will start at this "hot spot". The hot-spot stress may be determined by strain gage measurement, finite element analysis or empirical formulas. However, empirical formulas to determine an SCF to be applied to a nominal stress have been developed primarily for tubular structures. Therefore, only strain gage and finite method methods are discussed herein.

Because the hot spot is located at a local notch and notch effects are to be excluded, extrapolation of the stress from points removed from the notch is necessary. Therefore, the strain gage method of determining the hot-spot stress as presented in most recommendations consists of a linear extrapolation of geometric stress on the surface of the detail at adequate distances perpendicular to the weld toe. The first measured point is chosen at a point near the weld toe where notch effects are negligible. A second gage is placed at some distance away but still located within the influence of the geometric stress. A line passing through these measured stresses is extrapolated to the weld toe to define the hot-spot stress as shown in Figure 2.4. This method has been developed primarily for use in the offshore oil industry for the design of tubular structures. As a result, procedures developed for determining the parameters for the proper location of gages to measure this gradient are dependent on tube diameter and wall thickness [12,13]. However, extrapolations applicable to plate structures have also been investigated [27]. Table 2.1 lists several recommendations for the location of strain gages. As seen in Table

2.1, the AWS code differs from other guides in that it defines a single point as the definition of the hot-spot stress. No extrapolation of weld stress is required.

Finite-element analysis may also be used to determine the hot-spot stress. Since the finite-element method cannot give valid results at a notch, extrapolation of stress is again required. The element mesh must be refined near the hot spot so that stress at points similar to those defined above can be used to extrapolate to the weld toe. The results of a finite element analysis are very sensitive to the mesh size and element type. Therefore, careful consideration must be taken to gain accurate results. Recommendations have been proposed for circular hollow section (CHS) joints as well as rectangular hollow section (RHS) joints [23]. Best results are obtained when three-dimensional solid elements are used to model the joints in detail. Typically, however, quadratic thin shell elements have been used to determine hot-spot stress. The hot-spot stress is the stress computed at the intersection of the shells of the structural components. For thin shell elements, this intersection is actually the point of intersection of the midsurface planes of each shell. The stress at this location is only an index and obviously does not represent any actual physical stress in the joint. Nevertheless, for the special cases of certain tubular joints, empirical correlations have been developed between this computed index stress and the physical hot-spot stress measured with strain gages. Since the stiffness of rectangular sections or flat plate joints is quite different than in tubular structures, it is recommended that solid elements be used for modelling the weld and adjacent parts of the joint in order to get correct stiffness properties. Suitable transitions must be made between thin shell

and solid elements. If only thin shell elements are used, results may be obtained by shifting the stress distribution curve as shown in Figure 2.5 [28]. If consideration of the eccentricity of the detail is necessary, i.e. if eccentricity is small, use of thin shell elements with a curve shift may not be applicable. Solid elements may also be eliminated and correct stiffness maintained by using thin shell elements of different thickness at the intersection of structural components as shown in Figure 2.6 [23]. However, this method has yet to be verified. In addition to these many considerations, there is evidence that finite-element solution for hot-spot stress could become non-conservative as the severity of the structural stress concentration becomes less severe [29].

Since the hot-spot stress method is essentially the nominal stress approach with an SCF applied, similar behavior can be assumed. As in the nominal stress approach, the stress range is the dominant variable influencing the behavior. Parameters such as minimum stress, maximum stress and stress ratio have insignificant effect. And the type of steel and weld process are also negligible effects. Load reversal is fully effective due to the residual stress field present in all welds. The effect of load reversal is examined to a degree in this study.

There are several proposed baseline S-N curves for the hot-spot approach. The AWS Structural Welding Code D1.1 provides two design curves. Category X1 and X2 were developed using data from examination of tubular joints and pressure vessels [6]. As mentioned previously, this experimental data is from strain gages placed near the weld

toe and not from an extrapolation of stress as in other codes. Category X1 is applicable to welds that provide a smooth transition between the weld and base metal, i.e. welds that have been ground to improve the weld profile. Category X2 applies to as-welded joints. Explicit consideration of weld size and plate thickness is addressed. For thicknesses over a given limit, the following factor is applied to reduce the fatigue strength.

$$\left(\frac{t}{t_{ref}}\right)^{-0.25} \qquad (2.2)$$

where t_{ref} = 25 mm for Category X_2
t = actual thickness

The AWS curves X1 and X2 are the same as the curves X and X' as given by the API recommended practice for offshore structures RP-2A except for the definition of the CAFL. The implications of the CAFL are discussed later in this chapter. The same form of equation is used to describe the X1 and X2 curves as for the AASHTO nominal stress design curves. However, the curves have slopes of 4.30 and 3.74 respectively as shown in Figure 2.7 and Table 2.2.

Another design curve widely accepted is the UK H&SE category T curve. It is based on the geometric stress linearly extrapolated to the weld toe. Unlike the AWS curves it has a slope of 3 which is consistent with the AASHTO and Eurocode nominal stress design curves. In fact, the T curve is essentially the same as the AASHTO category C curve except for the definition of a fatigue limit. The T curve flattens to a slope of 5 at a cycle life of 10 million. The UK H&SE code includes the same thickness correction as AWS.

The baseline fatigue curves represent the fatigue strength of a groove weld when failure results from a crack that had initiated at the weld toe. The AASHTO category C curve also represents this condition. Therefore, it is also a good candidate as a baseline curve for the hot-spot stress approach. The hot-spot and nominal stress approaches are essentially equivalent. The hot-spot approach uses the concept of a structural stress concentration factor (SCF) to represent stress at the weld toe. Ignoring the CAFL, the AASHTO fatigue curves are all parallel. Therefore, each category could be represented with SCF's [30]. The SCF of a particular category is equal to the ratio of the fatigue strength of category C to the fatigue strength of the category required. Since the curves are parallel, the ratio is independent of the number of cycles at which fatigue strengths are compared. For example, category D is equivalent to an SCF of 1.3 and category E is equivalent to and SCF of 1.6. These SCF's are calibrated or determined from full-scale test observations.

2.1.3 Local Notch Strain and Fracture Mechanics

The notch strain is the controlling factor for crack initiation and initial crack propagation. Fracture mechanics assumes an existing initial crack. Therefore, a combination of the two analysis methods may be used to determine an estimated total life.

In the local notch strain approach a fatigue notch factor (K_f) is defined as the ratio of fatigue strength of a specimen with no stress concentration to the fatigue strength of a specimen with a stress concentration. Notches generally effect the distribution of stress

through the thickness of the material. Figure 2.8 shows examples of local notches. The total notch strain can be determined several ways. The notch strain can be measured with strain gages placed over the weld toe. Or a very fine mesh finite element model may be developed. Fortunately, a two dimensional FEA model using plane strain elements yields satisfactory results. Another method is to determine the elastic-plastic stress and strain state at the notch root using Neuber's rule [31] and the elastic stress-strain curve with the previously known fatigue notch factor as a basis. Material properties for base metal, weld metal and the heat affected zone are required. In addition, the results are sensitive to assumed mean and residual stresses.

In the fracture mechanics approach the defects and cracks inherent in welds are evaluated based on the stress intensity at the crack tip. This is a very complex process. A detailed knowledge of the stress field along the path of the crack growth is needed. In addition, local weld geometry and initial flaw size are required. The fracture mechanics approach must accurately predict crack growth rates to the threshold level. This approach uses the least amount of empiricism. Data are generated from small-scale compact-tension specimens. Therefore, the effect of many variables can be examined by substituting appropriate crack growth rate data into the analysis. This presents a good method for predictions of behavior of a known crack. Fitness-for-purpose concepts can then be applied to verify safety.

2.1.4 Choosing an Analysis Method

The nominal stress approach would prove difficult to apply to a welded detail with a large eccentricity such as a ship foundation attachment. If the hull plate were rigid, if the attachment passed through the plate, or if there was a corresponding shape that continued on the other side of the plate (intercostal), this detail could be designed with respect to the nominal stress in the angle as a Category C detail. However, if there is significant eccentricity or misalignment, the fatigue resistance in terms of the nominal stress in the angle can be much lower than Category E' (AASHTO's lowest category). The nominal stress in the angle is very small (3-10 MPa). The bending stress induced in the plate to which the angle is mounted is much higher than the nominal stress in the angle. In fact, fatigue cracking in these experiments typically initiated at the weld toe in the hull plate perpendicular to the bending stress in the hull plate. Defining a nominal stress in this small gap between the angle and longitudinal support would be difficult. Therefore, the nominal stress fatigue analysis approach is not a reasonable method.

The notch stress approach requires a greater amount of measuring, testing and calculation compared with the nominal stress approach. In addition, the geometry of the local notch at the weld toe varies significantly along the weld and between welds. This causes a varying value of peak stress. Also, the analysis is sensitive to estimation of residual stress. In the nominal stress and hot-spot stress approaches, these variations are absorbed in the scatter band of the S-N curve. Notch stress approach is most applicable for crack initiation in details with no precracks at the root [27]. Welding almost always produces

small crack-like discontinuities. Therefore, to estimate total fatigue it must be combined with fracture mechanics which is too complex to apply to design. Data such as weld toe geometry and initial flaw size necessary for the fracture mechanics approach is difficult to quantify. Analyses are very sensitive to this input. A calibration to full-scale test data is necessary to eliminate uncertainty in the stress distribution near the weld and in the definition of the stress-intensity factor. Fracture mechanics is best suited to evaluating the safety of existing cracks and is not generally accepted as a basis for fatigue life predictions [7].

The hot-spot stress approach is suitable mainly for joints where the weld is transverse to the applied stress and the crack is expected to initiate at the weld toe. In addition, it can be used when a nominal stress is not easily defined. The hot-spot method has other attributes that make it a desirable fatigue design tool. For example, varying joint geometries are placed on a common ground, difficult to measure attributes such as notch effects and residual stresses are included in design curve, and a margin of safety consistent with other methods is provided. Unfortunately, methods for measuring and evaluating hot-spot stress vary. Despite this uncertainty in the correct method of application, the hot-spot method of fatigue analysis is the most appropriate for foundation details with large eccentricity. Therefore, hot-spot analysis was chosen to evaluate the foundation detail.

2.2 Fatigue Loading

Fatigue design curves are typically developed using a range of constant amplitude loadings inducing uniaxial stress. However, in reality, loading will be of a varying amplitude. A damage summation rule credited to Palmgren and Miner (referred to as Miner's rule) has been used to reduce a variable amplitude loading into discrete intervals of stress range. While there is evidence of load effects in fatigue [32-34], Miners's rule has produced acceptable results suggesting that load effects are cancelled under service loading. For the purposes of this study, a constant amplitude loading was used with the assumption that the constant and variable loading can be equated. Various publications may be consulted for further discussion concerning variable loading and its relation to fatigue resistance.

Also, in many instances, loading does not induce a uniaxial state of stress. Loadings may produce two or three principal stresses that may by nonproportional or out of phase in time. In addition, the directions of these stresses may change over time. This multiaxial stress state is not accounted for on the detail level. Though many studies examining multiaxial fatigue loading have been conducted, the majority have been for fatigue of base metal at a notch or discontinuity. Relatively limited research has been performed on welded details.

2.2.1 Multiaxial Loading

Loads used in ship design are categorized according to three designations. Primary loads

are those that induce overall hull bending. Secondary loads are those that induce local bending of frames and stiffeners in combination with an effective width. And tertiary loads cause plate bending between stiffeners. Often, secondary and tertiary loads and the resulting stresses are not considered in design.

Foundations attached to the inner hull of a double-hull ship are subjected to multiaxial state of stress. As shown in Figure 2.9, the primary hull bending would induce a stress in the plane of the hull plate. At the same time, inertial loads due to ship motions or equipment vibration would induce bending and axial loads in the foundation legs. Several problems are posed by this multiaxial loading, including:

1. To what extent does a small superposed "primary" stress range influence the fatigue resistance of the detail which is dominated by the much larger "distortion" stress range perpendicular to the web?

2. Stress will occur randomly in several directions and will most likely be out of phase. If necessary, how should the primary and distortion stress ranges be combined?

Constant amplitude fatigue testing of various beam web stiffener details correlated the maximum principal tensile stress including the effect of shear at the point of failure [38]. A plot of this data showed a distinct band of scatter suggesting the principal stress at the point of crack initiation as a valid measure of fatigue strength.

A more recent study of multiaxial loading on full-scale welded structural details indicated that loading perpendicular to the weld toe dominates fatigue life [5]. The data suggest that an orthogonal nominal in-plane stress, if less than 83 Mpa, would have no effect on

the fatigue resistance due to distortion. A stress greater than 83 MPa would have only a small effect. This is based on a plot of strain range measured perpendicular to the weld toe where the crack typically started versus number of cycles to first observation of a crack. Data distinguishing between two different orthogonal nominal stresses (41 MPa and 83 MPa) showed an earlier initial detection for the larger in-plane stress.

Another study using small-scale welded specimens examined the out-of-phase loading effects on fatigue life [35]. Evaluation of data was examined using the local strain approach and the various local stress criteria. Though testing indicated an order of magnitude difference in life for in-phase and out-of-phase loadings with identical maximum local principal stress amplitudes, all data falls within the scatter band of the in-phase data. Important to note is that these tests incorporated stress relief of welds to reduce residual stresses and thus, reduce data scatter. Stress concentration factors were developed using complex finite element models with specific data on weld geometry. This type of analysis is not conducive to the design process. The local strain notch approach and its applicability to multiaxial fatigue of welded structures has been the subject of several studies [7,36].

In the experiments reported in sections 3 and 4, in-phase biaxial loading of a typical foundation detail with large eccentricity is examined. The hot-spot stress as defined by a measured strain perpendicular and nominally 5 mm from the weld toe was used to assess fatigue resistance. Comparisons to uniaxial loading fatigue tests were performed

to assess the influence of two levels of an orthogonal in-plane stress. All tests were constant amplitude. The effects of nonproportional loading were not examined, i.e. in-phase loading is assumed to be the worst case.

Table 2.1 Hot-Spot Definitions

CODE OR GUIDE	S-N CAT.	DISTANCE FROM WELD TOE		COMMENTS
		a	b	
AWS	X1 X2	6mm to $0.1\sqrt{rt}$	not defined	defined by point a; not explicitly defined in code (see fig 2.4 & ref 10)
API	X X'	6mm to $0.1\sqrt{rt}$	not defined	same as AWS
UK H&SE	T	$0.2\sqrt{rt}$	$0.625\sqrt{rt}$	linear extrapolation in reference to tubular joints (see fig 2.4)
Eurocode/ ECCS/IIW	90	not defined	not defined	no guidance given on extrapolation of stress
IIW-XIII-1414-91	T	0.5t	1.0t	Various delphi opinion reported in IIW paper for use with linear extrapolation in plate applied to UK H&SE curve (see ref 14)
	T	0.5t	1.5t	
	T	0.4t	2.0t	
	T	1.0t	3.0t	
	T	4.0 mm	10.0 mm	
	T	$1.57\sqrt[4]{t^3}$	$4.9\sqrt[4]{t^3}$	

Notes: r = radius of tubular section
t = thickness of tubular section or plate

Table 2.2 Hot-Spot Fatigue Design Curves

CODE	Hot-spot	Category	log(N)=C-m*log(S)	
			m	C
AWS/API	YES	X1/X	4.30	11.31
	YES	X2/X'	3.74	10.30
H&SE	YES	T	3.0	12.17
Eurocode/ECCS/IIW	YES	90	3.0	12.17
BS5400/ABS	NO	D	3.0	12.18
AASHTO/AISC	NO	C	3.0	12.17

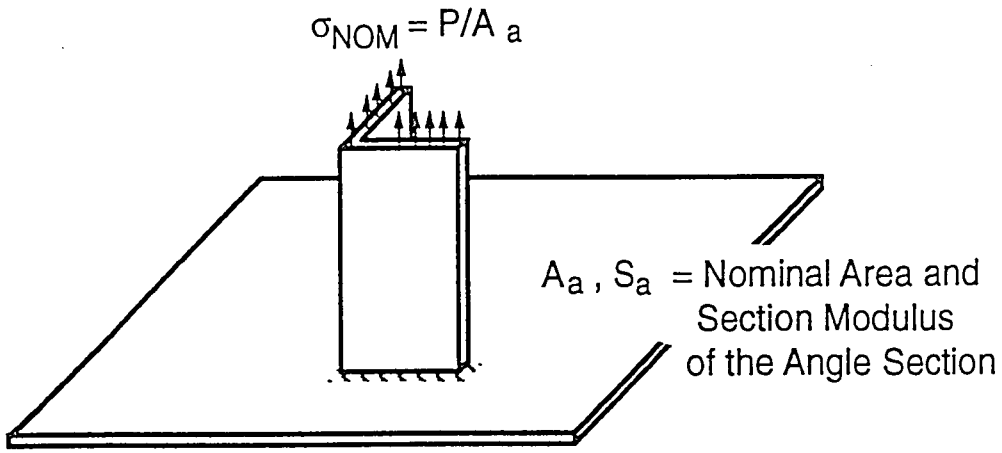

AXIAL LOAD

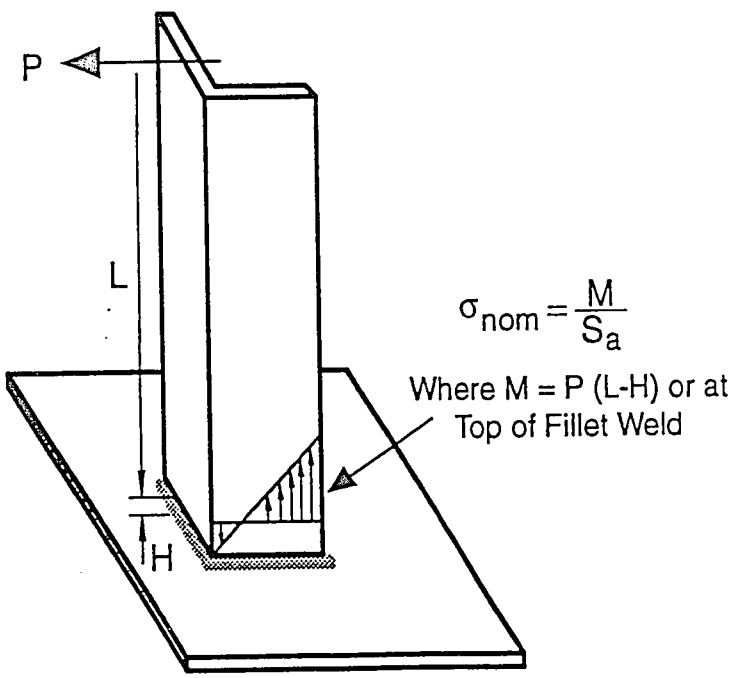

BENDING LOAD

Figure 2.1 Definition of nominal stress for axial and bending loads based on section properties of the angle excluding the fillet welds

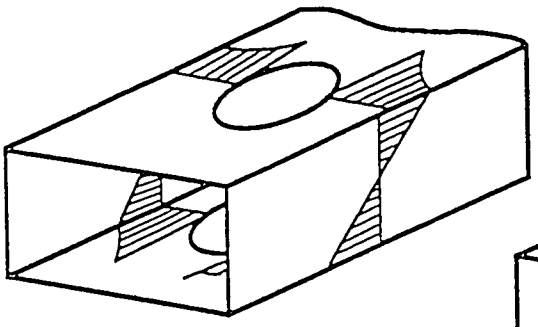

(a) Large Opening

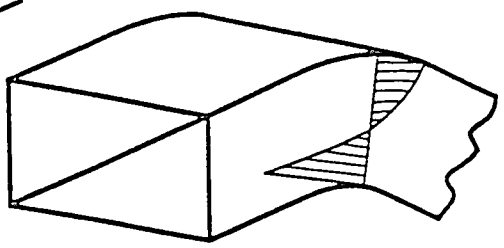

(b) Curved Beam

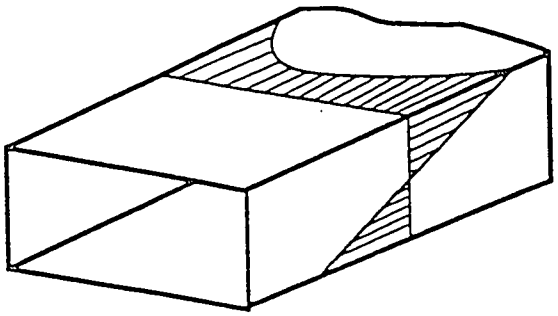

(c) Shear Lag

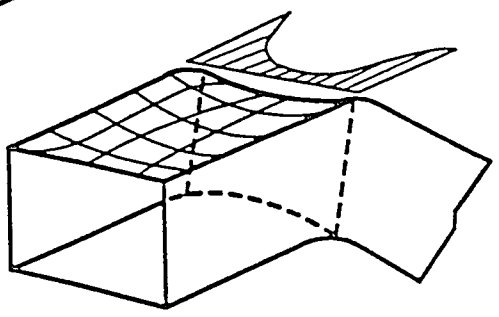

(d) Flange Curling

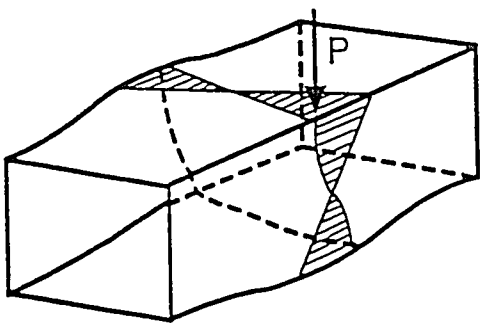

(e) Distortion of Cross Section

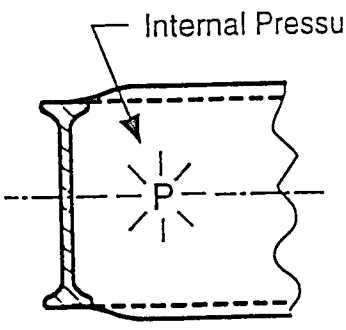

(f) Discontinuity Stresses in a Shell

Figure 2.2 Geometrical effects which produce stresses exceeding those calculated by elementary stress analysis

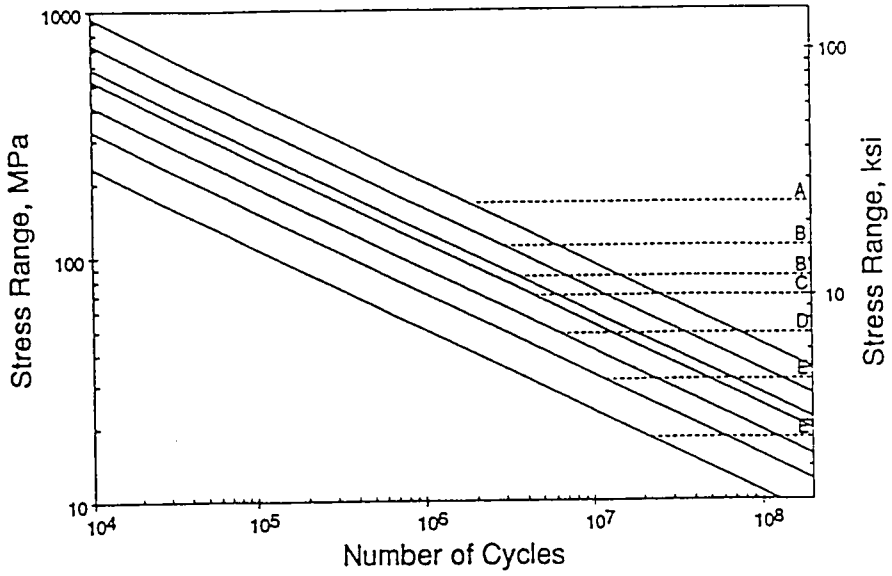

Figure 2.3 Fatigue Design Curves Used by AASHTO and AISC

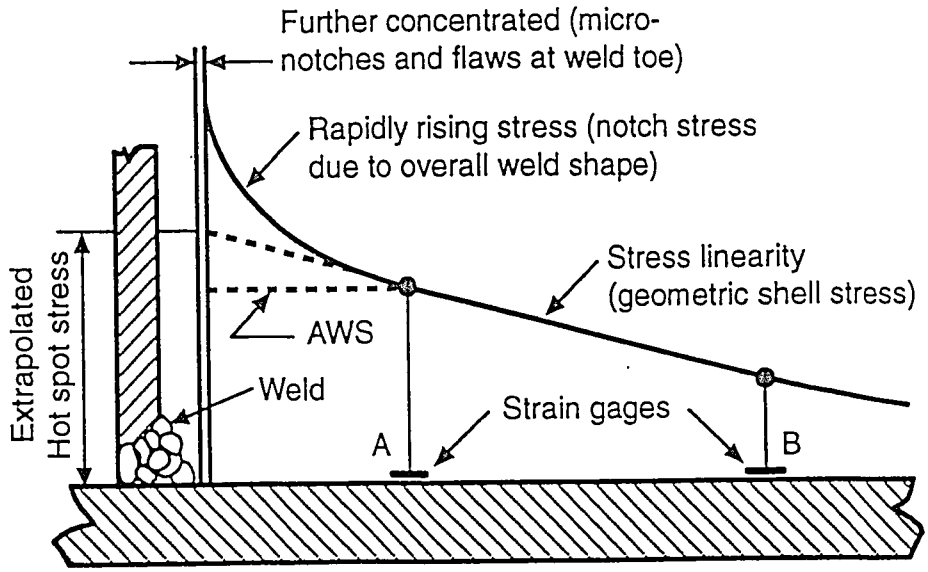

Figure 2.4 Definitions of 1) Hot Spot Stress According to AWS and European Conventions, 2) Geometric Stress and 3) Local Stress

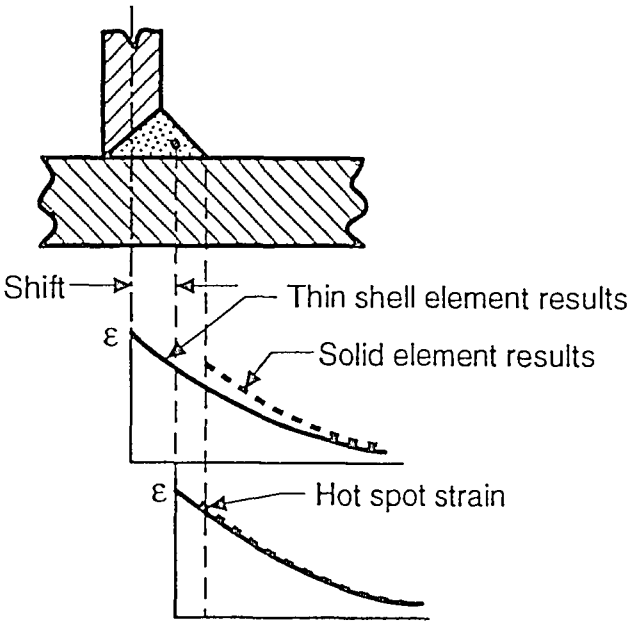

Figure 2.5 Shift of stress gradient as determined by thin shell finite element analysis to obtain realistic Hot- Spot Stress

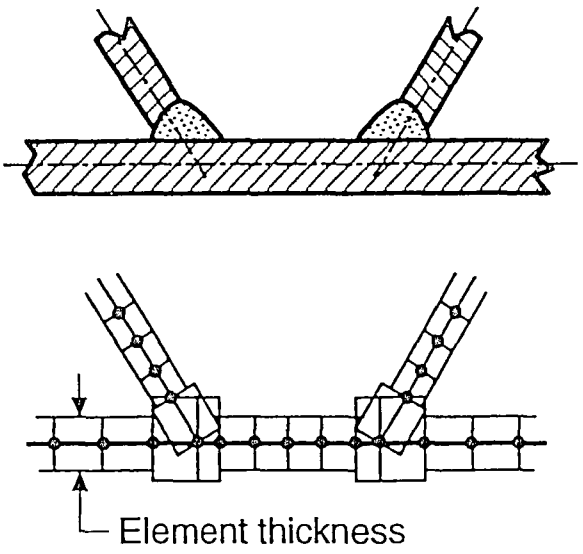

Figure 2.6 Use of thin shell elements with increased thickness at weld zone to approximate increased stiffness

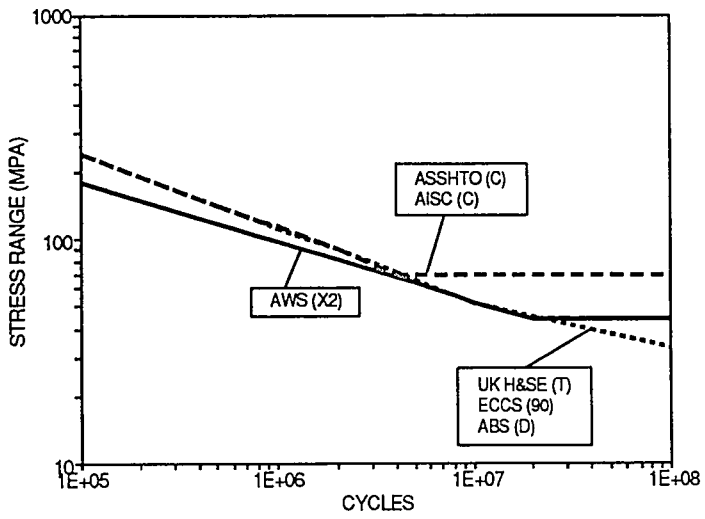

Figure 2.7 Various fatigue design curves applicable to the Hot-Spot Concept and similar Nominal Stress Curves

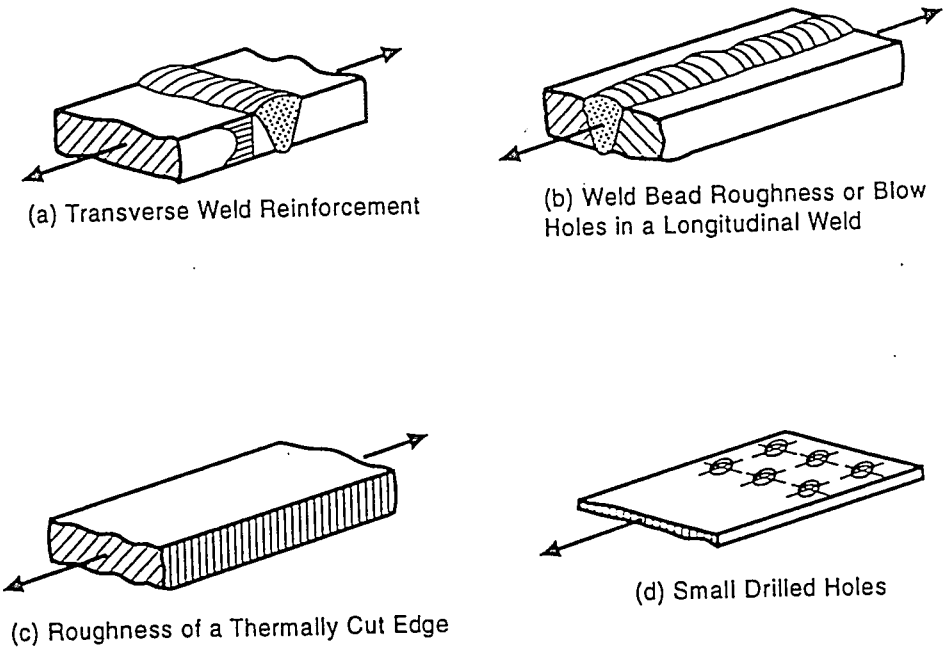

Figure 2.8 Typical notches in welded details

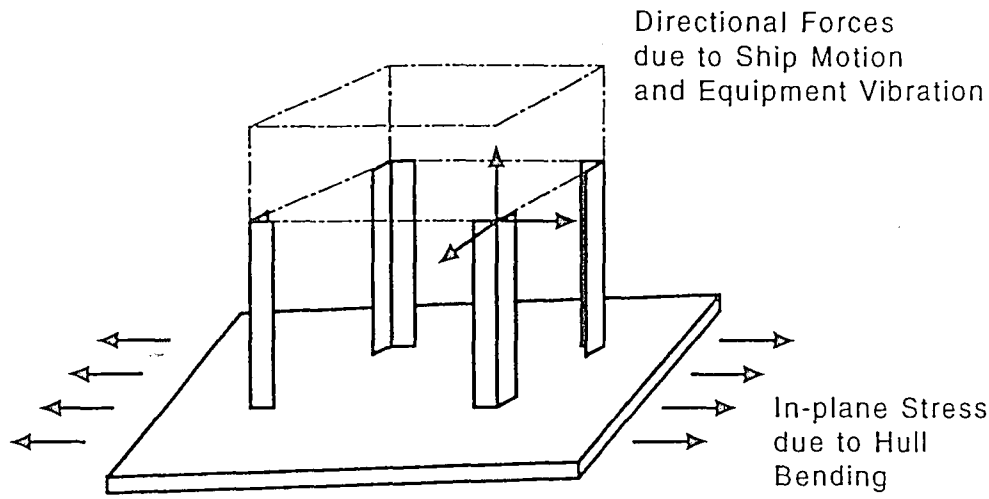

Figure 2.9 Foundation subject to various loads resulting in a multiaxial stress state

3.0 DESCRIPTION OF EXPERIMENTS

As described in Section 3 of reference 39, foundation configurations for testing were developed after analysis of the response of a typical foundation attachment to the double-hull cellular structure. These details included a primary configuration and three alternatives as shown in Figure 3.1. The Primary configuration was subject to three types of constant amplitude loadings to assess its fatigue resistance. The loadings consisted of a force acting axial to the foundation angle (Axial test), a force lateral to the angle (Bending test), and a simultaneous loading axial to the angle and in the plane of the hull plate (Biaxial test). The alternative configurations were subject to only axial loading and fewer tests were conducted than for the Primary configuration. The three alternatives were to examine the influence of eccentricity to the web.

3.1 Design of Test Specimens

3.1.1 Material and Fabrication

The test specimens were fabricated at Nazareth Machine Inc. using A572 (grade 50) material. After initial quotes for fabrication, it was decided to use this material in lieu of HSLA-80 (MIL-STD-S-24645(SH)-Class 3) which is the typical material used in surface combatants. Using HSLA-80 was too costly and delivery, due to availability of the material, would not suit the required test schedule. Several test programs indicate that the type of steel is not a significant factor in fatigue life of large scale weldment [17,18,37]. All welds were made using a Carbon-Dioxide gas shielded flux-cored welding (FCAW) process in accord with MIL-100TC. All welds were visually inspected.

Fillet welding of the angles to the cell was done by Nazareth Machine for the first specimens delivered. The remainder of the angles were attached at Lehigh University. This allowed flexibility in configuration of remaining specimens.

3.1.2 Axial and Bending Specimens

The Axial and Bending test specimens were designed to represent one cell of a multicell, unidirectional, double hull so that a representative structural response was simulated. A typical cell of 915 mm x 915 mm and constructed of 10 mm plate was used in accord with notional double-hull design for a CG-47 type ship. In order to compensate for the reduced stiffness resulting from the lack of the adjacent cell structure, the vertical height of the webs was reduced to 610 mm and transverse plate stiffeners were placed at each end of the box. A 50 mm overhang was provided at the corners of the cell to allow for a characteristic double fillet joint. The length (1830 mm) of the specimens was chosen so that the stress pattern in the vicinity of the test angle was not significantly affected by the specimen edge geometry. Equal leg angles (75 mm x 75 mm x 10 mm) were fillet welded to the top plate according to the configurations shown in Figure 3.1. Two angles were mounted on each cell or box except for the Alternative 3 specimens. The two-angle configuration provided a structural response representative of a foundation located above one cell (see Figure 3.2) and also provided the added benefit of testing two details simultaneously. This allowed more details to be tested in less time for an economical use of material and equipment. Figures 3.3 to 3.8 show details and photos of specimens.

3.1.3 Biaxial Specimen

The Biaxial specimens consisted of the same basic cell structure used in the Axial and Bending specimens. Axial stress in the hull plate was induced by bending a cantilever span on either end of the section, as shown in Figures 3.11 to 3.13. The specimen was required to be about 5 m in length. Two angles were mounted at each of the 1/3 points of the specimen. This placed the angle in the theoretical constant moment region and minimized the vertical displacement of the detail due to the bending of the cantilevers. Excessive vertical displacement could interfere with operation of the actuators applying the axial loads.

3.1.4 Test Matrices

The test matrix for each configuration (Table 3.1) was a factorial design with minimum stress and stress range as the main control variables. The stress ranges were chosen to give a range of fatigue lives that then can be used to plot a fatigue S-N curve. The minimum stress range corresponds to a predicted life of about 10 million cycles while the largest range corresponds to a predicted life of about 150 thousand cycles. Target stress shown in the matrix is local stress. This local stress is the hot-spot stress as defined by a gage at 5 mm from the weld toe at the point of highest stress along the weld length. Both positive and reverse loading tests were performed to verify that reversal of stresses typical of ship structures does not have a significant effect on fatigue life. Fatigue tests performed at Lehigh on longitudinal welds and welded attachments suggests that reversal loading has an insignificant effect [7].

Initially all alternate configurations were intended to be tested at the same stress range. However, the initial test of Alternate 2 failed at a low cycle life. It was decided to decrease the stress range on the second specimen to a measured hot-spot stress of 12 MPa to obtain a higher cycle life.

For the Biaxial tests, the in-plane stress range reflects a nominal stress. The ranges were chosen to determine the effect of a biaxial state of stress. Reference 5 suggests that an in-plane stress below 83 MPa does not affect the fatigue resistance of a detail which is similarly dominated by distortion in a perpendicular plane. Therefore, stress ranges on either side of this value were used.

3.2 Test Setup and Procedure

3.2.1 Axial Testing

As shown in Table 3.1, twenty-four attachment details were tested with a load normal to the hull (axial loading). Twelve of these details were the Primary configuration (refer to Figure 3.1). There are two of these Primary details on a given box for a total of six boxes. In addition, four details of each of the three alternate configurations were tested. Alternates 1 and 2 required two boxes with two details per box. Alternate 3 had only one detail per box; thus, four boxes were required.

Two identical test stations were constructed that were adjustable so that Primary as well as Alternate configurations could be tested easily in the same setup. As shown in Figure

3.9, a servohydraulic actuator with a capacity of 490 kN applied load to two details through a spreader beam attached at the end of the subject angles. A clamp was designed to attach to the top of the angle to transfer load from the spreader beam to the angles. This clamped the test angle between concentric tubular sections for use as a double shear slip-critical connection (Figure 3.14). The clamp was oriented in such a manner that the applied force acted through the centroid of the subject angle. The specimen was mounted to a plate fixed to the floor to provide a rigid connection as shown in Figure 3.15. Each actuator was individually controlled at a frequency of 2 to 4 Hz using a multichannel system on a personal computer.

Tests were performed in load control and strain gages were used to determine nominal and hot-spot stresses. Nominal stress refers to the average axial stress through the angle. Hot-spot stress refers to the stress at the weld toe measured with a strain gage as close as possible to the weld toe. Initial testing showed bending in the angle due to geometry of the welded connection and the flexibility of the plate (Figure 3.16). However, strain readings taken at the center of each face of the angle, 305 mm above the plate, indicated an average axial stress consistent with the applied load. Therefore, nominal strain was determined using a double-full bridge arrangement of strain gages as shown in Figure 3.19. Hot-spot strain was measured using a 3 mm gage placed 5-6 mm from the weld toe. See Chapter 4.0 for locations along the weld length specific to each configuration.

At initial startup of each test, loads were applied to attain the target hot-spot stress range.

The nominal stress range was noted. Stress at the hot-spot gages was also monitored to detect cracks. Since these were placed at the point of highest stress, cracking was most likely initiated near the gage. Therefore, a change in stress usually indicated cracking. So, the nominal stress was periodically monitored to insure initial loading was maintained throughout the test. Each specimen was visually inspected for cracks approximately every 4 hours (except 4 a.m.).

At first visual observation of cracking, the number of cycles, location and surface length of the crack were recorded. Loading was continued until the crack propagated to failure. Failure was defined as a through thickness crack, since this leads to leaking problems on a ship. Observation of stress at the adjacent detail indicated that a crack at one detail did not influence the nominal or hot-spot stress of the other detail. Cracking of both details was nearly simultaneous in most cases. Therefore, a repair procedure was not used except for Alternate 2 tests (see discussion below). However, both cracks were seldom propagated to failure. In general, one detail failed first and the test was ended. Periodic measurements of crack surface length were used to estimate the through thickness cycle life of the unfailed detail.

The testing of the Alternate 2 configuration did not exhibit the same characteristics as the other configurations. The two details of given specimen or box did not crack simultaneously. Therefore, a repair procedure was developed to continue cycling of the adjacent detail. Since the weld in this case propagated through the throat of the weld, the

plate was not cracked. Failure was then defined as a crack length of at least 75 % of the total weld length. To repair this, the cracked detail was removed and the plate was ground smooth. A new angle was welded in place and testing was resumed until the second original angle (not the angle just replaced) reached failure. Further discussion of the failure mode is contained in Section 4.1.3.

3.2.2 Bending Testing

Twelve Primary details (two details per box for a total of six boxes) were tested with a load out of plane and parallel to the hull plate to induce bending in the test angle. One test station was constructed. As Figure 3.10 shows, a servohydraulic actuator with a capacity of 133 kN applied a lateral load to two details through a truss type member. The hinges of this member provided a true pinned condition insuring a pure bending in the angle. The actuator was controlled at a frequency of 2 to 4 Hz using a multichannel system on a personal computer.

Tests were performed in displacement control due to available equipment. As in the axial tests, nominal and hot-spot stresses were monitored. In this case, nominal stress refers to bending stress in the leg of the angle transverse to the cell web. Initial testing showed nearly all bending stress was carried through this angle leg (see Figure 3.17). For subsequent tests, nominal bending stress was measured with one strain gage located 200 mm above the plate and 25 mm from the toe of the angle leg. Hot-spot stress was measured at the center of the leg parallel to the web and at the toe of the transverse leg.

At first visual observation of cracking, the number of cycles, location and surface length of the crack were recorded. Loading was continued until the crack propagated to failure. Observation of stress at the adjacent detail indicated that a crack at one detail did not influence the nominal or hot-spot stress of the other detail. Cracking of both details was nearly simultaneous. Therefore, a repair procedure was not used. In general, one detail failed first and the test was ended. Periodic measurements of crack surface length were used to estimate the through thickness cycle life of the unfailed detail.

3.2.3 Biaxial Testing

Twelve Primary details were tested with a combination of loading in the plane of the hull and loading normal to the hull (biaxial loading). As discussed in section 3.1.3, each box had 4 angles. Only two of these four were expected to yield results. Therefore, a total of six boxes were required.

One test station was constructed as depicted in Figure 3.13. Two servohydraulic actuators with a capacity of 980 kN each applied positive load to the cantilevered ends of the specimen producing tension in the top plate due to bending. Simultaneously, two actuators each with a capacity of 490 kN applied an axial load in phase with the bending load to the four test angles through spreader beams and clamps similar to the axial tests. The location of the test angles over the support points minimized the vertical and angular displacement of the angles for ease in applying this axial load. All four actuators were controlled via computer software so that phase control and a frequency of 1 to 2 Hz was maintained.

Tests were performed in load control. Nominal stress and hot-spot stress were monitored as in the axial tests. In addition, a nominal bending stress at midspan of the cell was monitored with three strain gages across the width of the top plate of the cell. At first visual observation of cracking, the number of cycles, location and surface length of the crack were recorded. Loading was continued until the crack propagated to failure. Upon failure of one angle, the associated pair of angles was disconnected from the axial loading jack. This allowed continued biaxial cycling of the remaining pair. This pair was then cycled until failure in one angle. It was intended to obtain only two data points from each biaxial specimen though there were four angles per specimen. However, as in the other types of tests, cracking occurred approximately simultaneously. Thus, at least three data points were obtained for each specimen.

3.3.4 Strain Measurements

As discussed in Section 2.1.2, the hot-spot stress approach to fatigue life prediction requires knowledge of the stress gradient leading to the weld toe. To determine the point of highest stress at the weld toe, 3 mm strain gages were placed at various locations around the weld toe with the nearest gages 5 - 6 mm from the weld toe. The gage size and proximity to the weld toe were chosen to conform to previous strain measurements used in establishing the AWS hot-spot fatigue design curve [6]. Prior to fatigue testing and after shakedown, static positive and negative incremental loads were applied to the test specimens in accordance with the intended test mode, i.e. loads axial to the test detail for axial specimens etc. Static loads were repeated at least three times to check

consistency of gage readings. Using data from these initial strain measurements, the hot-spot was determined. Then on subsequent tests, only three gages measuring the strain gradient leading to the weld toe at the hot-spot were measured. Again, the nearest gage was nominally 5-6 mm from the weld toe and succeeding gages were 18 mm and 31 mm from the weld toe respectively (See Figure 3.18). Several different specimens were measured to obtain a mean stress gradient for use in determining a hot-spot stress as defined by an extrapolation to the weld toe (See Chapter 4).

Table 3.1 Test Matrices

Axial Test Matrix (Primary configuration)

S_{min} \ S_r	110 MPa	165 MPa	220 MPa
14 MPa	[1A] 2 details (1 spec)	[4A] 2 details (1 spec)	[2A] 2 details (1 spec)
-55 MPa	[3A] 2 details (1 spec)	---	---
-82.5 MPa	---	[5A] 2 details (1 spec)	---
-110 MPa	---	---	[6A] 2 details (1 spec)

Axial Test Matrix (alternate configurations)

S_{min} \ S_r	85 MPa	165 MPa	220 MPa
14 MPa	2 det (1 spec), [1A2]	---	---
14 MPa	---	2 det (1 spec), [1A1] 2 det (2 spec), [1A3,4A3]	---
-82.5 MPa	---	2 det (1 spec), [2A1] 2 det (1 spec), [2A2] 2 det (2 spec), [2A3,3A3]	---

Notes:

1. S_r = Stress Range at weld toe
   S_{min} = Minimum Stress at weld toe

2. Bracketed numbers are specimen numbers. The format is as follows:

   [1A1]
   - 1 — sequential number
   - A — axial loading
   - 1 — alternate number; no number indicates Primary specimen

Table 3.1 (cont.) Test Matrices

Bending Test Matrix (Primary configuration)

S_{min} \ S_r	110 MPa	138 MPa	165 MPa
14 MPa	[1B] 2 details (1 spec)	[4B] 2 details (1 spec)	[5B] 2 details (1 spec)
-55 MPa	[6B] 2 details (1 spec)	---	---
-82.5 MPa	---	[3B] 2 details (1 spec)	---
-110 MPa	---	---	[2B] 2 details (1 spec)

Biaxial Test Matrix (Primary configuration)

S^*_{rip}	S_{min} \ S_r	110 MPa	165 MPa	220 MPa
55 MPa	14 MPa	[2] 2 details (1 spec)	[3] 2 details (1 spec)	[5] 2 details (1 spec)
110 MPa	14 MPa	[1] 2 details (1 spec) note 2	[4] 2 details (1 spec)	[6] 2 details (1 spec)

Notes:

1. S_r = Stress Range at weld toe
   S_{min} = Minimum Stress at weld toe
   S_{rip} = In Plane Stress Range

2. Biaxial Specimen 1 was tested using matrix as original proposed, i.e. based on nominal stress. Therefore, position in matrix is in reference to nominal stress.

3. Bracketed numbers are specimen numbers. The format is as follows:

   [1B]
   - 1 — sequential number
   - B — bending loading, no letter indicates Biaxial Specimen

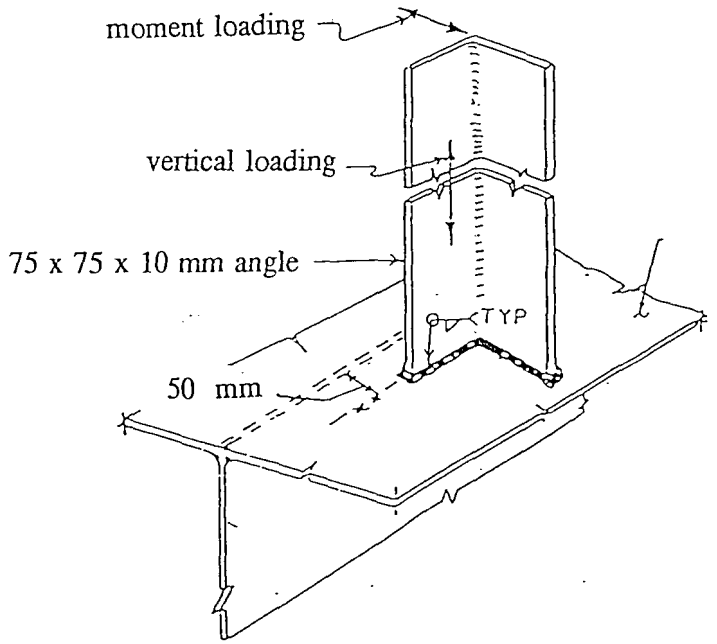

Primary Test Configuration

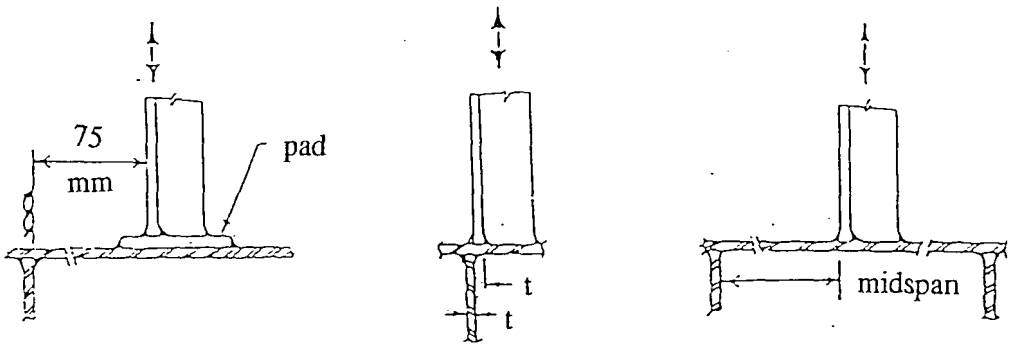

Alternative 1 Alternative 2 Alternative 3

Figure 3.1 Foundation attachment test details

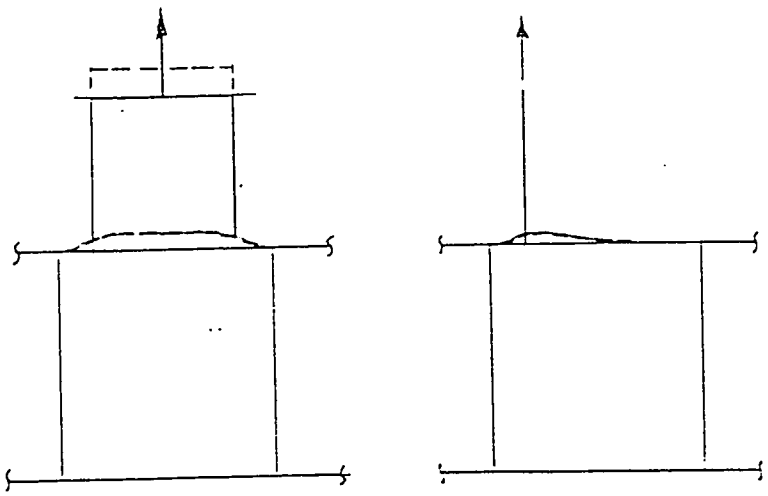

b. Foundation axial load response for one and two angles per cell.

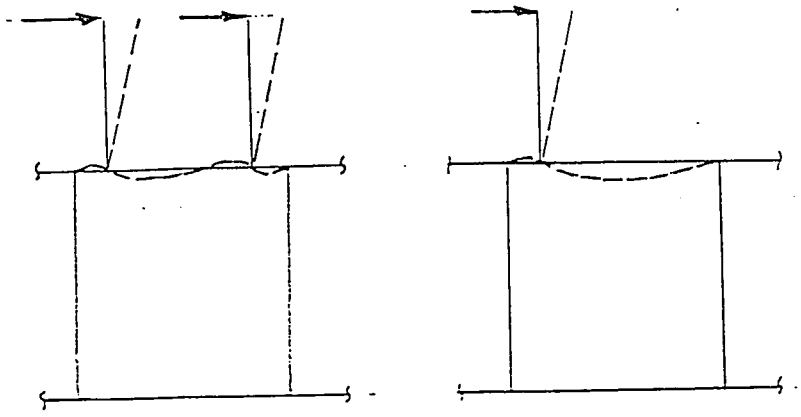

a. Foundation bending load response for one and two angles per cell.

Figure 3.2 Comparison of the structural response of double-hull cell under bending and axial foundation load

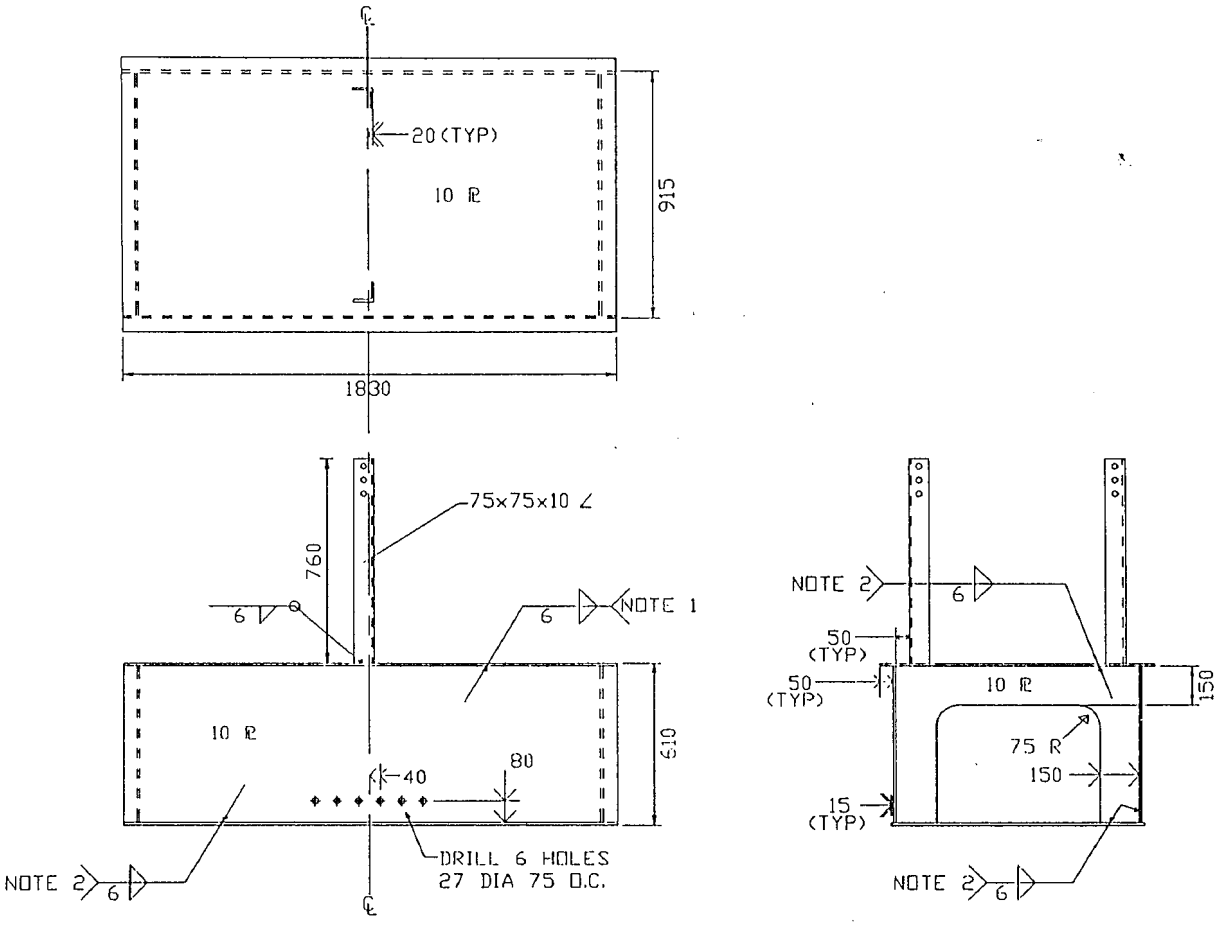

Figure 3.3 Primary detail Axial and Bending Specimen detail drawings

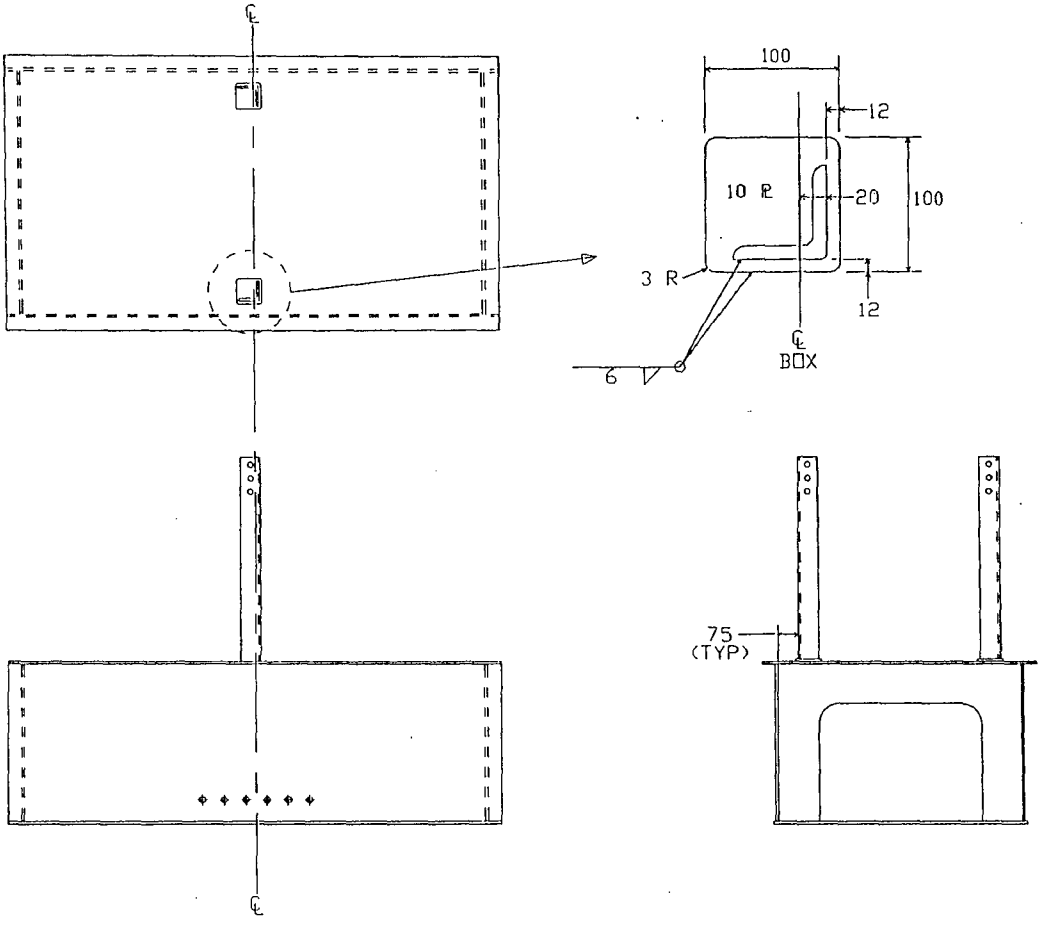

Figure 3.4 Alternate 1 - 85 mm eccentric detail Axial Specimen detail drawing

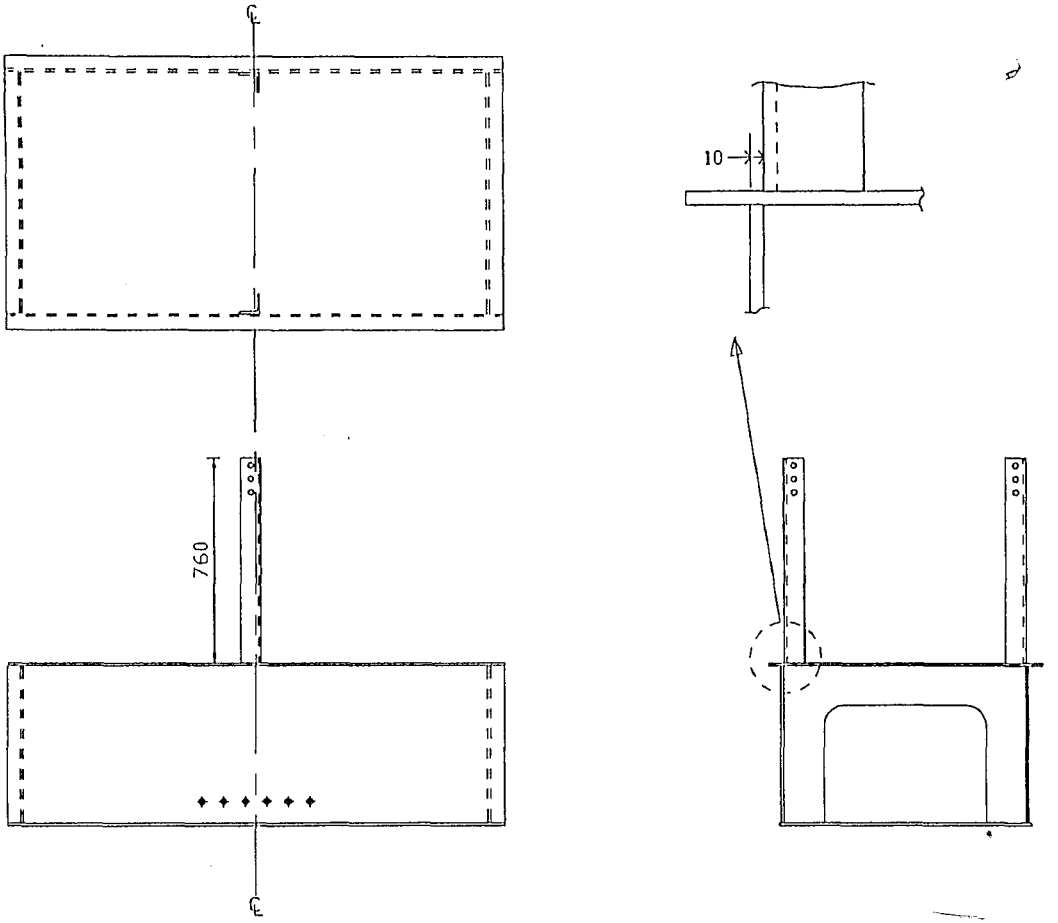

Figure 3.5 Alternate 2 - 1 plate thickness eccentric detail Axial Specimen detail drawing

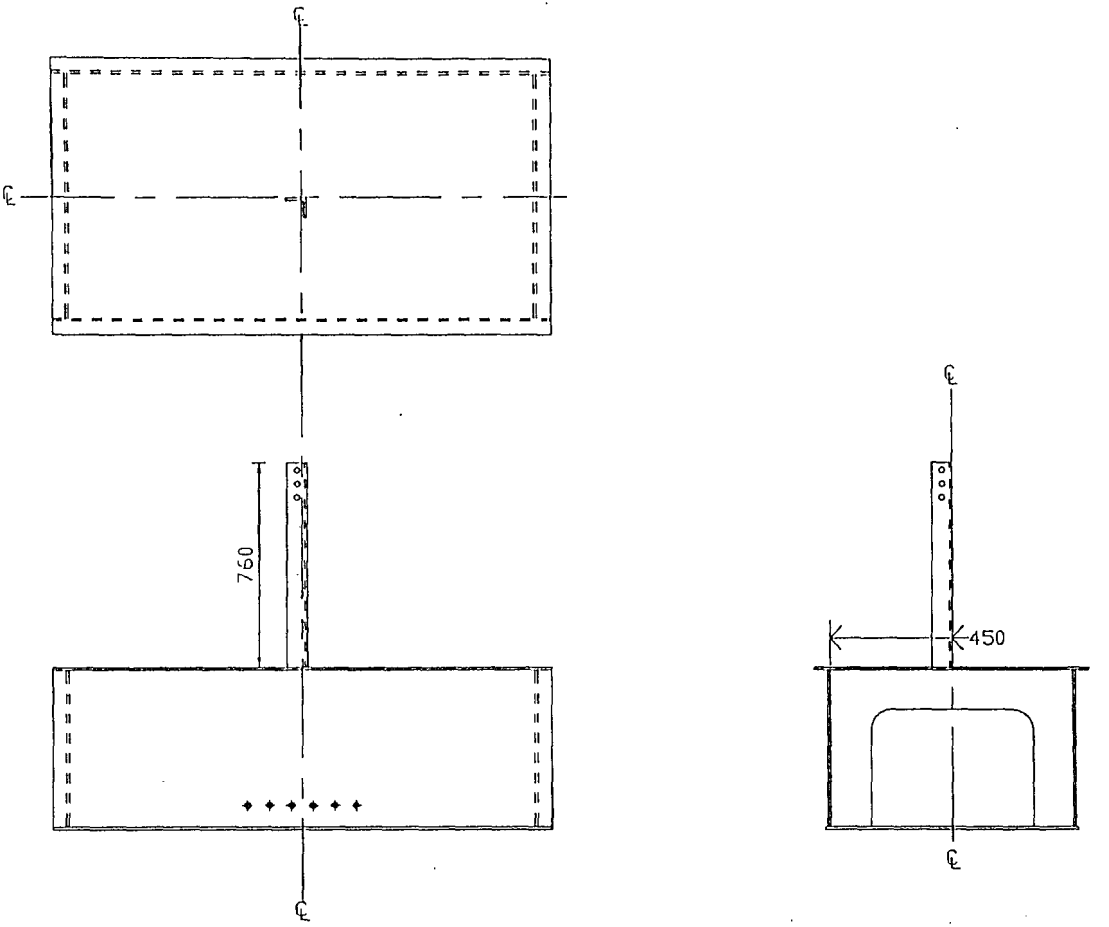

Figure 3.6 Alternate 3 - Midspan detail Axial Specimen detail drawings

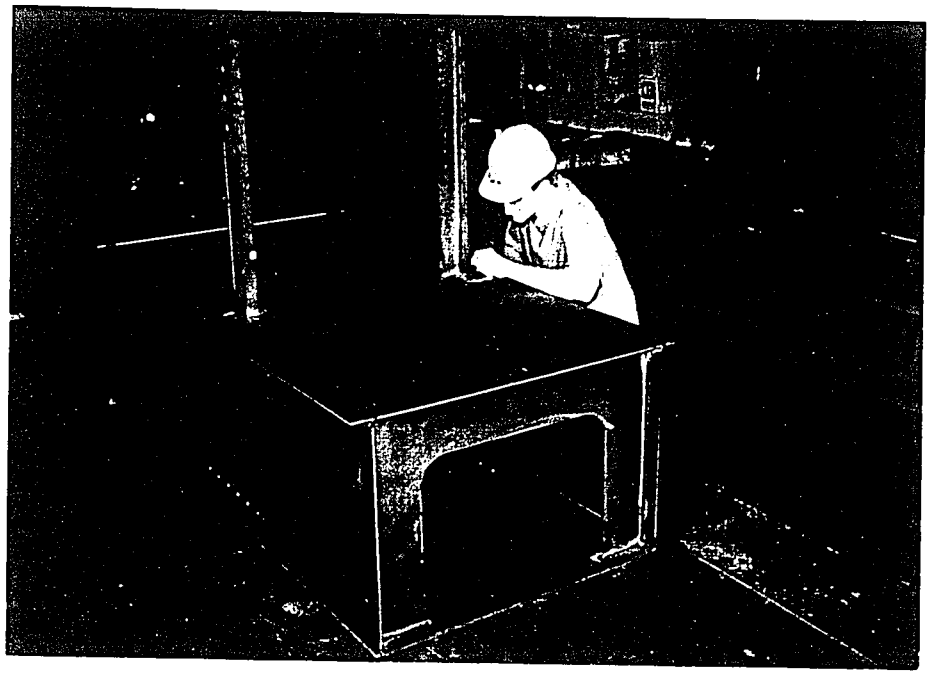

Figure 3.7 Typical Primary Detail Specimen

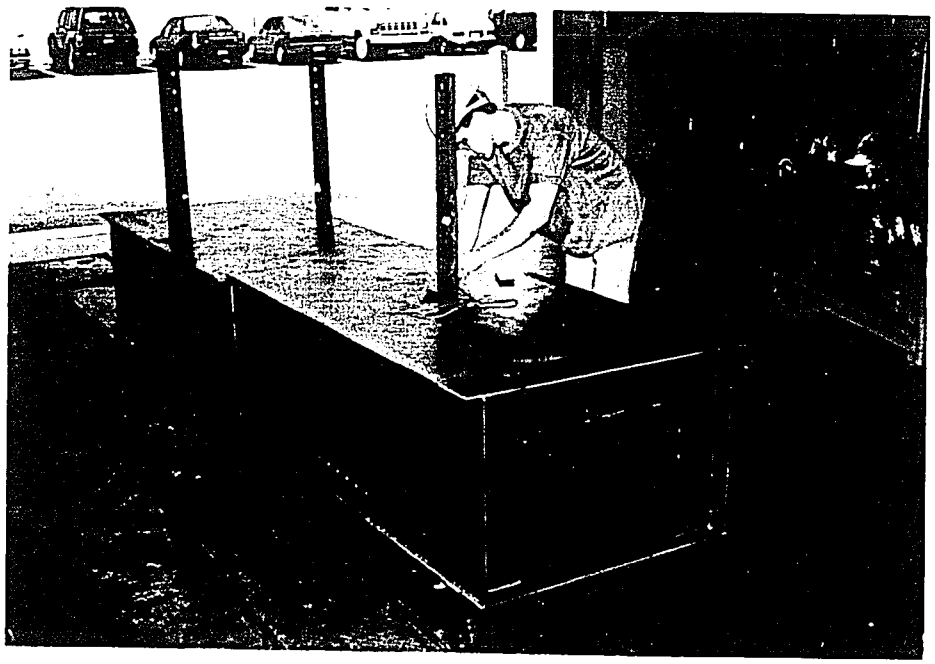

Figure 3.8 Typical center panel specimen

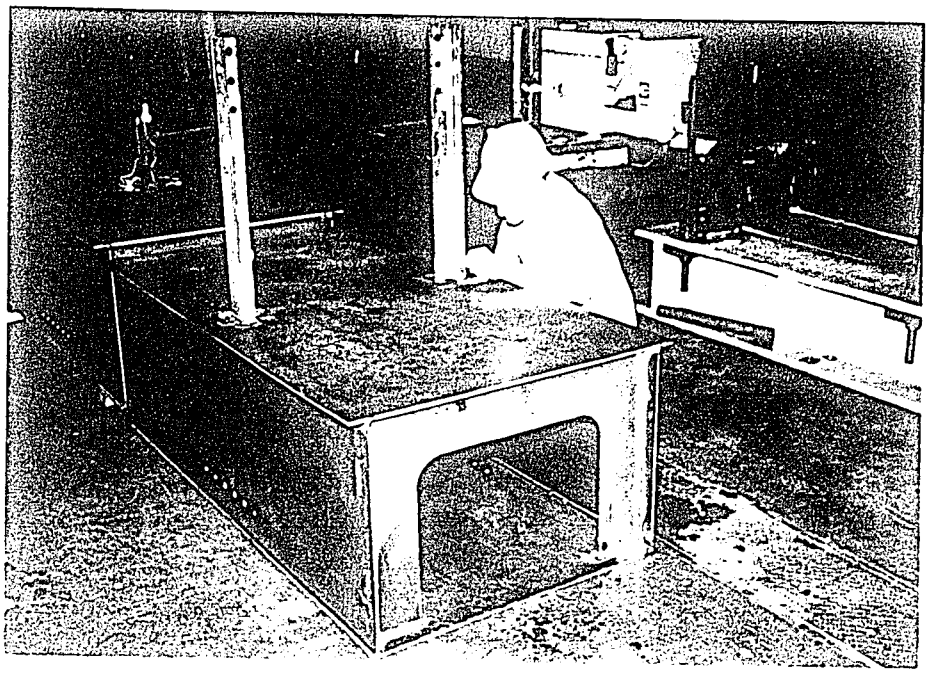

Figure 3.7 Typical Primary Detail Specimen

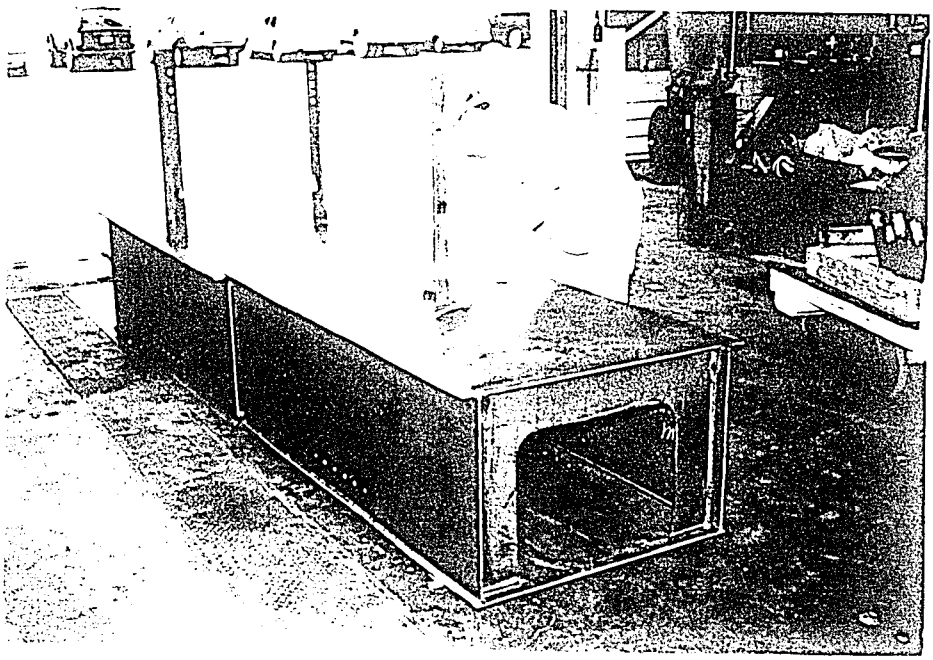

Figure 3.8 Typical center panel specimen

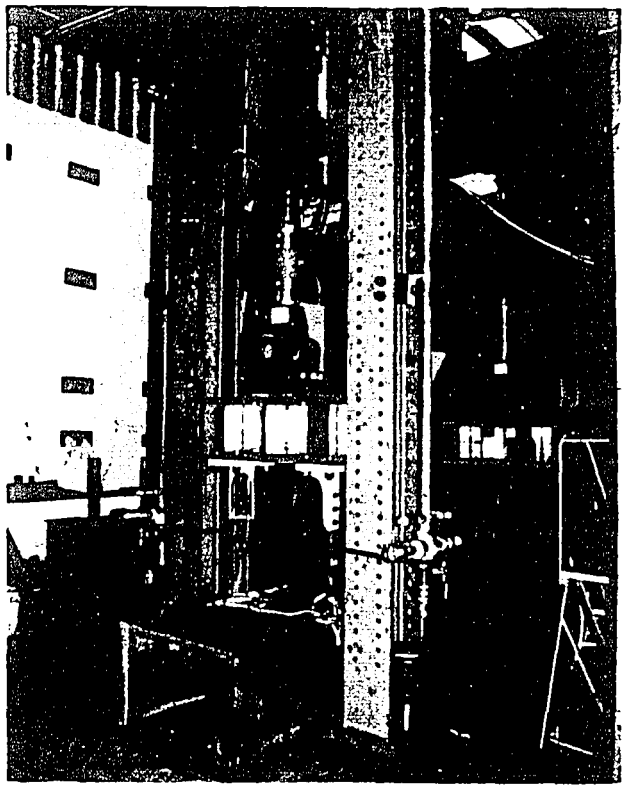

Figure 3.9 Axial test setup

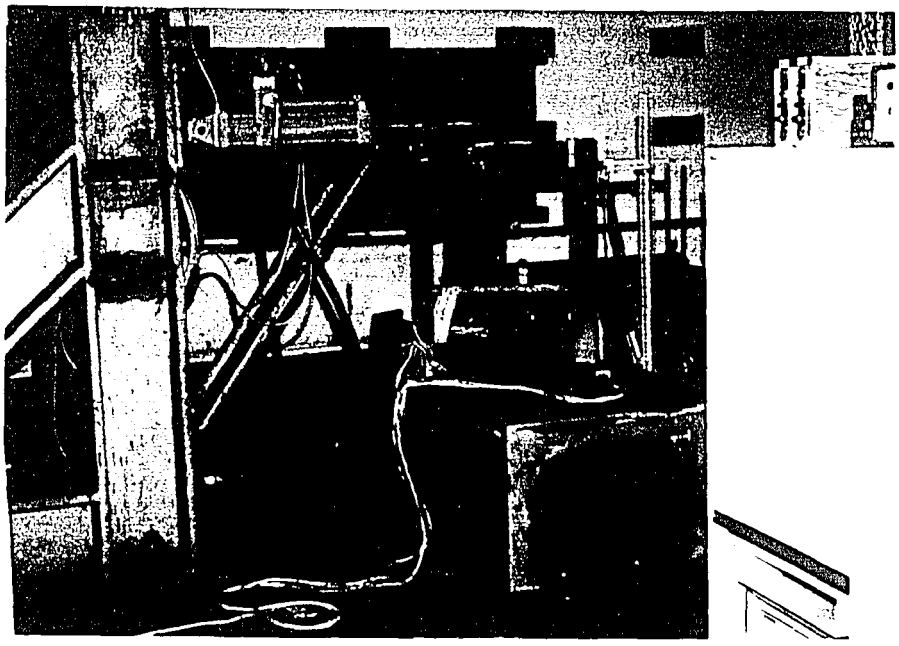

Figure 3.10 Bending test setup

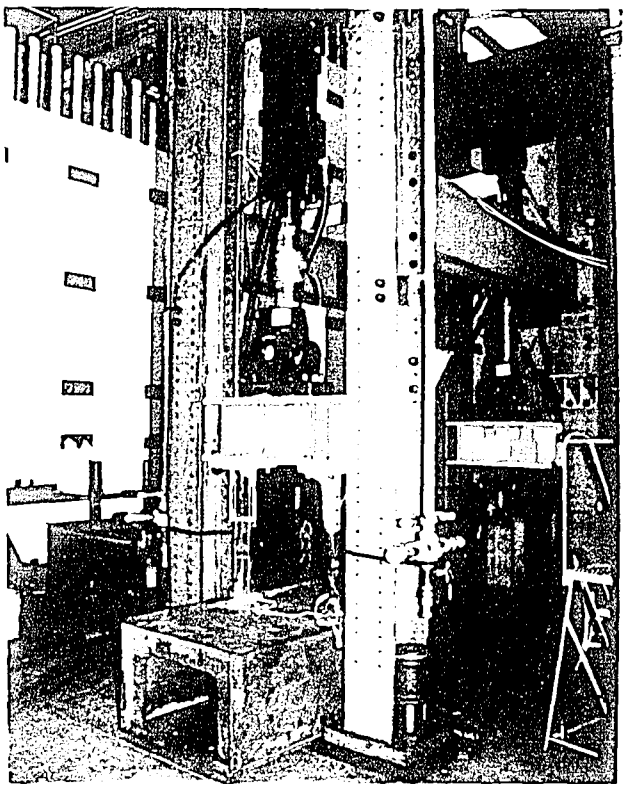

Figure 3.9 Axial test setup

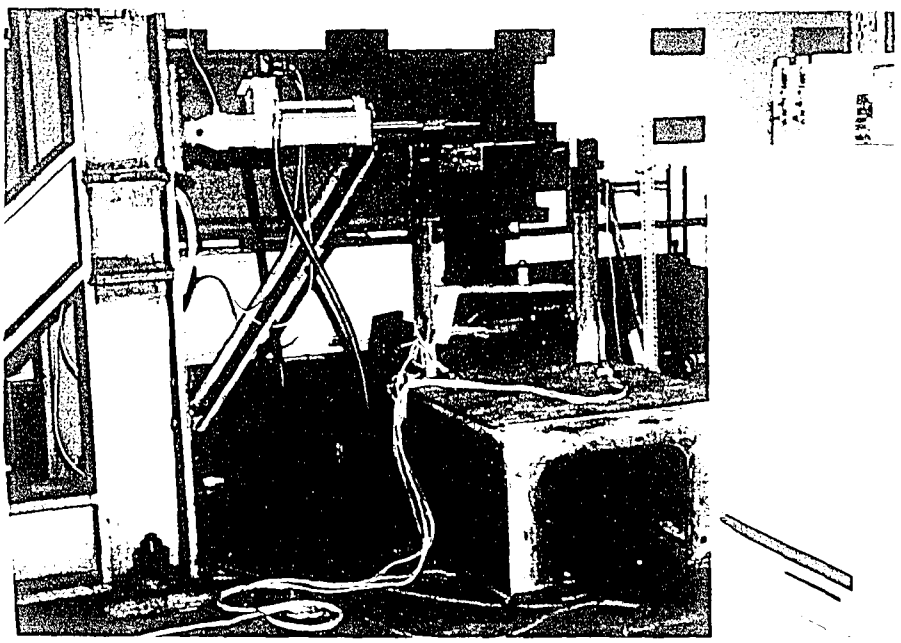

Figure 3.10 Bending test setup

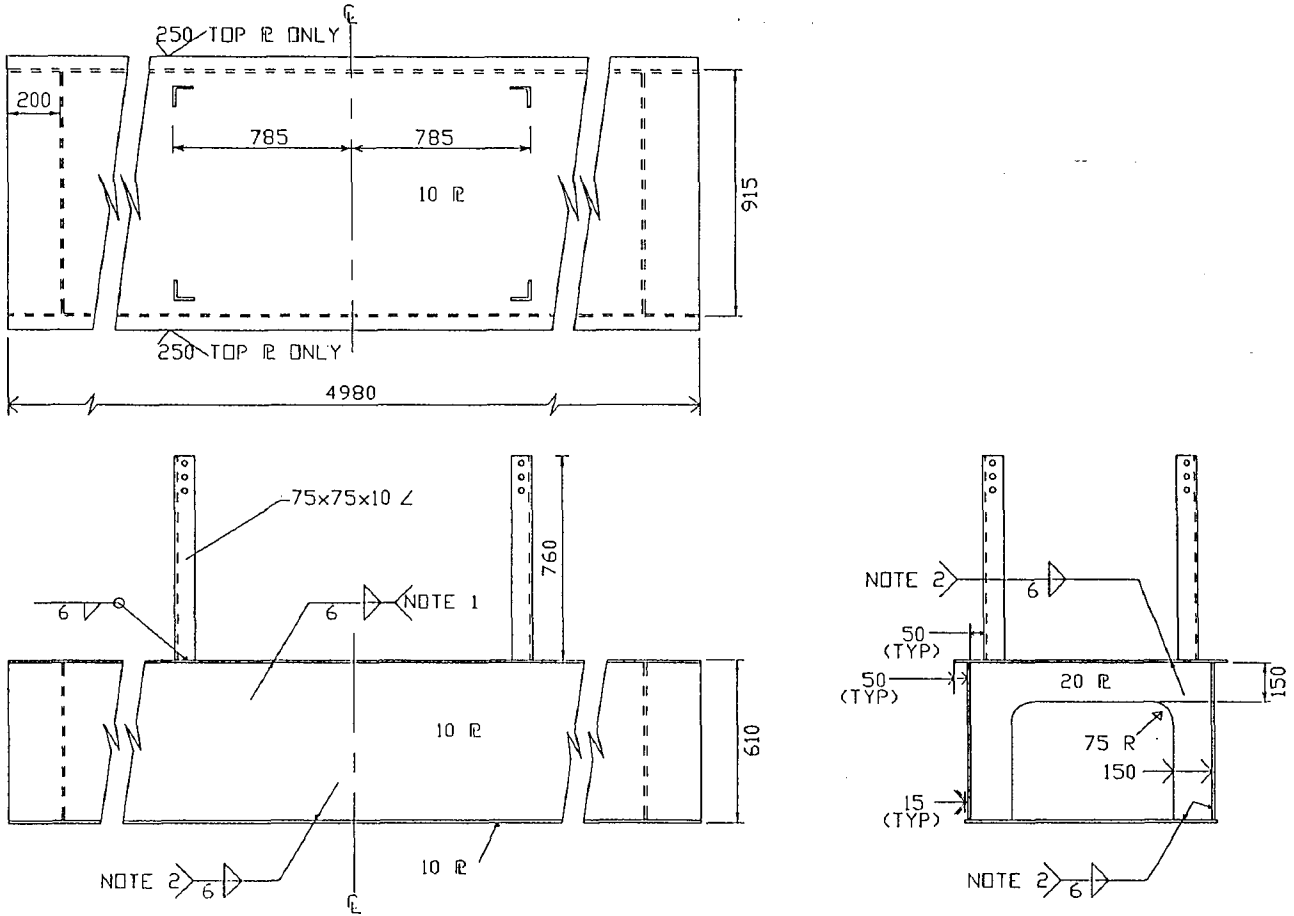

Figure 3.11 Primary Detail Biaxial Specimen detail drawing

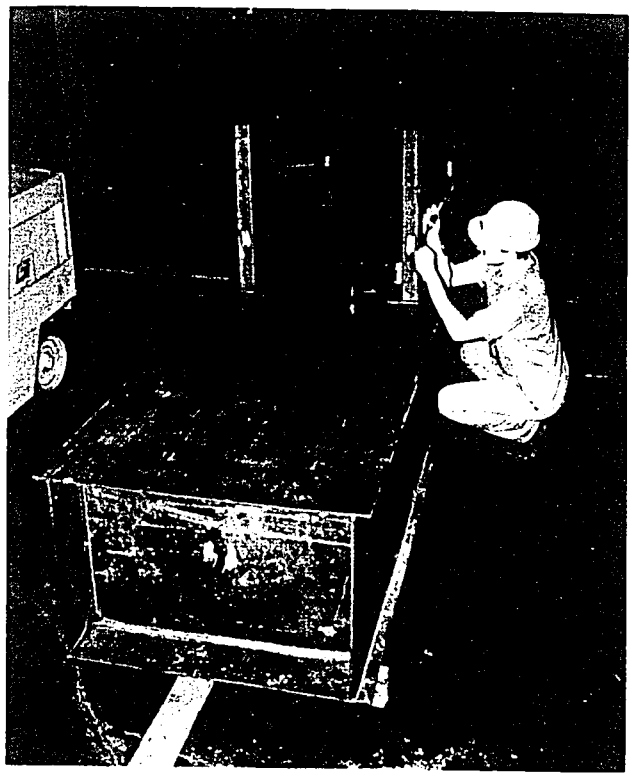

Figure 3.12 Typical Biaxial Test Specimen

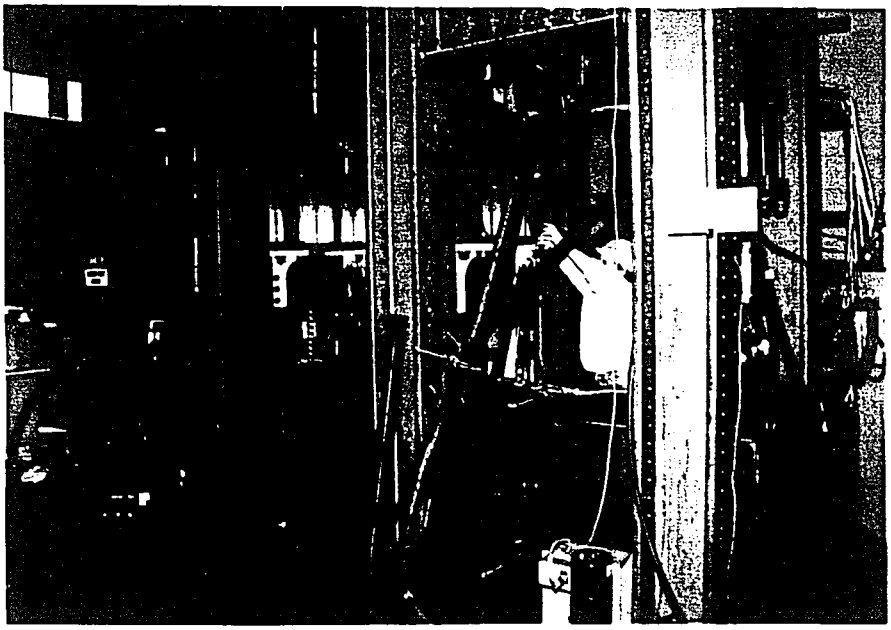

Figure 3.13 Biaxial test setup

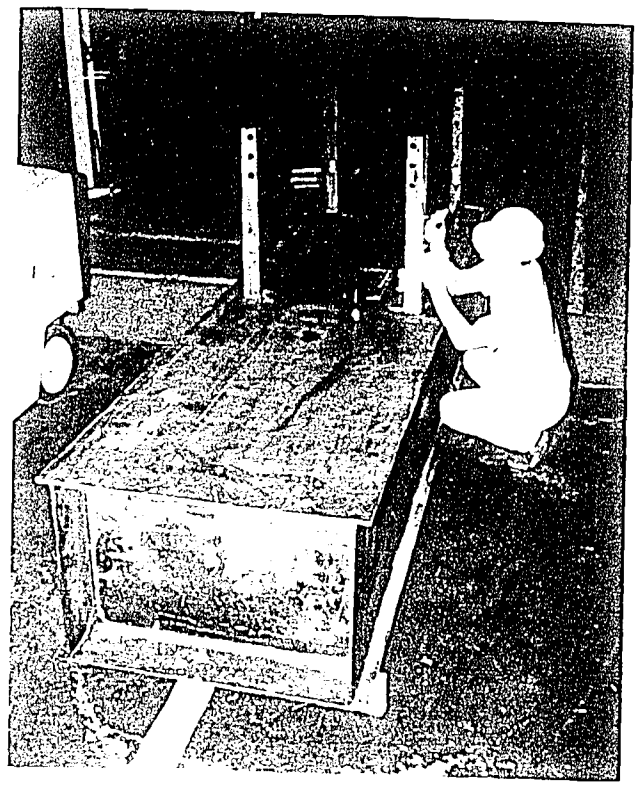

Figure 3.12 Typical Biaxial Test Specimen

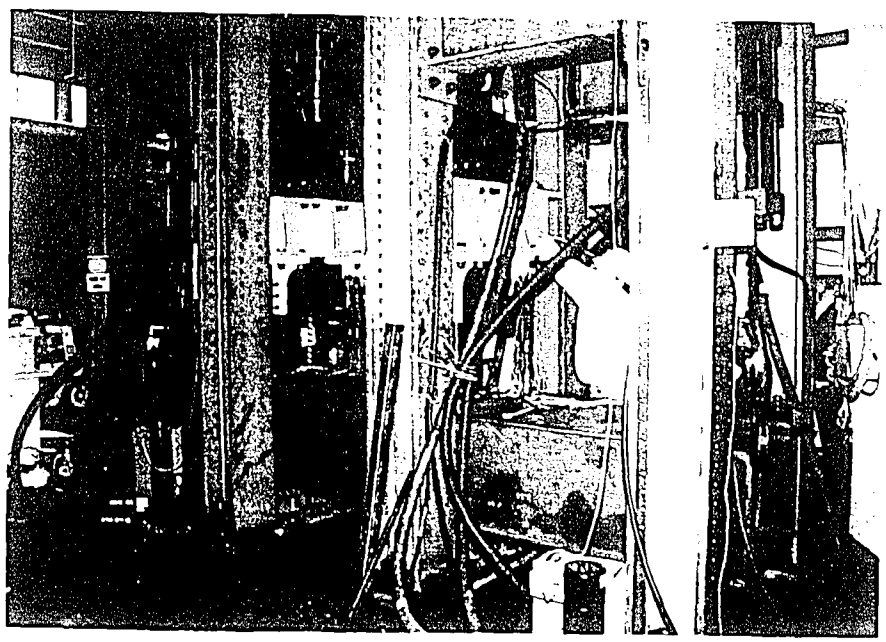

Figure 3.13 Biaxial test setup

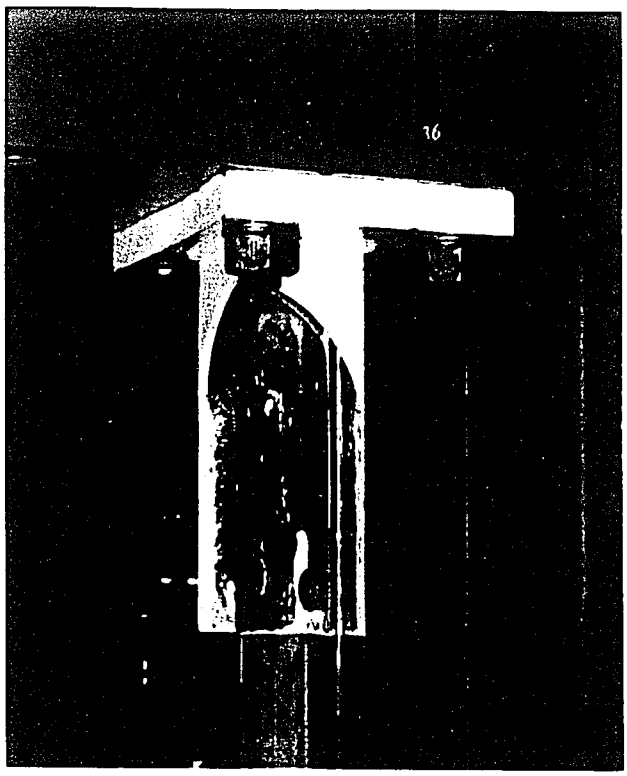

Figure 3.14 Clamp fixture used for Axial and Biaxial test setup

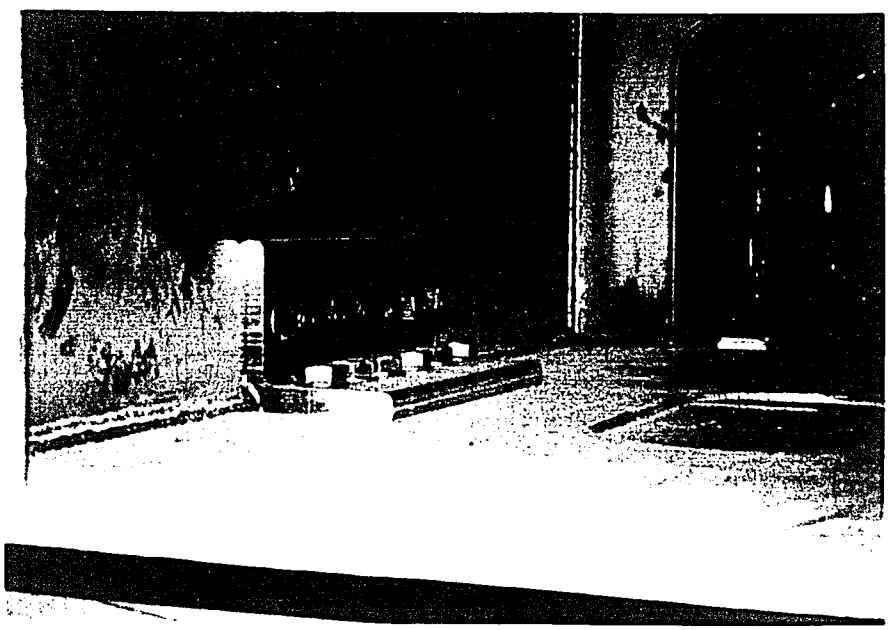

Figure 3.15 Rigid floor mount used for Axial and Bending test setups

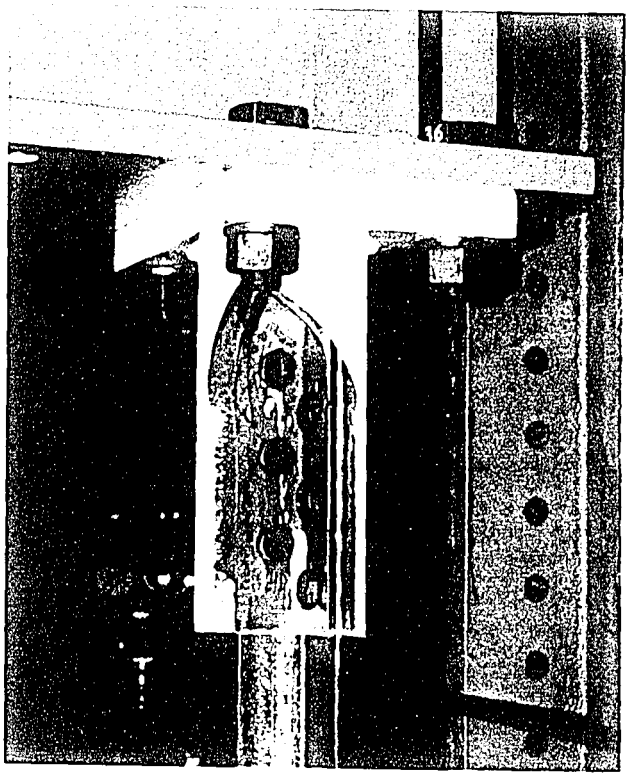

Figure 3.14 Clamp fixture used for Axial and Biaxial test setup

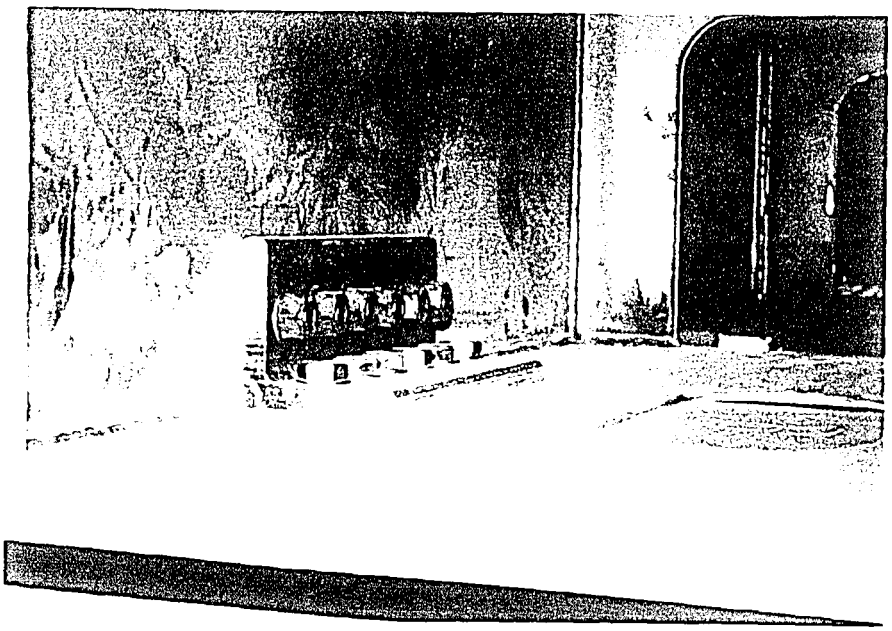

Figure 3.15 Rigid floor mount used for Axial and Bending test setups

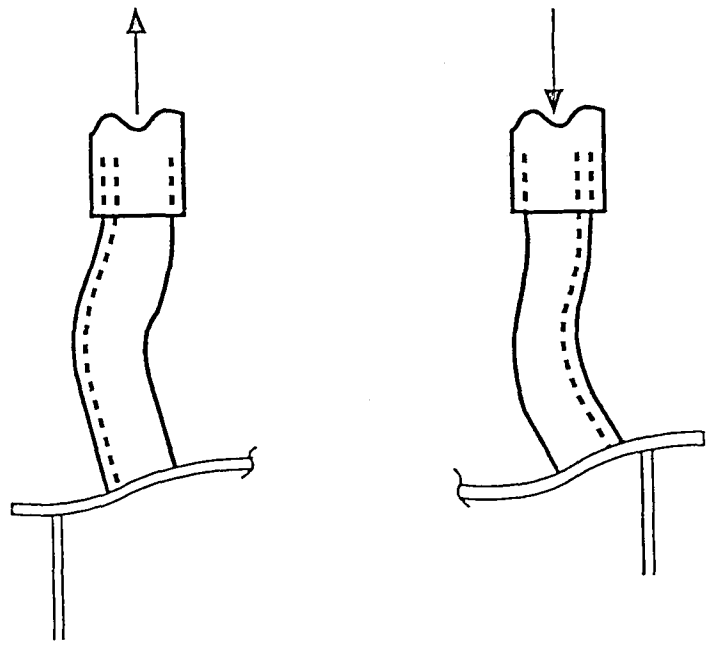

Figure 3.16 Bending induced in angle due to flexibility of plate and rigidity of clamp fixture

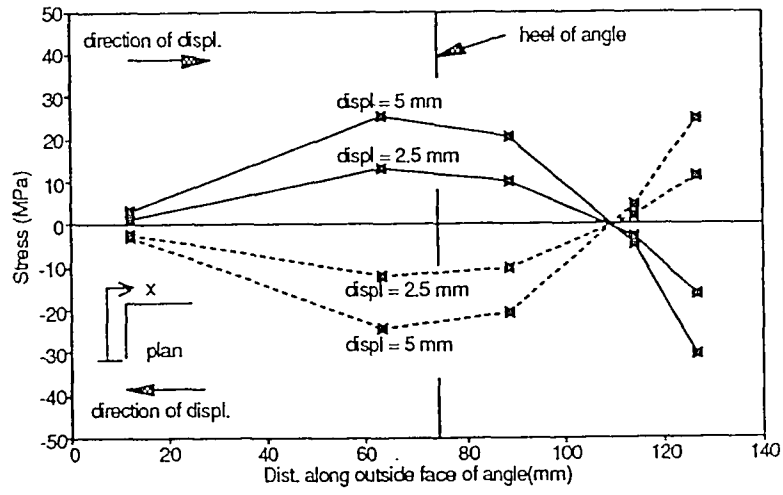

Figure 3.17 Stress gradient of angle leg due to applied lateral displacement as determined from gages on the outside surface of angle legs

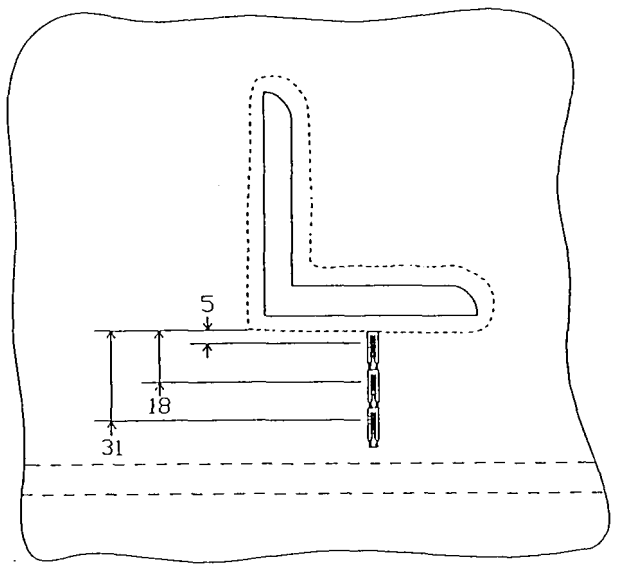

Figure 3.18 Typical hot-spot gage arrangement for determination of stress gradient leading to the weld toe

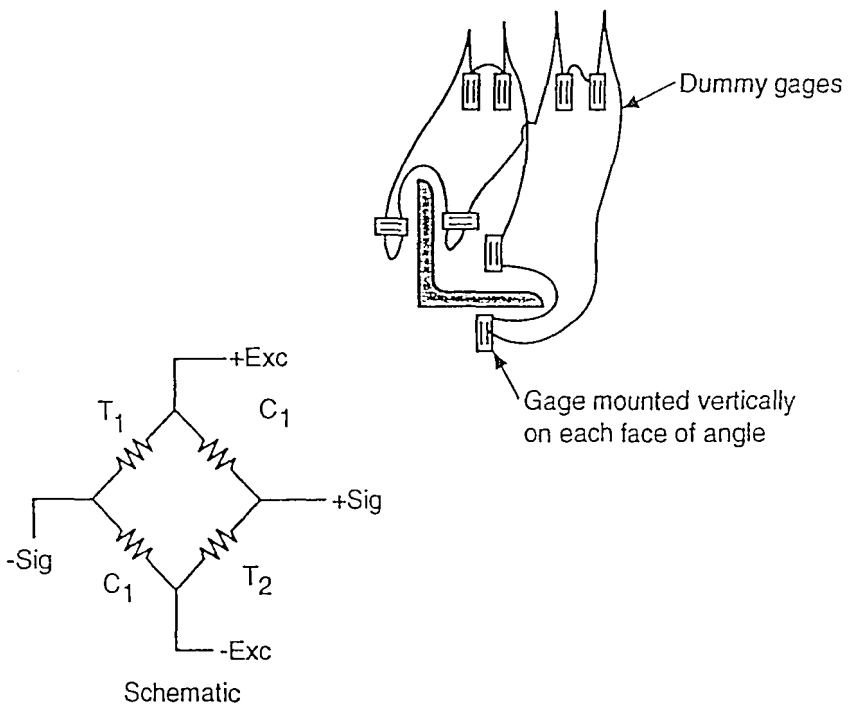

Figure 3.19 Full bridge arrangement of strain gages used to monitor nominal axial stress in angles for Axial and Biaxial tests

4.0 TEST RESULTS

Full-scale fatigue tests were performed on a variety of foundation attachment configurations loaded axially and in bending. The fatigue resistance of the details tested was characterized using the hot-spot concept as discussed in Section 2.1.4. In this study, the AASHTO Category C curve was chosen as the base-line S-N curve. This curve represents the fatigue strength of a groove weld when failure results from a crack at the weld toe. In other words, the Category C curve represents a weld with a "global" stress concentration factor (SCF) of one. The "local" SCF due to the weld toe and weld discontinuities is built into the C curve. The hot-spot method includes the "global" SCF in the analysis (i.e., the global SCF is on the applied loading side of the design equation). Therefore, the AASHTO Category C curve can be used with the hot-spot method as an appropriate baseline design curve for geometries with different global SCF's. In addition, the Category C curve is widely accepted in the U.S. (it is the same as the AISC or AWS Category C curve), it has a rationally determined and realistic slope and CAFL, and it is essentially the same as the U.K. Health and Safety Executive (H&SE) "T" curve (from the design guidance for offshore structures) which is widely used with the hot-spot approach.

In this study, a simple definition of the hot-spot stress was adopted and was found to adequately correlate the fatigue strength of the various details. The simple definition of hot-spot stress is the value of the stress as determined with a strain gage located nominally 5 mm from the weld toe. Actually, the 5 mm distance was not specifically

selected. Rather, this distance is just the closest that a 3 mm strain gage can be placed to the weld toe. This definition of hot-spot stress originated from early experimental work on pressure vessels and tubular joints and has persisted as the working definition of hot-spot stress in the U.S. offshore industry. This definition of hot-spot stress is consistent with the AWS welding code approach for tubular joints [6].

An alternative definition of the hot-spot stress was also considered. This definition was the linear extrapolation of stress in the plate, as shown in Figure 2.4. It was found that this definition of hot-spot stress gave a value up to 20 percent greater than the stress at 5 mm. As discussed in Section 2.1.2, there are varying definitions of this extrapolation. Only the definitions applicable to plate were used. Other definitions listed in Table 2.1 are dependent on the dimensions of tubular joints and are not applicable to the box section tested in this project. Since the extrapolated hot-spot stress was approximately proportional to the 5 mm stress and the 5 mm stress correlated well with the AASHTO Category C curve, the added complexity of the extrapolation technique was not considered warranted.

A typical S-N curve showing data from these experiments is shown in Figure 4.6. The following procedure was used to develop all S-N plots (unless otherwise noted). The mean of the "failure" data (the short dashed line shown in Figure 4.6.) was determined by linear regression analysis (excluding any runouts) using log(S) as the independent variable and log(N) as the dependent variable ("Failure" data are the S-N points where

N is the number of cycles to develop a through thickness crack.). In order to keep the curves parallel to the base line S-N curve, the slope of the regression curve was fixed at 3.0. The mean minus two standard deviations is the 97.5 percent survival limit referred to herein as the lower 95% confidence limit or lower bound and indicated with a long dashed line (See Figure 4.6). This simple confidence interval analysis assumes the data are normally distributed.

4.1 Axial Tests

4.1.1 Primary Configuration - 60 mm Eccentricity

In all details that were tested, cracking originated at the toe of the weld along the plate surface. As shown in Figure 4.1, cracking consistently occurred along the weld length parallel to the box web plate and at the toe of the fillet weld on the outside of the angle leg. In all cases, the crack first appeared in the vicinity of the angle heel. This is typically the location with the largest measured strain range. In some cases, cracks were detected elsewhere along the same length of weld after detection of a crack at the heel. These additional cracks soon coalesced with the initially detected crack. Cracking continued along the full length of the angle leg without a through-thickness crack developing. Only after the length of the surface crack extended beyond the ends of the angle section did a through crack develop. This extension of the crack along the surface is probably caused by the bending stress gradient through the thickness of the plate.

Figure 4.2 shows a typical crack surface at failure. The crack propagated in a curved

manner through the thickness of the plate eventually following a path that appears to be in a plane parallel to the plate surface. This path is most pronounced at the surface near the heel of the angle and is due to the change in the direction of primary stress. Initially the driving fatigue stress is due to bending of the plate. As the crack propagates, the driving stress is due more to the axial stress applied. This behavior is consistent with the large number of cycles between initial detection and through-thickness "failure". Obviously the curved path provides an increased length for fatigue propagation extending the time from initiation to failure. Also, as can be seen in Figure 4.2, the through-thickness crack required shear failure through the final 1-2 mm of plate thickness. As a result of this shear, failure was rarely recorded at a small through-thickness crack length. Despite frequent monitoring of tests, cracks on the underside of the plate appeared suddenly and at long lengths.

Of the twelve details tested, four were ground with a burr grinder. This was inadvertent and not intended to improve the fatigue resistance of the weld. In fact, it is important to note that the primary improvement was on the weld surface and not at the weld toe. Since all cracking occurred at the weld toe, it was not expected that the grinding would significantly affect results of the tests. It is unfortunate that these four details were tested at the same stress range (two in tension and two in reversal) so a direct comparison of fatigue life to an unground weld cannot be made. However, as discussed later, results agree favorably with other axially loaded details.

4.1.1.1 Determining the Hot-Spot Stress

As discussed in Section 3.3.4, strain gage measurements were used to determine the stress field in the vicinity of the weld. A series of strain gages were placed in a line approaching the weld toe at the centerline of the angle leg which was parallel to the web plate. These gages were used to measure the gradient in the strains approaching the weld and to determine the hot-spot stress. This line of gages was placed at the centerline of the weld length because measurements on the first few specimens indicated the stress at that point was at least as great as, if not greater than, the stress at the heel. Examples of such measurements are labelled 1A and 2A in Figure 4.3. As testing progressed, initiation of the crack was consistently observed to occur at the heel of the angle. This observation suggested that the heel of the angle was the hot-spot (i.e. the point of highest stress). Subsequent measurement of strain along the weld length supported this observation. Figure 4.3 shows a least squares fit of the data for all details that were gaged to measure the gradient along the toe of the weld indicating that the stress at the heel is about 25% greater than that at the centerline of the leg.

Results of measurements of the stress gradient leading to the weld toe for several loads are shown in Figure 4.4. The gradient is linear and passes through zero at a point about 25 mm from the weld. The linearity of this gradient indicates that the geometric stress concentration at the weld toe is due primarily to bending of the plate. The existence of a linear stress gradient facilitates determination of the hot-spot stress. As discussed in Section 2.1.2, the hot-spot stress is determined by a linear extrapolation of the stress from

two points near the weld. However, the points used to make the extrapolation are not well defined and are in a nonlinear gradient. Therefore, the result is sensitive to which points are used. However, if a linear gradient (such as shown in Figure 4.4) is used to determine the hot-spot stress, the result is not sensitive to which points are used. Using this linear extrapolation, it can be seen in Figure 4.4 that the stress extrapolated to the weld toe is consistently about 20 percent greater than the stress at 5 mm.

Using the measured and extrapolated hot-spot stresses from Figure 4.4, a plot of hot-spot stress versus nominal axial stress was developed as shown in Figure 4.5. This shows the linear increase in stress measured at 5 mm from the weld toe at the centerline of the weld length, the corresponding stress at 5 mm from the weld toe at the heel of the angle, and the extrapolated hot-spot stress at the heel as load is increased. The ratio of the stress at 5 mm from the weld toe at the angle heel to the nominal axial stress in the angle (i.e. the stress concentration factor or SCF) was 14.3. Since the extrapolated hot-spot stress is approximately 20 percent greater than the stress at 5 mm, the SCF in terms of the extrapolated stress would be about 20 percent greater.

4.1.1.2 Comparison to Design Curve

The results of the experiments on the Primary detail are shown in Table 4.1. The measured or estimated stress range at the angle heel is the appropriate corresponding hot-spot stress range. For information purposes, the measured hot-spot stress range at the centerline of the weld leg is shown along with the nominal axial stress range in the angle.

Figure 4.6 shows an S-N plot of all axial test data on the Primary detail in terms of the hot-spot stress at 5 mm from the weld toe. The mean and lower bound curve correspond to a regression analysis on the "failure" data. The lower bound curve is slightly greater than the Category C curve, indicating that the Category C curve and the 5 mm hot-spot stress would be an appropriate estimate of fatigue life for design purposes. The cycles to failure at first observation of the crack, referred to as "initiation", are also shown in Figure 4.6. With one exception, these initiation data also fall above the Category C line.

If a straight line extrapolation was used to establish a hot-spot stress range, the data would merely be shifted vertically because the stress range would be increased 20 percent. Since this shift would not improve the agreement with the Category C curve and the procedure to determine the extrapolated hot-spot stress is more complex, further comparisons of axial test data were made using the 5 mm hot-spot stress convention.

A comparison of tension only tests and reversal tests is made in Figure 4.7. Though statistically there are insufficient data, a regression was performed on the reversal data separately, and the resulting lower bound curve is shown in Figure 4.7. The apparent trend is that the life tends to be greater and there is less variability in the reversal data. However, since data are limited and actual in-service stress is ill defined, a conservative approach is to include both tension only and reversal data in the database. That is, all data should be considered and no allowance should be made for reversal loading.

Finally, the effect of the details with ground welds are examined for their impact on the results. Figure 4.8 shows an S-N plot with ground welds indicated separately from other data. The mean and lower bound curves correspond to the as-welded data. There are tension and reversal data considered together in each group. The ground details do not show any improvement in the fatigue life.

4.1.2 Alternate 1 - 85 mm Eccentric with Pad

In these experiments on details with pads beneath the angles, cracking originated at the weld joining the pad and the cell top plate. Cracking was always at the toe along the plate surface. As shown in Figure 4.9, cracking occurred along the nearest weld length parallel to the box web plate. Typically, the cracks appeared simultaneously in the vicinity of the angle heel as well as elsewhere along the weld length. These cracks eventually coalesced. Cracking continued along the full pad length without a through-thickness crack developing. Only after the crack had extended beyond the pad did a through thickness crack develop. Note that none of the welds on these details were ground.

Figure 4.10 shows a typical crack surface. As in the Primary detail crack surface, the crack propagated in a curved path that approaches a direction parallel with the plate surface. This can be seen at both ends of the crack surface near the corners of the pad. Again, the final failure was due to shear through the final 1 - 2 mm of plate thickness.

4.1.2.1 Determining the Hot-spot Stress

Measurements of strain perpendicular to the weld toe along the length of weld parallel to the web plate are shown in Figure 4.11. These measurements show that the stress is nearly uniform along this length. The first detection of cracking was often at the angle heel but in most cases cracks were detected at about the same time elsewhere along the same weld length. The assumption of a uniform stress along the weld is supported by observation of the crack surface as shown in 4.10. Note the symmetry of the crack surface as compared to the Primary configuration surface shown in Figure 4.2. This symmetry suggests a uniform stress field along the length of the pad. Therefore, the point chosen to define the hot-spot stress is arbitrary, and the measurement of the strain gradient approaching the weld toe taken at the centerline of the pad was valid.

Results of measurements of the stress gradient leading to the weld toe for several loads are shown in Figure 4.12. The gradient is linear and passes through zero at a point about 30 mm from the weld toe. Therefore, the stress concentration at the weld toe was primarily due to plate bending stress. Using the 5 mm hot-spot stress definition, an SCF of 13.2 applied to the nominal axial stress in the angle can be used to determine the stress at 5 mm from the toe of the weld. Again, a similar relation could be developed for the extrapolated stress but this would be merely proportional and offer no advantages.

4.1.2.2 Comparison to Design Curve

The results of these experiments are shown in Table 4.2. Figure 4.13 shows the data in

an S-N plot with the mean and lower bound to the through-thickness failure data with the Category C curve shown as well. The lower bound is significantly greater than the Category C curve in this case. Though the data are very limited, this suggests that the use of a pad may provide an improved fatigue life for the foundation detail. However, in view of the uncertainty, the relatively small apparent increase in fatigue strength, and the fact that the crack initiation data do not show any improvement relative to the data without pads, Category C is appropriate for design purposes. It should be recognized that although the pad does not have improved fatigue strength, the pad generally would reduce the stress by reducing eccentricity and stiffening the plate. For example, the SCF in terms of the ratio of the 5 mm hot-spot stress to the nominal stress was 14.3 for the Primary detail and was 13.2 for this detail despite the greater eccentricity. Thus, for a given load in the angle, the detail with the pad would have greater fatigue life because of the lower hot-spot stress.

Figure 4.13 also indicates tension and reversal load. There is a marked improvement in fatigue resistance of the reverse loaded details. However, as seen in Table 4.2 and Figure 4.13, initial detection of a crack occurred at about the same time. Initially detected lengths were between 15 and 24 mm. Therefore, there was no apparent effect on initiation but the crack propagation life was prolonged for the reversal tests.

4.1.3 Alternate 2 - 1 Plate Thickness Eccentricity

Cracks initiated at the fillet weld root in all the Alternate 2 details tested, as shown in

Figure 4.14. This is characteristic of load-carrying welded cruciform joints [40] which this detail approximates (see Figure 4.15). For cruciform joints, the fatigue life has been shown to increase with an increase in weld penetration [40]. The fatigue strength can be increased to an upper bound at which the mode of failure changes from a crack starting at the lack of penetration at the weld root to one initiating at the weld toe. Essentially, the lack of penetration at the weld root is an existing crack. Increasing weld penetration decreases this "initial crack size" improving the fatigue resistance.

The fatigue of a joint when failure occurs as a result cracking at the weld toe is equal to Category C. A reduction factor to be applied to Category C has been developed, based on fracture mechanics and the lack of penetration at the weld root as an initial crack size, to provide a simple means to determine the fatigue strength of a load-carrying cruciform joint [40].

$$S_R = S_{R,C} \frac{0.06 + \frac{0.79H}{t}}{(0.64\ t^{0.17})} \qquad (4.1)$$

Where:

S_R = stress range of cruciform joint (MPa)
$S_{R,C}$ = stress range of Category C (MPa)
H = length of fillet weld leg (mm)
t = thickness of loaded member (mm)

This reduction factor accounts for the pre-existing "crack" at the lack of penetration at the weld root. Since the stress range 5 mm from the weld toe approximates the stress range at the "crack", it follows that this definition of hot-spot stress may be applied to the reduced Category C curve to assess fatigue resistance. The following sections discuss

determining the hot-spot stress value and compare the failure data of these tests to a reduced C curve as determined using the reduction factor as defined by Equation 4.1.

4.1.3.1 Determining the Hot-spot Stress

Strain measurements were taken leading to the weld toe on the centerline of the outside face of the longitudinal angle leg. Measurements of strain in the web plate directly below the angle detail were also recorded. Figure 4.16 shows a typical gage arrangement. The resultant gradient on the face of the angle leg is shown in Figure 4.17. A least squares fit of the data was made. If the square of the correlation coefficient (R^2) was greater than 0.9 when a linear fit was attempted, then the gradient was considered linear. In this case, the R^2 was less than 0.9 and therefore a power law was fit to the data. The solid line shown is a least squares fit of the data.

With the small eccentricity, it would be expected that the weld between the box web and top plate would experience a high stress concentration also. The stress data for the web is plotted in Figure 4.17. This data indicates that the fillet weld joining the angle to the top plate is the higher stressed weld. Therefore, the SCF for this point was determined (SCF = 2.7).

An SCF for this condition of a small eccentricity or misalignment of a load carrying cruciform joint has been addressed in the ABS guide for Fatigue Assessment of Tankers [25]. The following equation is provided by ABS for determining such an SCF.

$$SCF = 1 + \frac{1.5e}{t} \qquad (4.2)$$

where t = the smaller thickness of the two opposing loaded members
e = eccentricity

Using Equation 4.3 for this configuration with the known eccentricity of 1 plate thickness (10 mm) an SCF of 2.5 was calculated. This agrees well with the measured SCF of 2.7 as determined by the ratio of the stress measured at 5 mm from the weld toe and the nominal axial stress in the angle. Therefore, Equation 4.2 provides a simple method for approximation of the hot-spot stress from a known nominal axial stress.

4.1.3.2 Comparison to Design Curve

As discussed previously, for this case of eccentricity of 10 mm, a reduction factor can be applied to the Category C curve to give a reduced fatigue design curve applicable to a load carrying cruciform joint. Examination of the tested joints after testing showed a weld penetration of about 10% of the angle leg thickness. Therefore, a reduction of the C curve was calculated using Equation 4.2 and 90% of the leg thickness (t) for the weld root opening. A plot of the failure data for the 10 mm eccentric detail with respect to this estimation of the reduced C curve is shown in Figure 4.18 (Failure in this case is defined as a crack that extends at least 75% of the weld length). This S-N plot shows that the lower bound of the failure data plots near the reduced curve when the 5 mm hot-spot stress range is used. Also note that in the data presented there is a very short life from initial detection to failure. This short life is due to the fact that the majority of the growth life is spent propagating the crack from the weld root to the surface of the weld

(i.e., the crack is not visible for most of its life). Therefore, the initial detection data all plots above the reduced C curve. Thus, assuming 10% weld penetration at the root of the weld to determine a reduction factor for the AASHTO Category C and plotting failure or initial detection data using the hot-spot stress range is valid.

All four details were ground. Unfortunately grinding was considerably more extensive than other details that were ground. The extent of grinding is apparent in Figure 4.15. However, the most critical load condition in most load-carrying welds will be fatigue crack growth from the weld root [40]. Therefore, these details would be expected to fail at the weld root not the toe. Grinding would provide no improvement. Figure 4.18 supports this assumption.

4.1.4 Alternate 3 - Center Panel

The Alternate 3 configuration had a single angle in the center of the panel between the webs as shown in Figure 3.8. The weld was not ground on any of these Alternate 3 details. In all of these fatigue tests on the Alternate 3 details, cracking was first detected at the toe of the weld at the toe of the transverse leg of the angle, as shown in Figure 4.19 and 4.20. This was also the point of highest stress as determined by strain gages placed near the toe of the weld.

The propagation behavior of the cracks (subsequent to the initial detection) was significantly different between tests where the loading was tension only and tests where

the load was reversed. For both types of loading, the crack continued around the radius of the wrap around portion of the fillet weld to about the tangent with the straight part of the weld. In the tension only tests, the crack then progressed into the surrounding plate as shown in Figure 4.19. The crack continued growing without a through thickness crack developing. Finally at a surface length of about 175 mm the crack penetrated through the plate. Figure 4.20 shows the crack surface just after such penetration. The crack curved toward a path that was parallel to the surface of the plate and eventually sheared through the remaining 1 - 2 mm of plate thickness. This behavior of the crack is similar to that exhibited by the Primary and Alternate 1 configurations.

In the loading reversal tests, the crack at first propagated in a similar fashion to the tension only tests, i.e. the crack initiated at the toe of the transverse leg and grew to about the tangent of the weld wrap around radius and straight section of weld. However, at this point the crack growth arrested in the load reversal tests. The total crack surface length at 5 million cycles was between 40 and 50 mm. Due to schedule constraints, one of the two reversal tests was stopped at this point. The second and last test continued to run to 10 million cycles with no further crack growth. The test was ended at this point.

4.1.4.1 Determining the Hot-Spot Stress

The hull plate is thin and flexible and therefore it is not expected to exhibit bending behavior when the detail is located so far (475 mm) from the web. Rather, the plate is expected to behave more like a membrane with local bending in the vicinity of the detail.

Therefore, the stress gradient approaching the detail was expected to be nonlinear. Figure 4.21 shows the measured stress gradient at the toe of the transverse leg of the angle in three specimens. An SCF of 23 was calculated in terms of the 5 mm hot-spot stress divided by the nominal axial stress in the angle. This very large SCF was expected given the flexibility of the plate and the abrupt change in stiffness at the location of the angle.

In both of the tension only tests, secondary cracks developed at the longitudinal leg toe and at the heel of the angle after the initial detection of the crack at the transverse leg toe. The locations and sequence of cracking were consistent with strain measurements. The strain measurements showed the strain range at the transverse leg toe was the greatest, followed by slightly lower strain ranges at the longitudinal leg toe and the heel. Though the secondary cracks grew throughout testing, they did not develop as through thickness cracks. No secondary cracking developed in the reversal tests.

4.1.4.2 Comparison to Design Curve

The results of the experiments on the Alternate 3 details are shown in Table 4.2 along with the nominal stress range and the 5 mm hot-spot stress range. The 5 mm hot-spot stress range is plotted with the number of cycles to initiation and final runout or through-thickness failure in Figure 4.22. The runouts and failure points fall well above the Category C S-N curve. Therefore, it was not considered necessary to examine the extrapolation of stress in the nonlinear gradient since the extrapolated stress range would be even greater. Although it might appear that the Category C curve is too conservative,

there are too few data to reach this conclusion. Also, the initiation points fall below the Category C curve in some cases, which did not occur for the other details. The arresting of the crack is a very interesting phenomena and should be investigated further in some future research. It may be possible to design details to exhibit this desirable fail-safe behavior so that there is adequate time to discover a crack prior to failure.

4.1.5 Comparison of Primary and Alternate Details

An S-N plot of the through-thickness failure data for the Primary detail as well as Alternates 1 and 3 is shown in Figure 4.23. Alternate 2 is excluded, since the failure mode was cracking through the weld root due to partial penetration and the fatigue resistance curve for this behavior is reduced relative to Category C. The apparent trend in the data is that the Primary configuration gives the lowest fatigue strength in terms of the 5 mm hot-spot stress. The mean and lower 95 percent confidence limit shown are from linear regression analysis of the data from all three details. Note that the lower bound is just slightly above the Category C line, indicating that the data as a group give about the same lower bound obtained from the regression on the Primary configuration data only (Figure 4.6). When the alternate details are considered separately, the lower bounds appear slightly greater (Figures 4.13 and 4.22), but there are too few data for these alternates. In analysis of fatigue data, the lower bound typically decreases as additional data are included in the database. This decrease is due to the statistical nature of the discontinuities, poor weld shape, stop/starts, and other attributes that influence fatigue resistance.

In Figure 4.24, the data are separated according to the load ratio, i.e. tension only and reversal loading. The regression lines shown are for the reversal data only. The lower bound for the reversal loading appears to be greater than the lower bound for all data shown in Figure 4.23. However, the reversal data falls within the scatter band of the tension only data (except for the runouts of Alternate 3) and it is possible that additional tests would decrease the lower bound for the reversal data. The analysis of a large number of fatigue tests recently completed at Lehigh [21] showed that the distribution of load reversal data was different and the mean life for load reversal was typically greater than for tension only. However, it was also found that the variability was greater for reversal loading, and consequently the lower bound was essentially the same as for the tension only data. There are not enough data in the present study to assess the variability of the reversal loading, so it is safe and simpler for the purposes of design to ignore the apparent benefit of reversal loading. Therefore, given the uncertainty in actual loads it would be considered appropriate to use the Category C curve for design. If loads are well defined an allowance for reversal loading may be considered.

The baseline fatigue strength of these details is the same in terms of the 5 mm hot-spot stress (except Alternate 2 which is reduced for partial penetration effect). However, it must be remembered that certain details have a profoundly different SCF and therefore much different fatigue strength in terms of the load or the nominal axial stress. Table 4.6 presents each of the four types of axial details tested and their associated SCF in terms of the 5 mm hot-spot stress. From this table, it is easily seen that Alternate 2 has the

greatest fatigue strength in terms of nominal stress range. The better fatigue strength of this detail was expected given the smaller eccentricity from the web. More notable is the difference between the Primary detail (60 mm eccentricity) and Alternate 1 (85 mm angle eccentricity). Alternate 1 has a lower SCF than the Primary configuration, despite the increased eccentricity. The decrease is apparently due to the pad which more evenly distributes the load from the angle reducing the stress near the heel of the angle. This clearly indicates that the fatigue strength is substantially improved by the pad. The economics of installing the pad should be investigated to see if the increase in fatigue strength justifies the cost increase.

4.2 Bending Tests

Six tests, with two Primary details each, were performed in bending in a transverse direction. As discussed in Section 3.2.2, static strain measurements along the outside surface of both legs of the angle showed that the load was carried by the transverse leg (see Figure 3.17). The two ends of this transverse leg were the locations of the highest hot-spot stress, i.e. at the angle heel and toe of this transverse leg. The magnitude of the 5 mm hot-spot stress was approximately equal at these two locations.

The strain measurements were consistent with the cracking in these tests, which occurred at both of the critical locations. Figure 4.25 shows a photograph of a detail which had cracks at both locations. As in the axial tests of the Primary configuration, cracking occurred along the weld length parallel to the box web plate at the toe of the fillet weld

near the angle heel. In some cases cracks formed elsewhere along the length of weld at approximately the same time as that of the heel and eventually coalesced. As was the case for the Primary axial details, these cracks propagated the full length of the angle leg and into the adjacent base plate before a through thickness crack developed (see Figure 4.26). Figure 4.27 shows a typical crack surface at failure. Though not as pronounced as in the axial tests, the crack front at the heel of the angle again followed a curved path into the plane of the base plate. However, away from the heel the crack propagated in a more direct path through the plate. Also, as in the axial tests, the through-thickness crack required shear failure through the final 1 - 2 mm of plate thickness.

In addition, cracking also occurred at the toe of the angle transverse to the box web plate. Cracking that initiated at the toe of the transverse leg quickly propagated into the base plate. In general the crack would first be detected at the top of the arc of the weld wrap around. This crack would propagate along the weld toe to approximately the end of the radius of the wrap around. The crack would then progress into the base plate. Occasionally small branches or secondary cracks were also observed near this primary crack as shown in Figure 4.28. Figure 4.29 shows that these cracks also curved toward a plane parallel to the plate surface and suddenly became through thickness cracks by shear failure of the remaining 1 - 2 mm of plate thickness.

Of the twelve details tested, four were ground with a burr grinder. This was inadvertent and not intended to improve the fatigue resistance of the weld. The toe of the weld was

not significantly improved. The face of the weld received most of the grinding. Therefore, given the nature of the grinding, it was expected that grinding would have an negligible impact on results.

4.2.1 Determining the Hot-Spot Stress

As discussed in Section 3.2.2, the bend tests were performed in displacement control. The transverse displacements were applied to the angles 840 mm above the hull plate through a pinned connection. Loads were determined from finite-element analysis that was calibrated to give good agreement with the measured strains and displacements. This analysis is described in the main body of the report in Section 4.4.

Figure 4.30 shows the hot-spot stress 5 mm from the weld toe along the longitudinal leg in three details. This plot shows that the stress on this leg is greatest near the heel of the angle. Measurements of the stress gradient perpendicular to the weld toe were made at the toe of the transverse leg and at the centerline of the longitudinal leg. In retrospect, it would have been better to have measured the gradients at the angle heel. However the stress at the angle heel is generally 1.25 times greater than the stress at the centerline as shown in Figure 4.30.

The measurements of the stress gradient at the centerline of the longitudinal leg at several displacements are show in Figure 4.31. As in the axial tests, the stress gradient is linear indicating the plate is primarily in bending between the angle and the web.

Results of measurements of the stress gradient at the toe of the transverse leg at 5 mm displacement is shown in Figure 4.33. In this case, the gradient was considered nonlinear (i.e., $R^2 < 0.9$) and therefore a power law was fit to the data. Based on this gradient, extrapolation of the stress to the weld toe can be done. However, as discussed previously and in the next section, good results were obtained using the 5 mm hot-spot stress so this extrapolation was unnecessary.

Figure 4.32 shows the nominal extreme fiber bending stress and the hot-spot stress at 5 mm at both the angle heel and the toe of the transverse leg as a function of displacement imposed at the top of the angle. The SCF in terms of the 5 mm hot spot stress is 2.2.

4.2.2 Comparison to Design Curves

The results of these experiments are summarized in Table 4.3. The hot-spot stress range at 5 mm from the weld toe is shown for both the angle heel as well as the toe of the transverse leg. The nominal extreme fiber bending stress at the plane of the weld is also given and the location of the dominant fatigue crack is noted. There does not appear to be any difference in the cycles to failure with respect to location of this crack.

Figure 4.34 shows the points for initial detection as well as through-thickness failure for details which failed at both the angle heel and the toe of the transverse leg. Note that the variability is relatively small for the failure points. The initial detection points for this detail are well below the Category C line which is very different than the axially-loaded

tests. However, the lower bound of the failure points is well above the Category C curve. Use of an extrapolation to define the hot-spot would only move the lower bound farther from the design curve.

Figure 4.35 shows the failure points separated according to load ratio, i.e. tests in which the loading was in one direction only and tests in which the loading was fully-reversed. The mean and lower bound shown are from a regression analysis of the reversal loading only. The reversal data appear to give a greater fatigue strength but are contained within the scatterband of the one-sided loading. In the one-sided loading tests, cracks were detected at either end of the transverse leg without any regard for which end was in tension. However, cracks located at the tension end consistently propagated to failure before those at the compression end.

Finally, the effect of details with ground welds was examined for the impact on the results. Figure 4.36 shows an S-N plot with ground welds indicated separately from the unground welds. The ground welds appear to give slightly greater fatigue strength. However, the ground welds were all tested in load reversal, where most of the unground welds were tested in one-sided loading. Therefore, these two effects were confounded and it is difficult to draw any conclusions.

4.3 Biaxial Tests

In the biaxial tests, cracking generally occurred along the weld length parallel to the box

web plate on the outside of the angle leg. In all cases, the crack first appeared in the vicinity of the angle heel. This is typically the location with the largest measured strain range. In some cases, cracks were detected elsewhere along the same length of weld after detection of a crack at the heel. These additional cracks coalesced with the initially detected crack. Cracking continued along the full length of the angle leg without a through-thickness crack forming.

Up to this point the cracks behaved in a manner that was similar to the axial tests of this same configuration. In about 75% of the biaxial-test details, the crack continued in a longitudinal direction into the base plate, as had occurred in the axial tests (Figure 4.37). A through crack developed shortly after this extension beyond the angle. In the remainder of the biaxial-test details, the crack turned 90 degrees at the angle heel and continued to follow the weld toe as seen in Figure 4.38. This phenomena is obviously due to the influence of the in-plane stress. An extreme example of this transverse path is shown in Figure 4.39. This crack had propagated the length of the weld and continued unchecked through one half the top plate and nearest web.

Figure 4.40 shows a typical crack surface of a failure that followed the weld toe transverse to the cell. Note the curved surface of the crack face and the shear failure through the final 1- 2 mm which is characteristic of all the experiments (except the Alternate 2 which was very close to the web). However, the crack surface along the transverse direction does not have this curved surface or shear failure. This face

experienced fatigue through the depth of the plate in a vertical path. Based on this observation it can be concluded that the transverse cracking is primarily due to the uniform in-plane membrane stress. If the axial stress in the angle was the primary factor, the crack surface would be expected to curve with the change in Primary stress as the detail cracked.

Of the 24 details tested, four were ground with a burr grinder (the details of specimen 3). This was inadvertent and not intended to improve the fatigue resistance of the weld. In fact, it is important to note that the primary improvement was on the weld surface and not at the weld toe. Since all cracking occurred at the weld toe, it was not expected that the grinding would significantly affect results of the tests.

4.3.1 Determining the Hot-spot Stress

The strain measurements used for determination of the hot-spot of the axial tests were also used for the biaxial tests. Therefore, measurement of the strain gradient leading to the weld toe was also taken at the centerline of the longitudinal leg of the angle. It was found that the hot-spot stress at the angle heel was approximately 25 percent greater than at the centerline.

Static tests were done applying axial stress in the angle and the stress in the plane of the hull plate separately as well as simultaneously. The axial stress had to be in compression when there was no in-plane stress because of the test setup. Since the static tests of the

Primary configuration indicated that axial tension and compression yielded stresses of equal magnitude but opposite sign, resultant stresses due to tension in the biaxial tests was assumed to be the absolute value of those due to compression. Figure 4.41 shows the gradients at the centerline of the weld length for three different details. Note that a small compressive transverse hot-spot stress was induced by the tensile in-plane longitudinal stress. Figure 4.42 shows the strain gradients when both loads are applied simultaneously. This verifies that the magnitude of the stresses could have been predicted by superposition of the stresses from the individual load components. A least squares fit of the points indicates a linear gradient.

Measurements of the stress gradient leading to the centerline of the weld length for several proportional loads are shown in Figure 4.43. The gradient is linear and passes through zero at a point about 25 mm from the weld as in the axial tests on these details. Examining these gradients for stress due to nominal axial stress and in-plane stress separately, SCF's for each nominal stress were determined. Obviously the axial SCF = 14.3 as was determined in the axial tests (Section 4.1). An SCF = -0.48 is applicable to an in-plane stress. Since the two types of loading can be superposed, any combination of in-plane and axial stress can be used to determine a worst case (in phase) hot-spot stress.

4.3.2 Comparison to Design Curves

The results of these biaxial experiments are given in Table 4.5 along with the nominal

axial and in-plane stress range as well as the hot-spot stress at 5 mm from the weld toe in a transverse direction at the weld heel. Figure 4.44 is an S-N plot of the all biaxial data using the 5 mm hot-spot stress. The lower bound from the regression on the through-thickness failure data is in good agreement with the Category C design resistance curve. The initiation data are only slightly below the Category C line.

A comparison of tests with an in-plane stress range ($S_{r,ip}$) of 55 MPa and those with a $S_{r,ip}$ of 110 MPa is made in Figure 4.45. This indicates that a higher $S_{r,ip}$ reduces the fatigue resistance of the foundation detail. However, note that the lower bound of the higher $S_{r,ip}$ data is still applicable to the C curve. Although for low in-plane stress range (i.e. 55 MPa or less) the C curve is slightly conservative, given the knowledge of actual in-plane stresses it is considered appropriate to use the AASHTO Category C curve.

Figure 4.46 examines the impact on the results of the details with ground welds. This figure shows an S-N plot with ground welds indicated separately from other data. The ground welds were all tested at the lower value of in-plane stress, so the comparison is inconclusive.

4.4 Summary and Comparison of Test Results

Table 4.6 presents a summary of the linear regression parameters for the different loadings of the Primary detail. This includes regression of positive and negative load ratio tests. The alternate configurations are not listed separately since there are too few

data points to give meaningful regression parameters. However, the Alternates 1 and 3 are included in a regression analysis of all tests of this study assuming they are of the same population as the Primary details. Alternate 2 data is not included since the mode of failure is different and a reduced S-N curve applies.

Figure 4.47 shows an S-N plot of the data for the Primary configuration and Alternate configurations 1 and 3. The lower bound plots directly on the Category C curve if a slope of -3 is imposed on the regression analysis. Though there is a wide range of scatter, especially in the axial data, the individual means of each set of data fall near the mean of all data combined. Therefore, the results of the tests are assumed to be of the same population.

Since the results of the data are in terms of a hot-spot stress range as defined at 5 mm from the weld toe which is consistent with the applications to tubular joints based on AWS D1.1 Chapter 10, the AWS category X2 line is also shown. The X2 line is applicable to tubular T, Y and K joints that have not been improved. Although this curve converges with the Category C curve near the CAFL, it is far too conservative in comparison to these data.

Table 4.1 Primary Configuration - Hot Spot Stress Due to Axial Load

Spec. No. and load direction	Angle No.	Measured Nominal Axial Stress Range (MPa)	Hot-spot Stress Range at 5 mm from Weld Toe		Cycles to Initial Detection (x 10^3)	Cycles to Failure (x 10^3)
			Weld Centerline[1] (MPa)	Angle Heel[2] (MPa)		
1A tension	1	13	117	117[3]	1330	2128
	2	13	117	146	1330	2500
2A tension	1	16	219	252[3]	43	188
	2	16	226	283	118	165
3A reversal	1	12	110	138	786	4540
	2	12	123	154	786	7300
4A tension	1	14	165	206	884	4200
	2	14	165	206	656	3540
5A reversal	1	14	172	215	519	2000
	2	14	144	164[3]	417	1365
6A reversal	1	16	239	299	202	428
	2	17	192	240	202	700

Notes:

1. Measured stress range was determined by a strain gage nominally 5mm from the weld toe at the centerline of the leg parallel to the web plate.
2. Estimated hot-spot stress range at the angle heel, 5 mm from the weld toe. (1.25 times the hot-spot stress range at the centerline of the angle leg.)
3. Measured hot-spot stress range at the angle heel, 5 mm from the weld toe.

Table 4.2 Axial Alternates 1 thru 3 - Hot Spot Stress

Speci. No. and load direction	Angle No.	Measured Nominal Axial Stress Range (MPa)	Measured Hot-Spot Stress Range[1] (MPa)	Cycles to Initial Detection (x 10^3)	Cycles to Failure (x 10^3)
1A1 tension	1	11	133	584	2700
	2	12	169	494	2023
2A1 reversal	1	13	165	604	4016
	2	13	162	604	6000
1A2 tension	1	31	76	747	854
	2	35	92	568	671
2A2 reversal	1	61	168	71	76
	2	61	149	47	47
1A3 tension	1	7	187	178	3814
2A3 reversal	1	8	165	243	RUNOUT
3A3 tension	1	6	165	304	RUNOUT
4A3 reversal	1	6	159	169	4132

Notes:

1. Measured stress range was determined by a strain gage nominally 5 mm form the weld toe. Position in reference to the angle differed for each alternate.

2. Alternate 1 - the gage was located on the plate at the centerline of the leg parallel to the web plate.
   Alternate 2 - the gage was located on the leg of the angle parallel to the web plate.
   Alternate 3 - the gage was located on the plate at the toe of the transverse angle leg.

Table 4.3 Primary Configuration Hot-spot Stress Due to Bending

Spec No. and load direction	Angle No.	Nominal Stress Range (MPa)	Hot spot range at 5 mm from weld toe		Cycles to Initial Detection (x 10^3)	Cycles to Failure[4] (x 10^3)	Point of Failure
			Angle Heel (MPa)	Angle Toe (MPa)			
1B one direction	1	28	117	117	108	RUNOUT	HEEL
	2	28	117	117	112	RUNOUT	TOE
2B reversal	1	62	278	230	92	630	HEEL
	2	69	289	193	92	780	HEEL
3B reversal	1	45	155	165	52	2760	TOE
	2	41	155	145	259	3400	HEEL
4B one direction	1	29	143	114	2310	RUNOUT	HEEL
	2	30	140	103	759	RUNOUT	TOE
5B one direction	1	66	250	221	152	534	HEEL
	2	68	241	221	152	534	TOE
6B reversal	1	43	155	172	463	1730	HEEL
	2	46	160	159	463	2464	TOE

Table 4.4 Primary Detail - Hot Spot Stress Due to Biaxial Load

Spec No and load direction	Nominal In-plane Stress Range (MPa)	Angle No.	Measured Nominal Axial Stress Range (MPa)	Hot-spot Stress Range at 5 mm from the weld toe at Angle Heel (MPa)	Cycles to Initial Detection (x 10^3)	Cycles to Failure (x 10^3)
1 tension	110	1	28	414	10	32
		2	28	414	13	35
		3	28	414	10	32
		4	28	414	16	40
2 tension	110	1	11	146	391	1673
		2	10	138	485	3100
		3	11	164	391	797
		4	10	138	485	10000
3 tension	55	1	14	190	465	990
		2	15	206	575	785
		3	15	215	465	1166
		4	15	199	NO CRACK	NO CRACK
4 tension	55	1	8	163	NO CRACK	NO CRACK
		2	13	223	229	422
		3	11	228	229	450
		4	12	210	317	550
5 tension	110	1	16	275	100	109
		2	15	224	100	230
		3	19	250	100	214
		4	20	266	100	262
6 tension	55	1	17	251	57	270
		2	14	269	57	270
		3	17	252	108	367
		4	13	215	108	931

Table 4.5 Linear Regression Parameters and Standard Deviations

Fatigue Details	No. of Data	Natural or Real Slope			Fixed Slope = -3	
		Slope	Intercept	Standard Deviation	Intercept	Standard Deviation
AXIAL						
Primary Tension Load	6	-2.873	12.631	0.491	12.922	0.492
Primary Reversal Load	6	-3.185	13.528	0.228	13.104	0.230
All Primary Configuration Data	12	-3.003	13.020	0.378	13.013	0.378
BENDING						
Tension Load	4	-2.783	12.442	0.129	12.932	0.132
Reversal Load	4	-2.526	11.668	0.198	12.726	0.205
All Bending Data	8	-2.577	11.879	0.188	12.829	0.194
BIAXIAL						
$S_{r,ip}$ = 55 MPa	10	-4.305	15.860	0.122	12.792	0.136
$S_{r,ip}$ = 110 MPa	11	-3.722	14.386	0.118	12.518	0.186
All Biaxial Data	21	-3.998	15.031	0.161	12.649	0.213
All Primary configuration data	41	-3.818	14.695	0.284	12.790	0.307
All configurations	51	-3.829	14.740	0.296	12.822	0.320

Table 4.6 Stress Concentration Factors Relating Nominal Stress to Hot-Spot Stress

Detail	SCF
Axial	
Primary	14.3
Alternate 1	13.2
Alternate 2	2.7
Alternate 3	23.0
Bending	2.2
Biaxial	
Axial Stress	14.3
In-plane Stress	-0.48

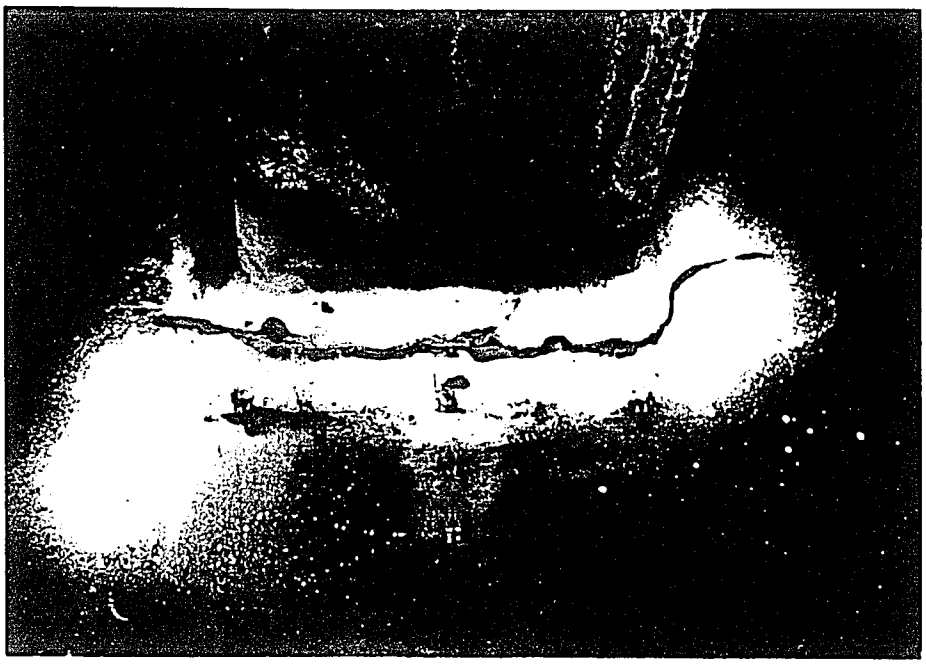

Figure 4.1 Typical crack due to axial loading of Primary configuration

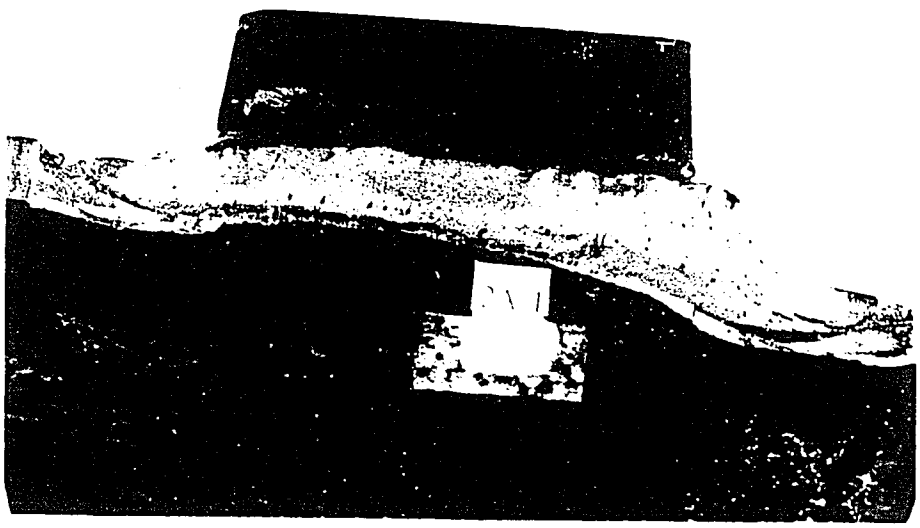

Figure 4.2 Typical crack surface of Primary configuration subject to axial loading.

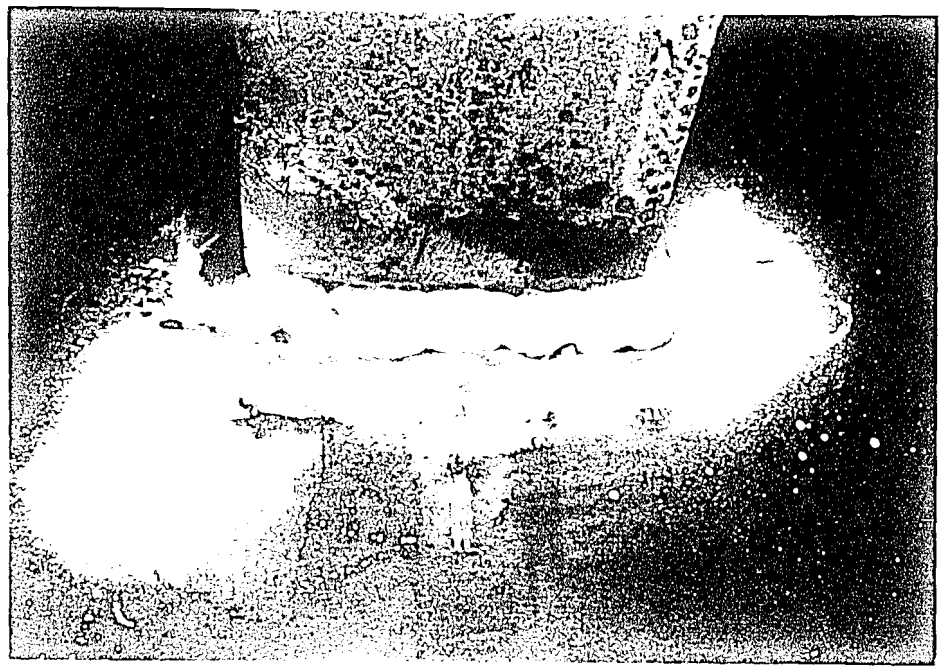

Figure 4.1 Typical crack due to axial loading of Primary configuration

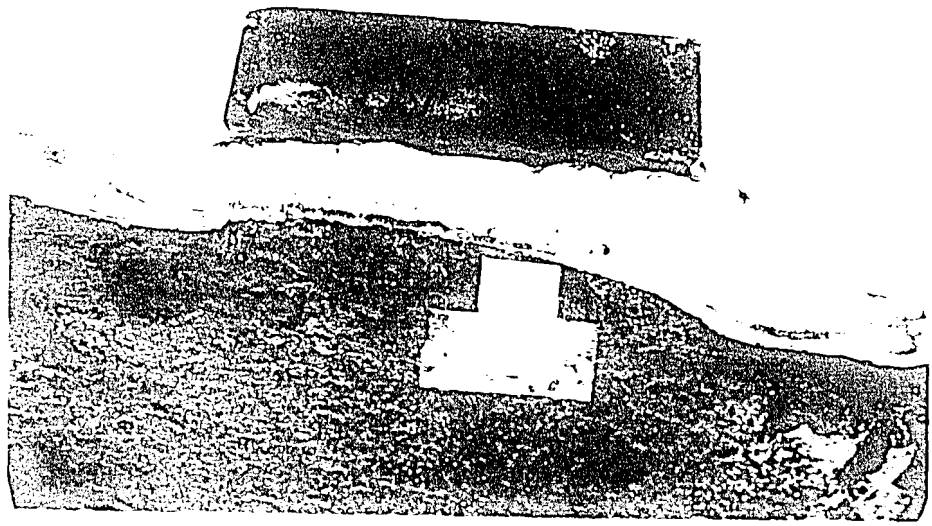

Figure 4.2 Typical crack surface of Primary configuration subject to axial loading.

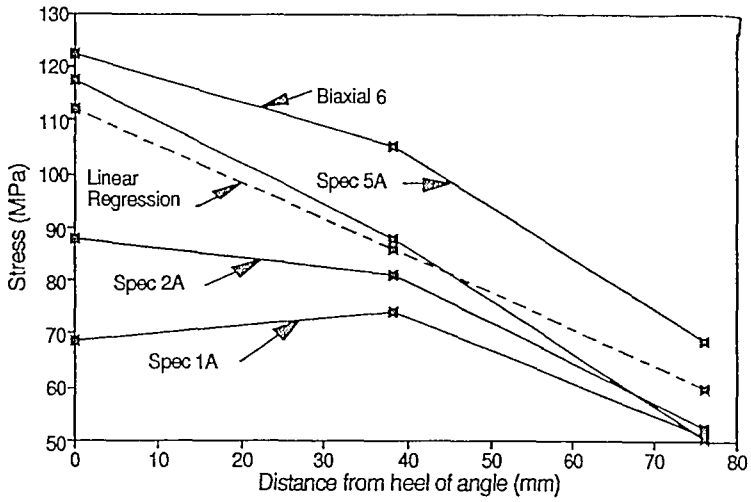

Figure 4.3 Stress gradient along angle leg parallel to web plate due to axial load of Primary detail. This indicates that the stress at the heel is on average 1.25 times that at the centerline of the leg.

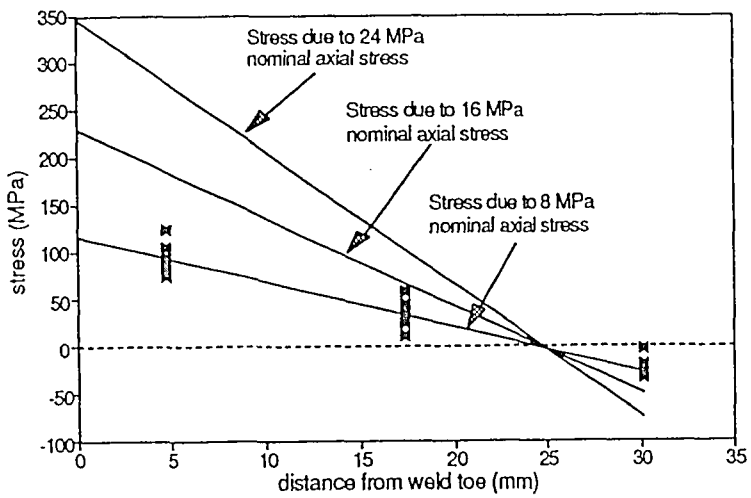

Figure 4.4 Stress gradient perpendicular to the weld toe at the centerline of the angle leg parallel to the web plate due to axial load of primary detail. Solid lines are results of a linear regression of data of several details. Actual data points are shown for several specimens subject to an 8 MPa nominal stress to indicate degree of scatter.

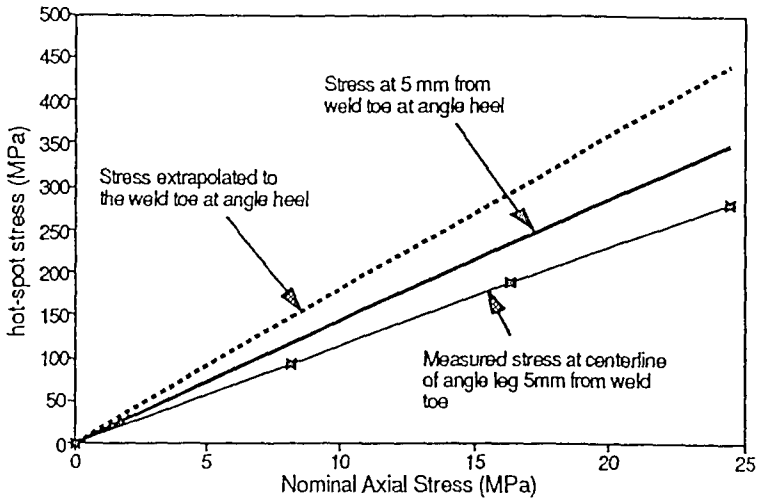

Figure 4.5 The 5mm hot-spot stress at the angle heel as a function of nominal axial stress of the Primary configuration

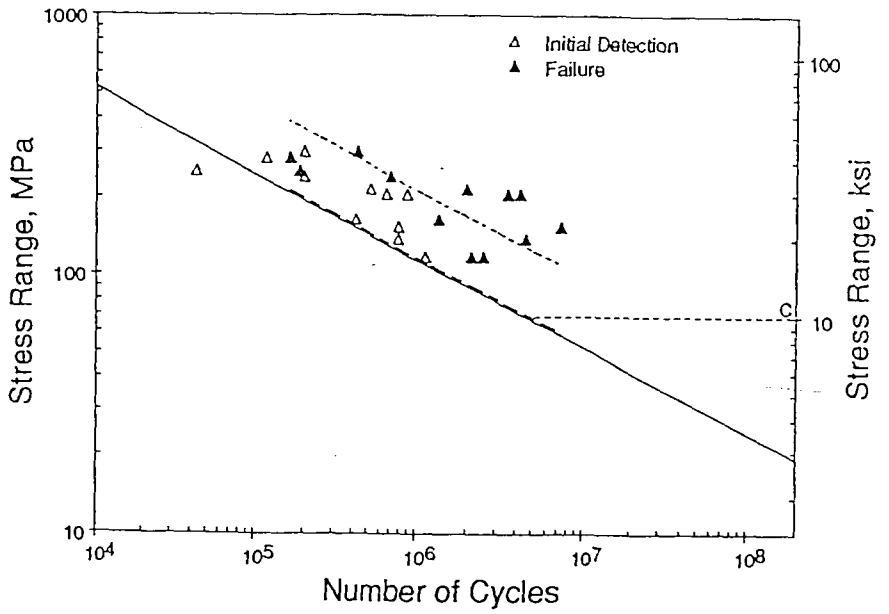

Figure 4.6 Primary configuration axial test data plotted with respect to the AASHTO C curve. The hot-spot stress range is that as determined at 5 mm from the weld toe at the heel of the angle. Regression is of failure data.

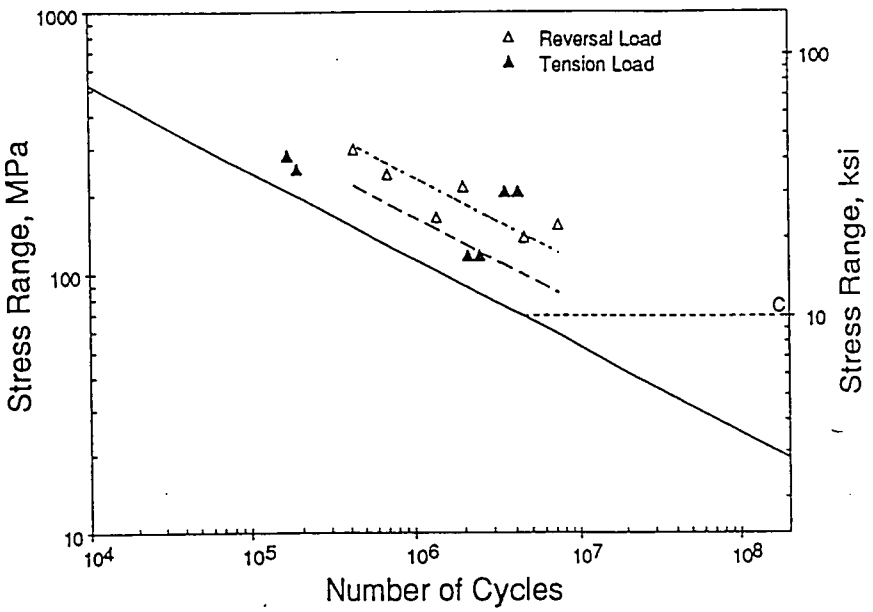

Figure 4.7 Comparison of reverse loaded, primary detail, axial failure data to the AASHTO C curve. Tension loaded data is also shown

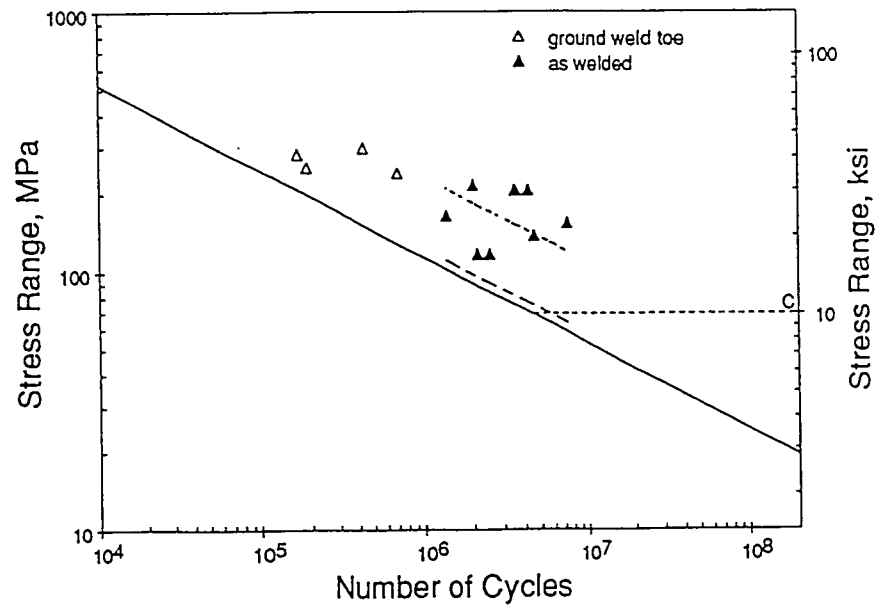

Figure 4.8 S-N plot of Primary configuration axial failure data showing comparison of ground and as-welded details in relation to the C curve.

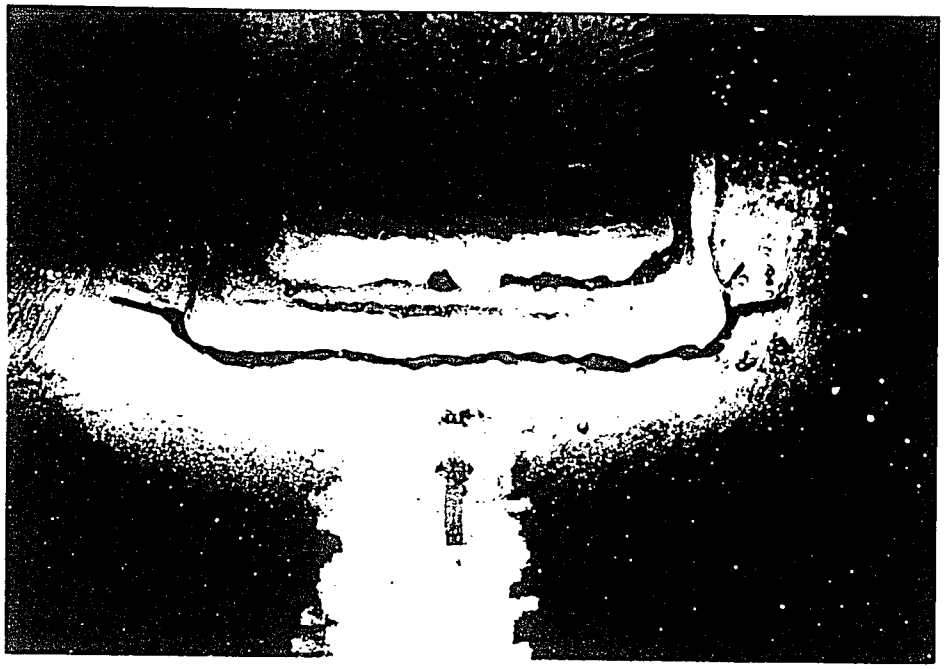

Figure 4.9 Typical crack due to axial load of Alternate 1 configuration

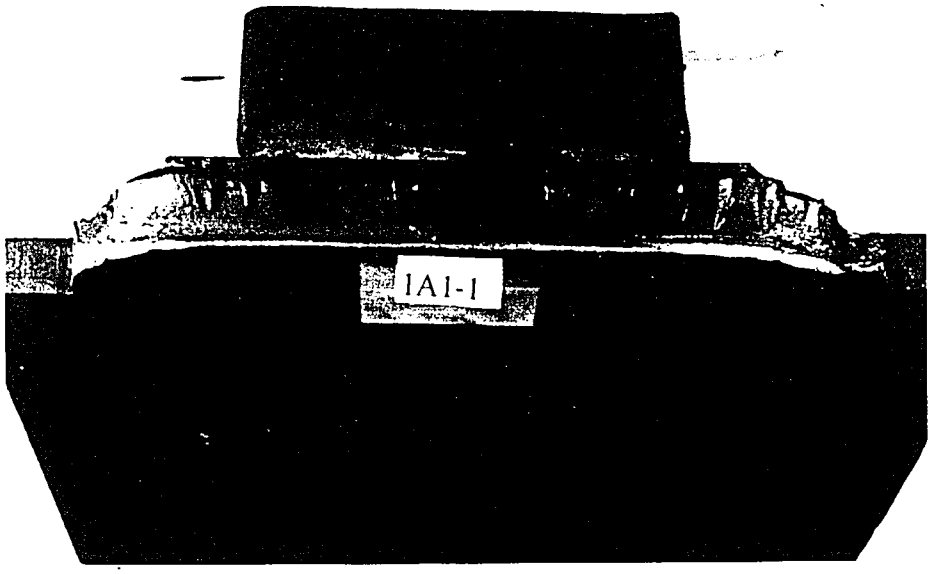

Figure 4.10 Typical crack surface of Alternate 1 configuration.

Figure 4.9 Typical crack due to axial load of Alternate 1 configuration

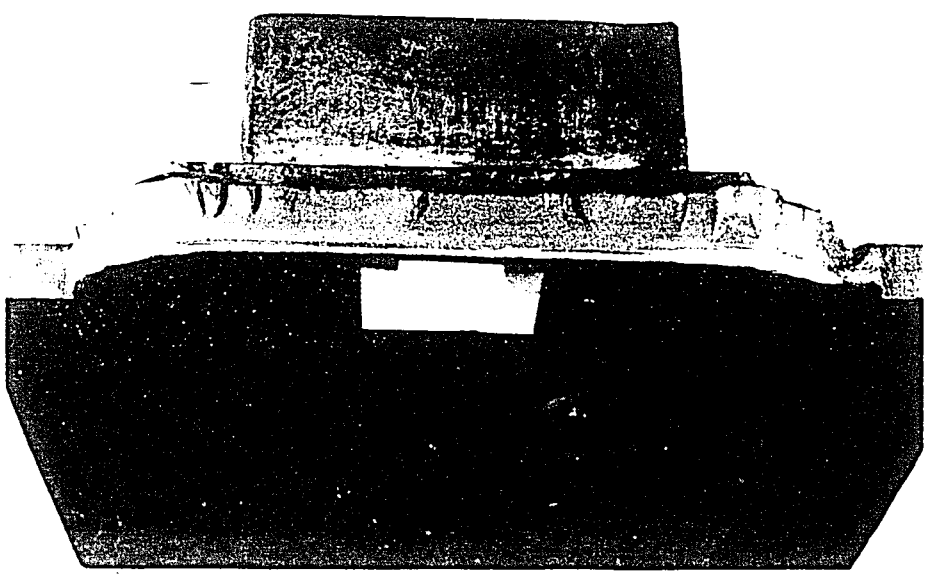

Figure 4.10 Typical crack surface of Alternate 1 configuration.

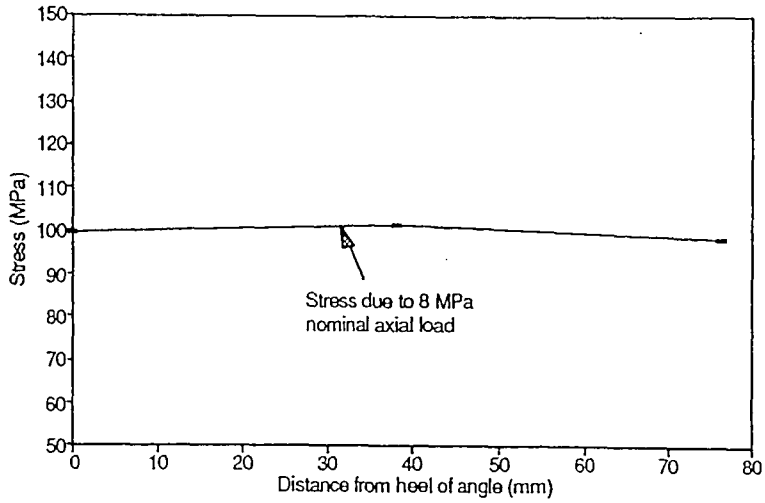

Figure 4.11 Stress gradient along the weld toe joining the pad and top plate indicating a uniform stress along the weld length

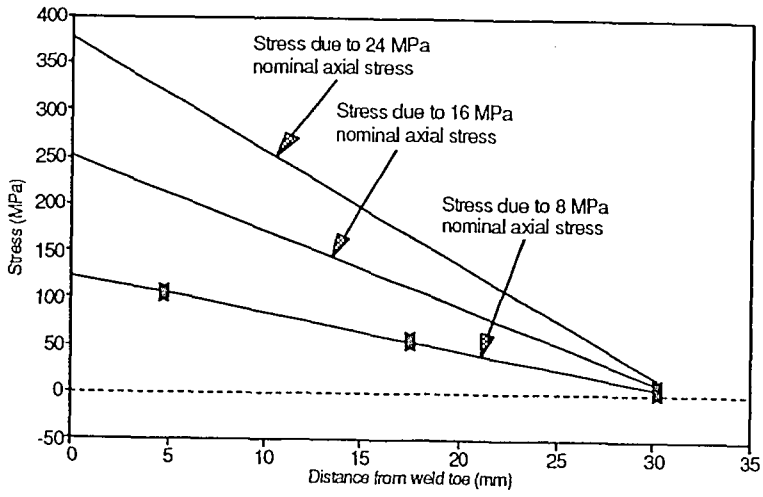

Figure 4.12 Stress gradient perpendicular to the weld toe at the centerline of the pad. Solid lines are results of linear regression of data of several details. Actual data points are plotted for 8 MPa nominal axial stress to indicate degree of scatter.

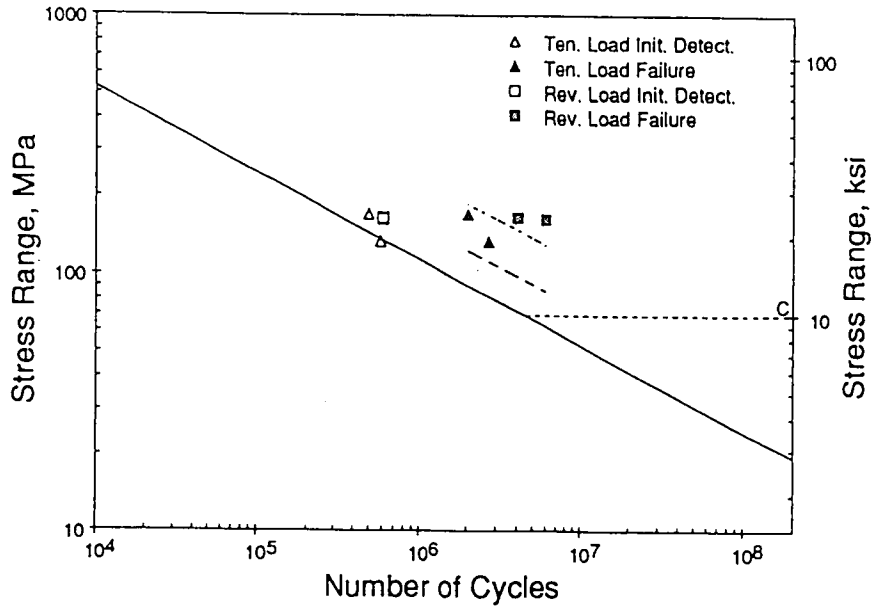

Figure 4.13 S-N plot of Axial Alternate 1 data with respect to the C curve. The 5 mm hot-spot stress range definiton is used. Tension and reversal data are also indicated.

Figure 4.14 Typical failure initiating from the weld root of Axial Alternate 2 configuration (10 mm eccentricity)

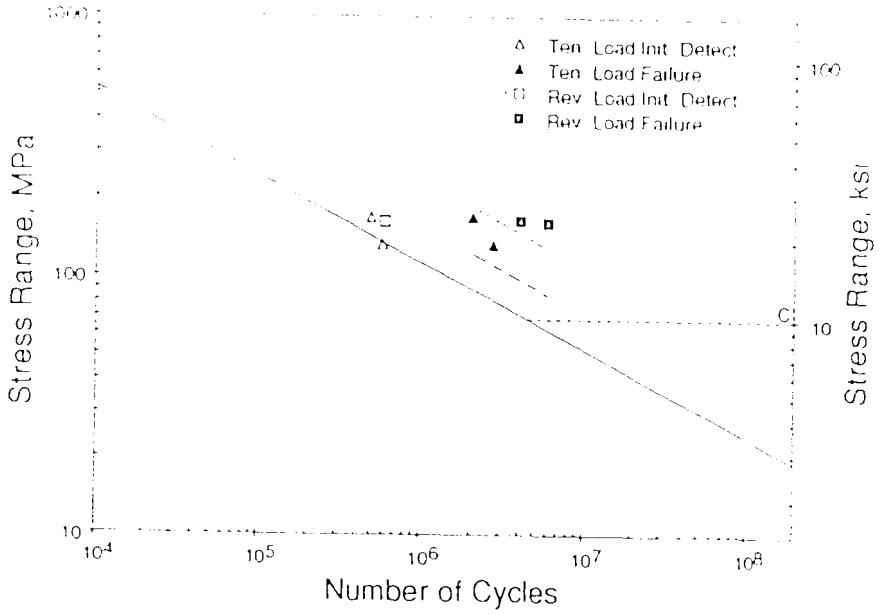

Figure 4.13 S-N plot of Axial Alternate 1 data with respect to the C curve. The 5 mm hot-spot stress range definiton is used. Tension and reversal data are also indicated.

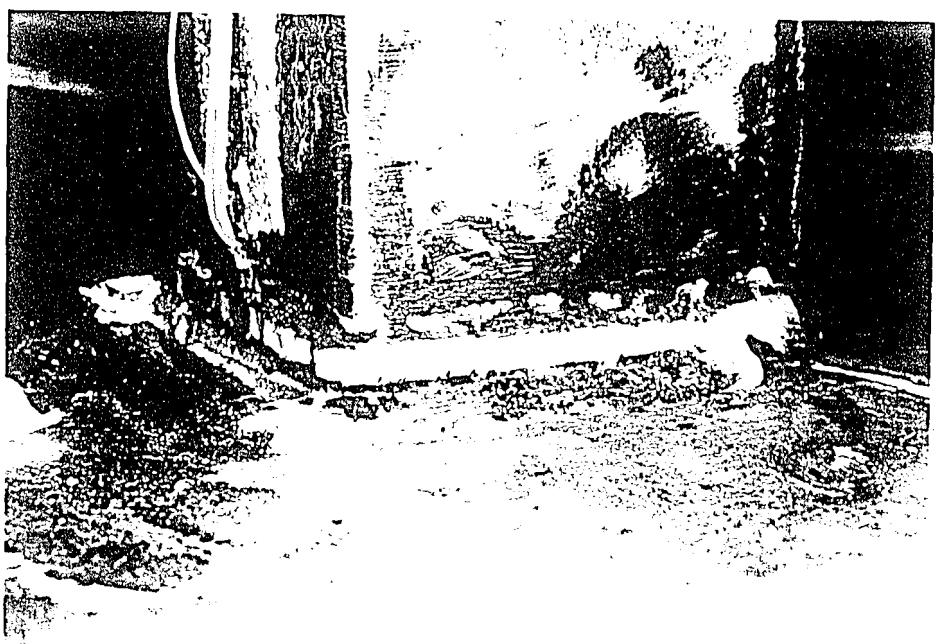

Figure 4.14 Typical failure initiating from the weld root of Axial Alternate 2 configuration (10 mm eccentricity)

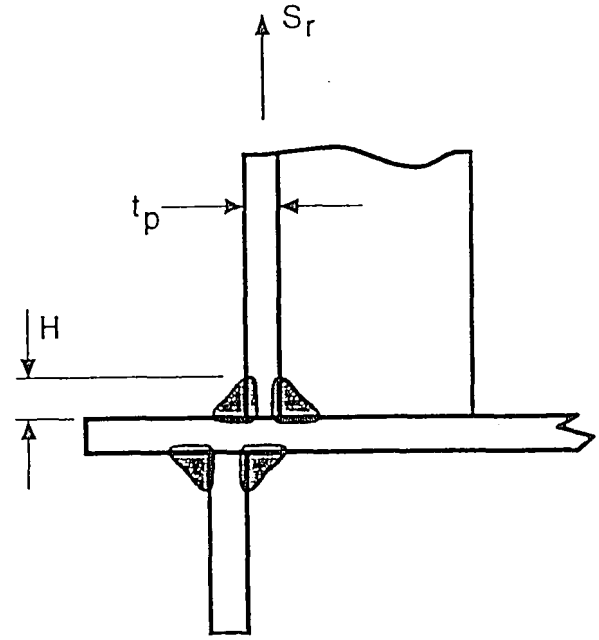

Figure 4.15 Cross section of Axial Alternate 2 detail showing eccentricity and definitions applicable to Equation 4.2.

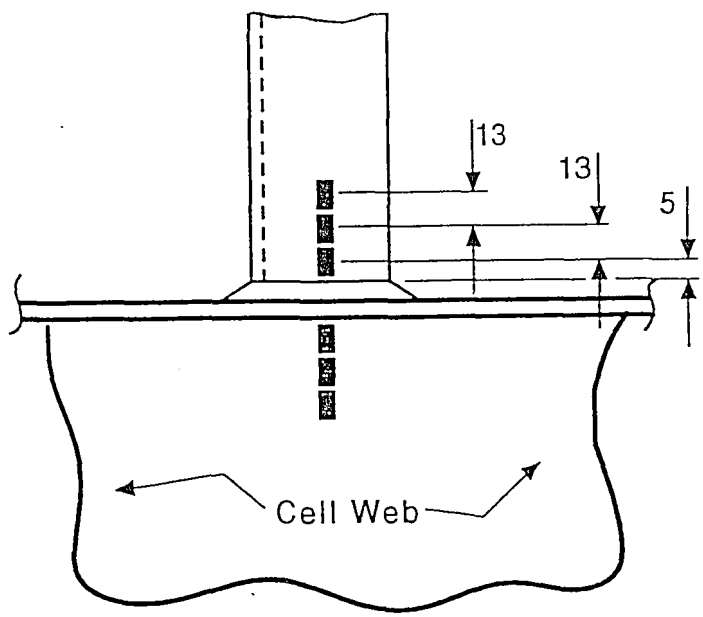

Figure 4.16 Typical gage arrangement for measuring strain gradients of Axial Alternate 2 details.

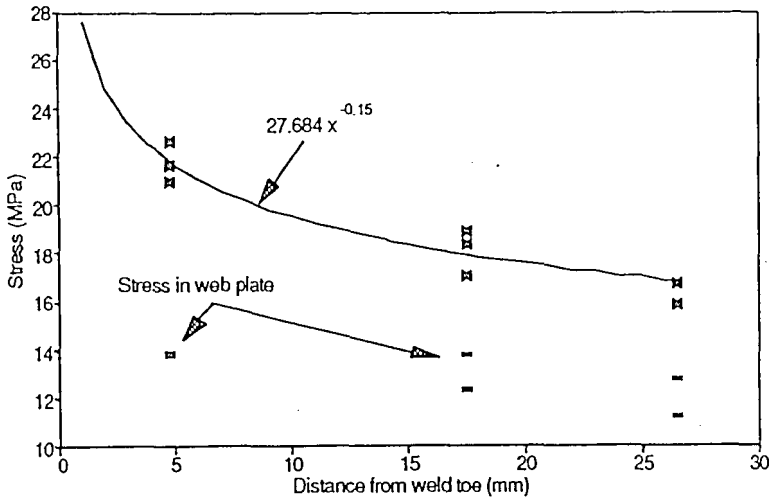

Figure 4.17 Stress gradient on centerline of face of longitudinal leg of Axial Alternate 2 configuration under a 8 MPa nominal axial stress. Also shown are stress data leading from the weld joining the web and top plate and in line with points measured on the leg of the angle.

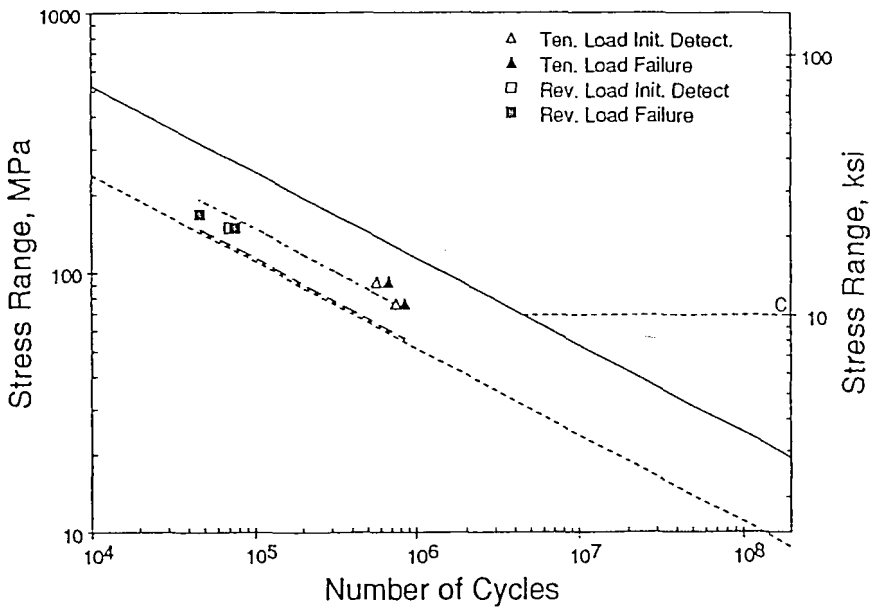

Figure 4.18 S-N plot of Axial Alternate 2 data with respect to a reduced AASHTO curve. A reduced curve is used to account for the pre-existing "crack" at the lack of penetration at the weld root of this cruciform joint. The 5 mm hot-spot stress range is used.

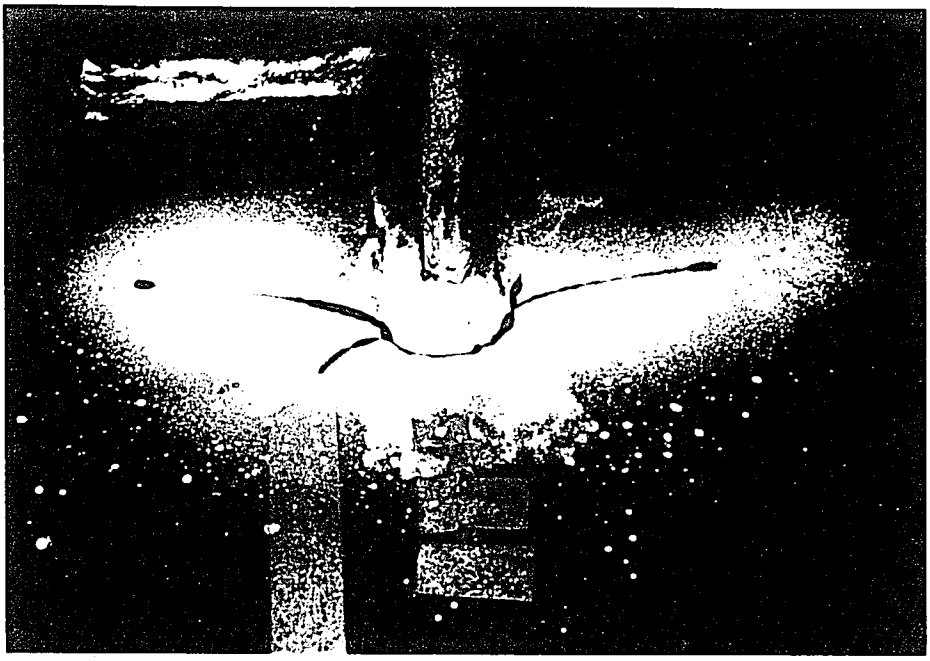

Figure 4.19 Typical crack at failure of Axial Alternate 3

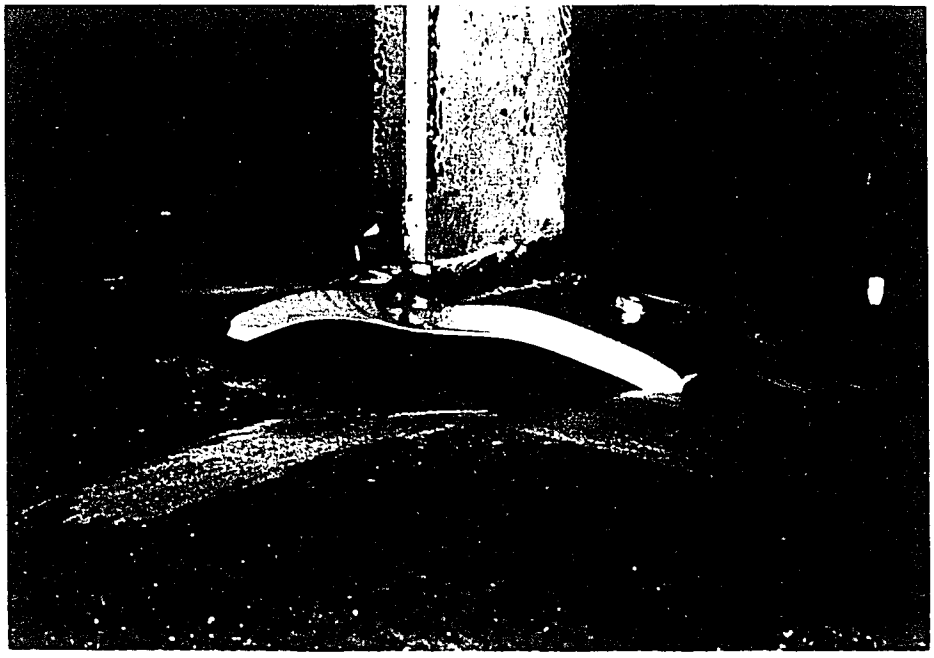

Figure 4.20 Typical crack surface of failure of Axial Alternate 3. The detail pictured was subjected to an ultimate tension load after a through-thickness crack developed.

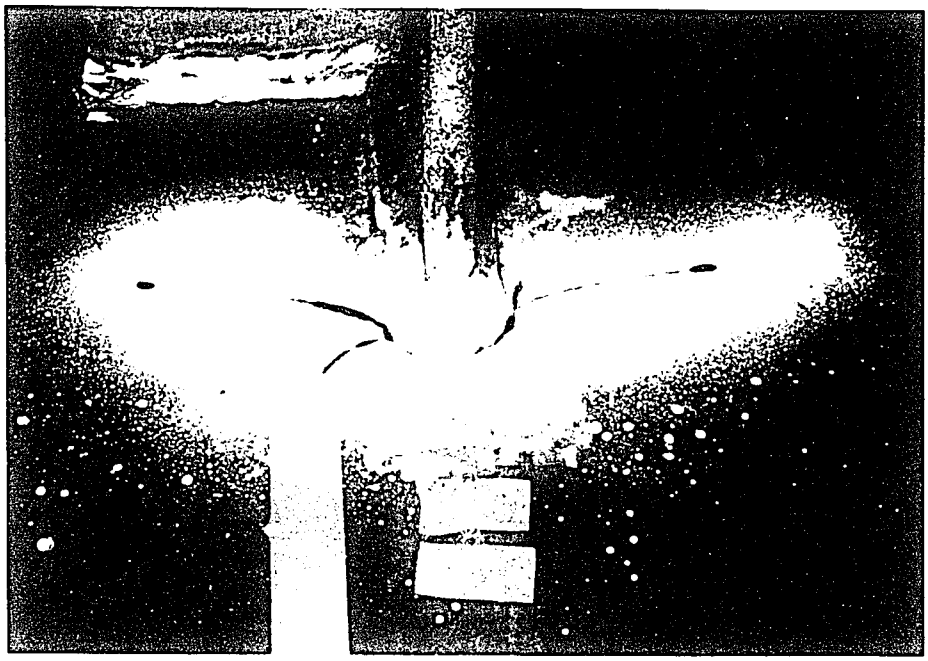

Figure 4.19 Typical crack at failure of Axial Alternate 3

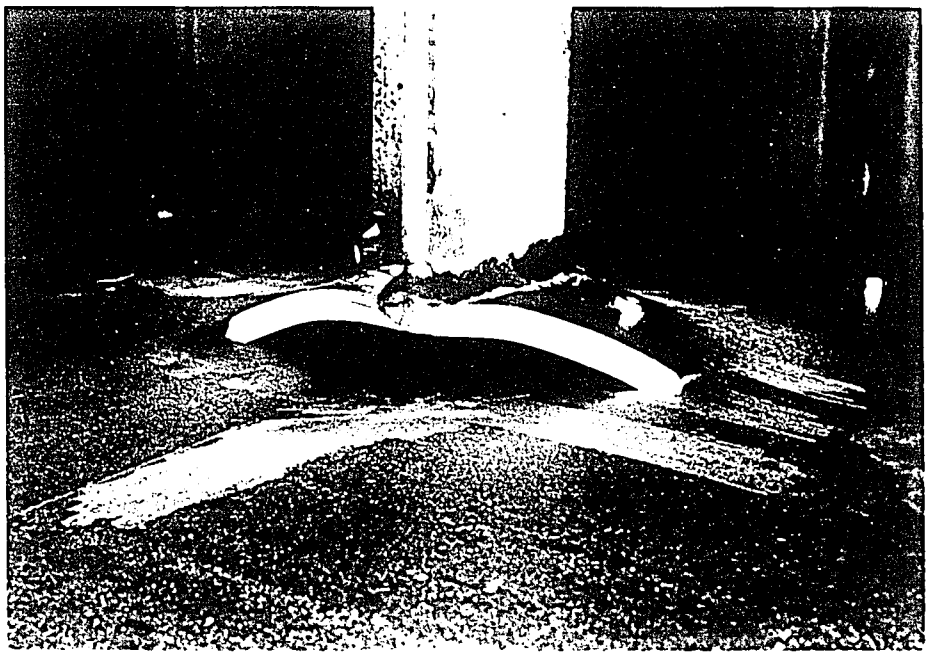

Figure 4.20 Typical crack surface of failure of Axial Alternate 3. The detail pictured was subjected to an ultimate tension load after a through-thickness crack developed.

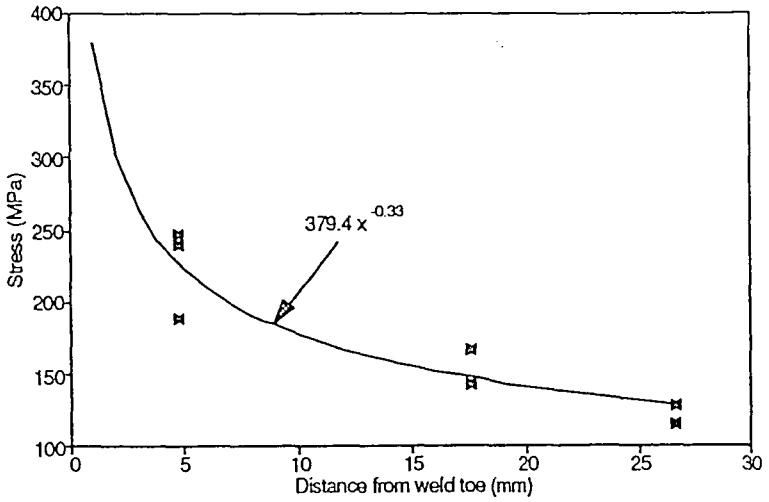

Figure 4.21 Stress gradient leading to the weld toe at the toe of the transverse leg of the angle for Axial Alternate 3 resulting from an 8 MPa nominal axial stress

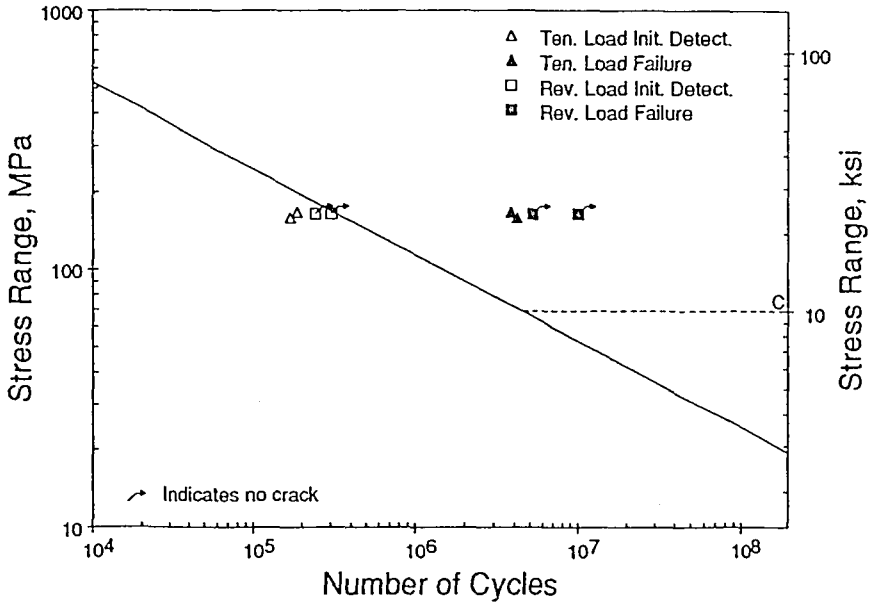

Figure 4.22 S-N plot of Axial Alternate 3 data using the 5 mm hot-spot stress range definition. This indicates tension and reversal loading.

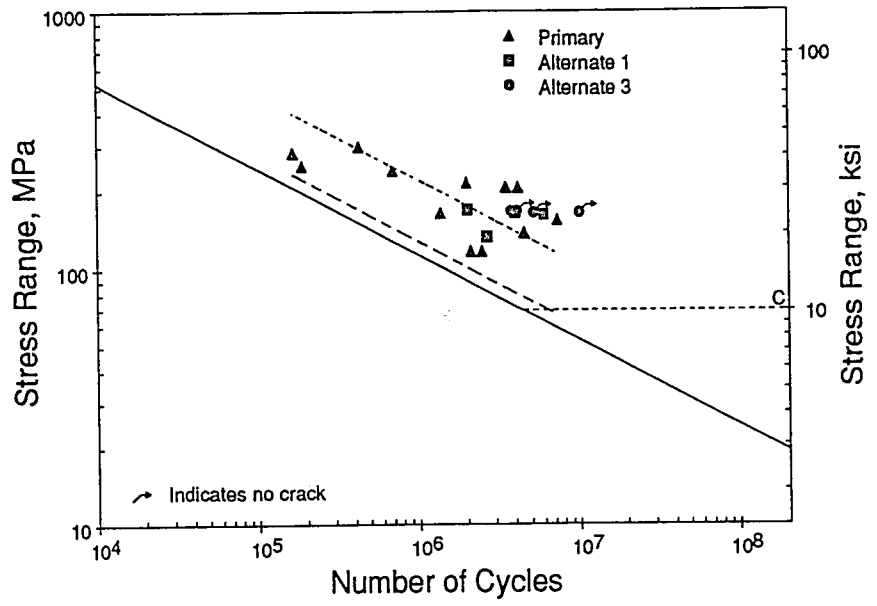

Figure 4.23 S-N plot comparing data for the Primary details, Alternate 1 and Alternate 3 details. Alternate 2 is not shown since it is not applicable to the C curve. Regression includes all data.

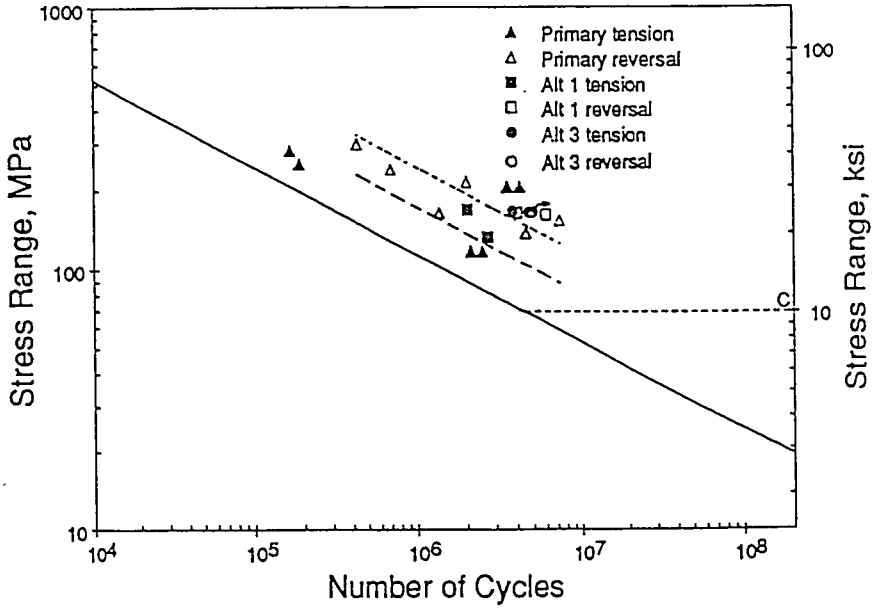

Figure 4.24 S-N plot comparing tension and reversal loading for all axial tests. The regression for the reversal data is indicated. Again Axial Alternate 2 is not applicable.

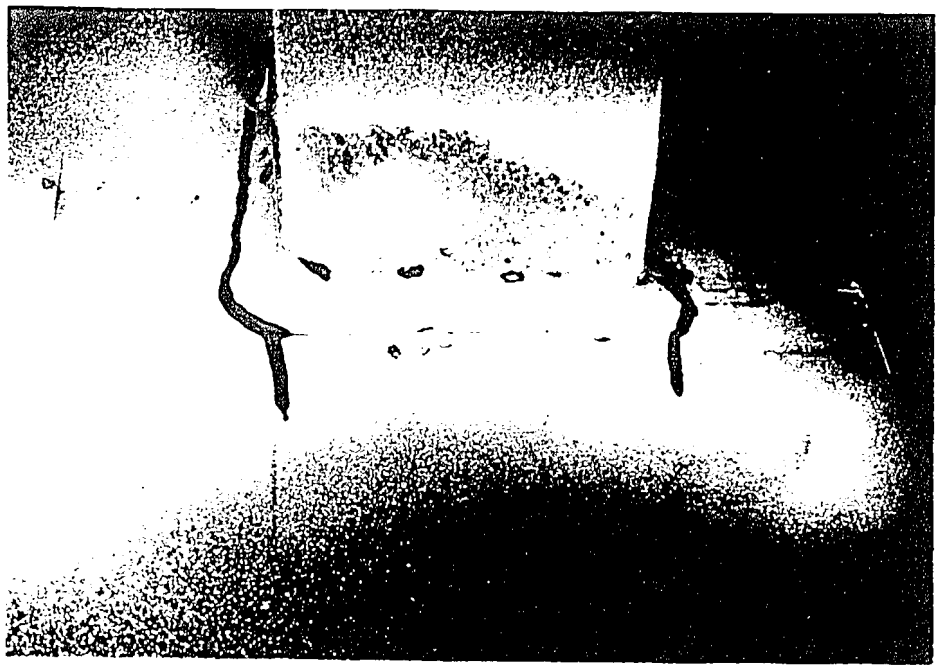

Figure 4.25 Cracks at the toe and heel of the transverse leg of a the Primary configuration subject to bending.

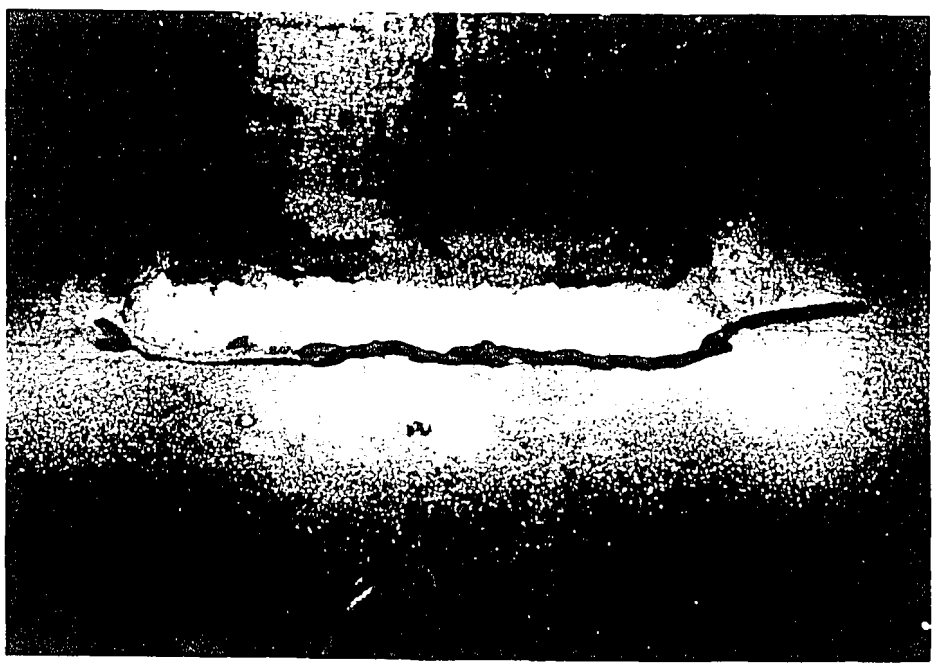

Figure 4.26 Typical crack that occurred along the longitudinal leg of the Primary configuration subject to bending

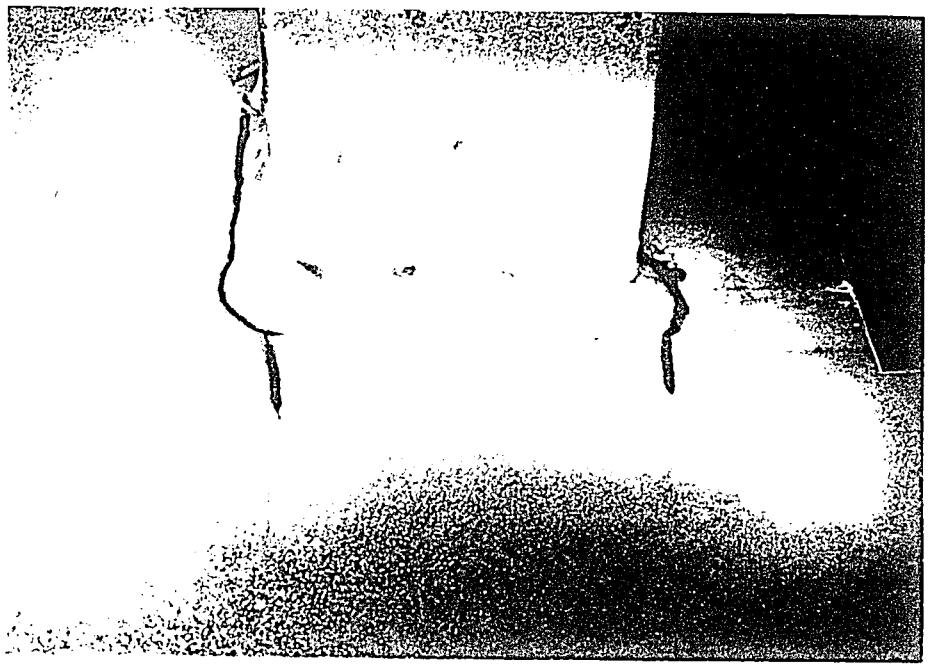

Figure 4.25 Cracks at the toe and heel of the transverse leg of a the Primary configuration subject to bending.

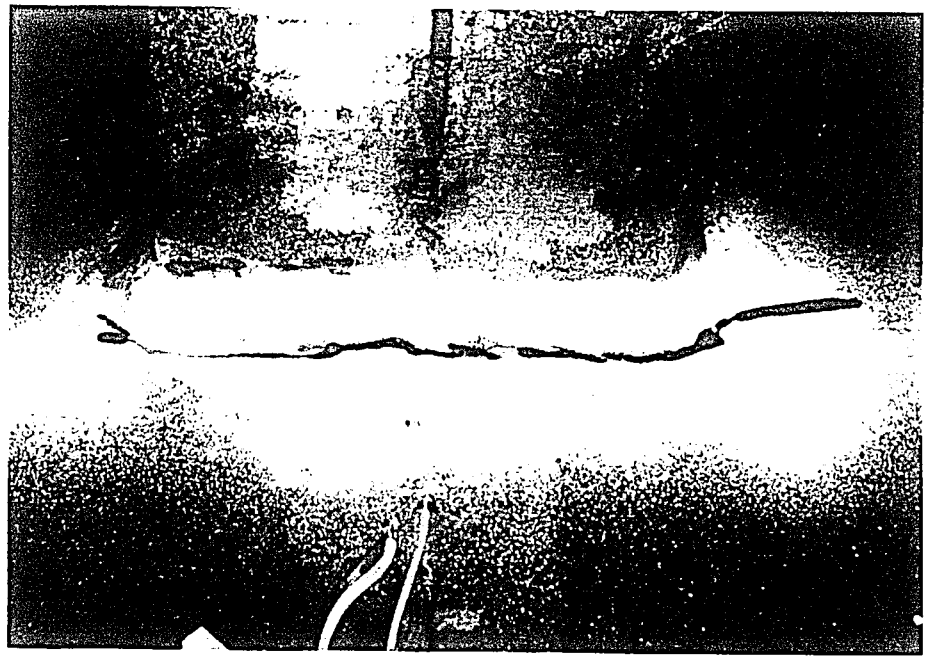

Figure 4.26 Typical crack that occurred along the longitudinal leg of the Primary configuration subject to bending

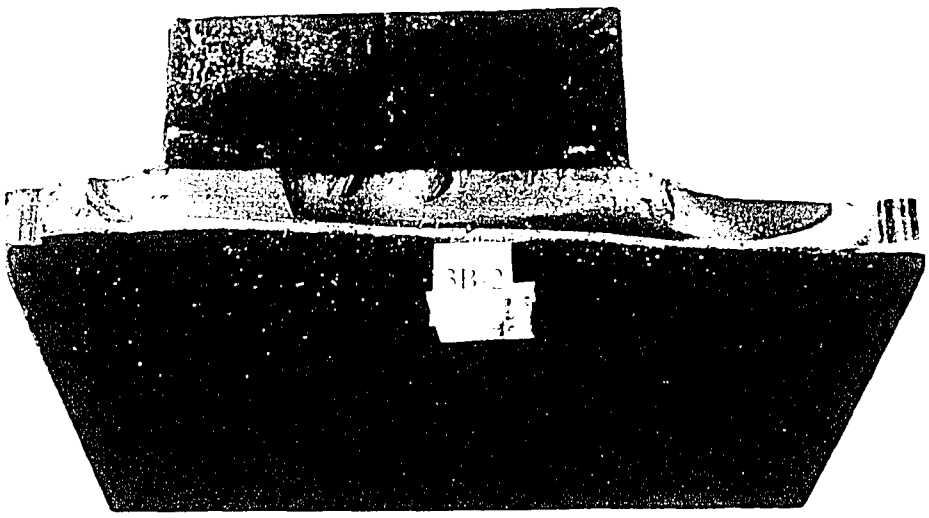

Figure 4.27 Typical crack surface of a crack along the longitudinal leg of the Primary configuration subject to bending

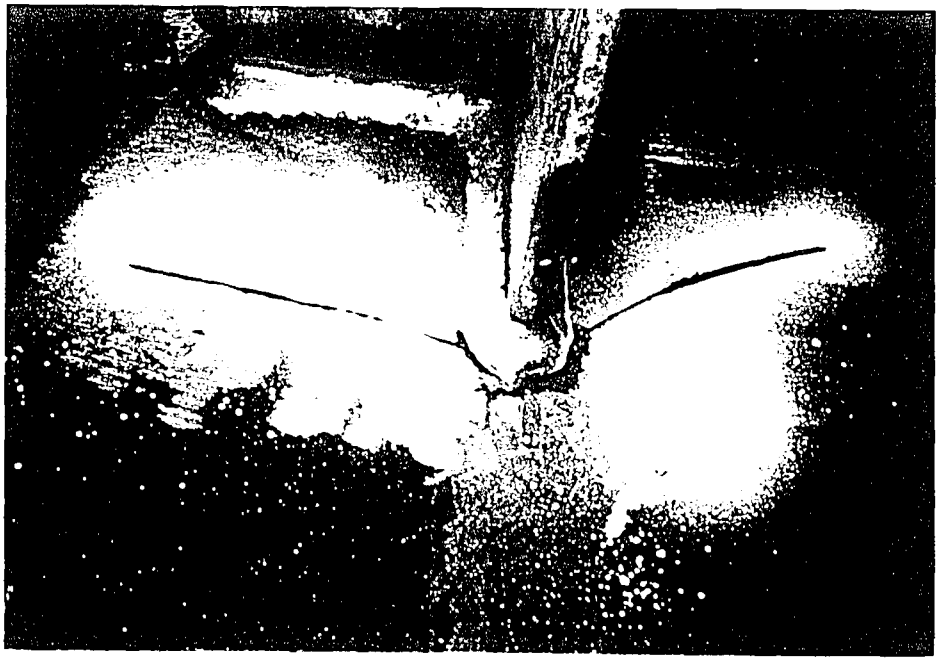

Figure 4.28 Typical crack at the toe of the transverse leg of the Primary configuration subject to bending

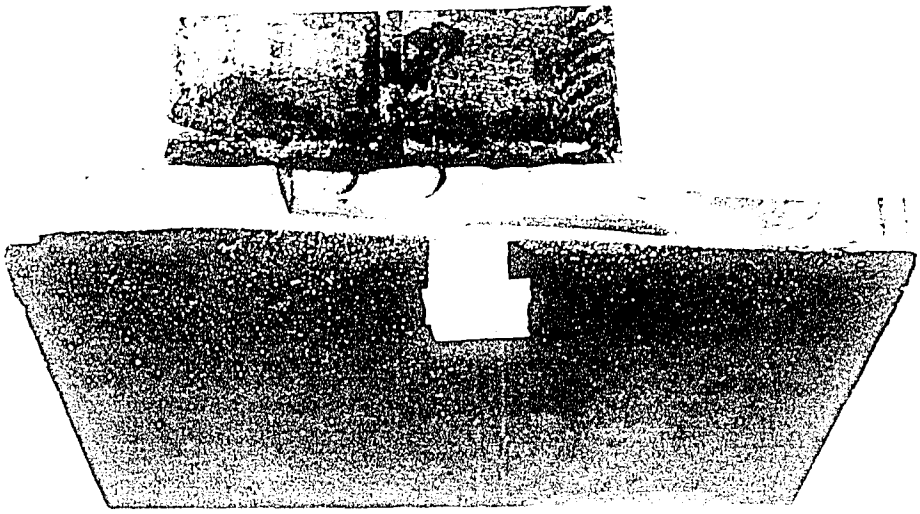

Figure 4.27 Typical crack surface of a crack along the longitudinal leg of the Primary configuration subject to bending

Figure 4.28 Typical crack at the toe of the transverse leg of the Primary configuration subject to bending

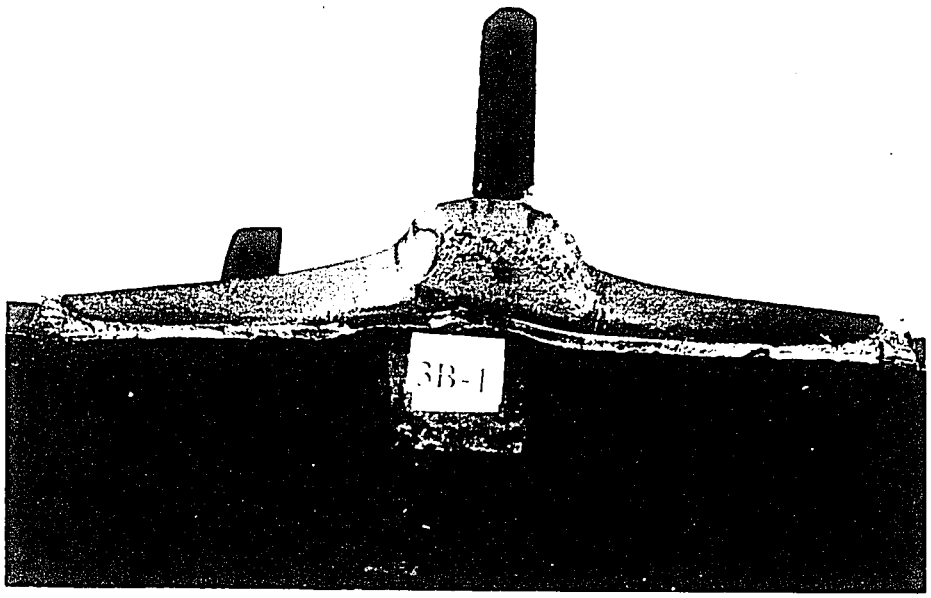

Figure 4.29 Typical crack surface of crack at toe of transverse leg of the Primary configuration subject to bending

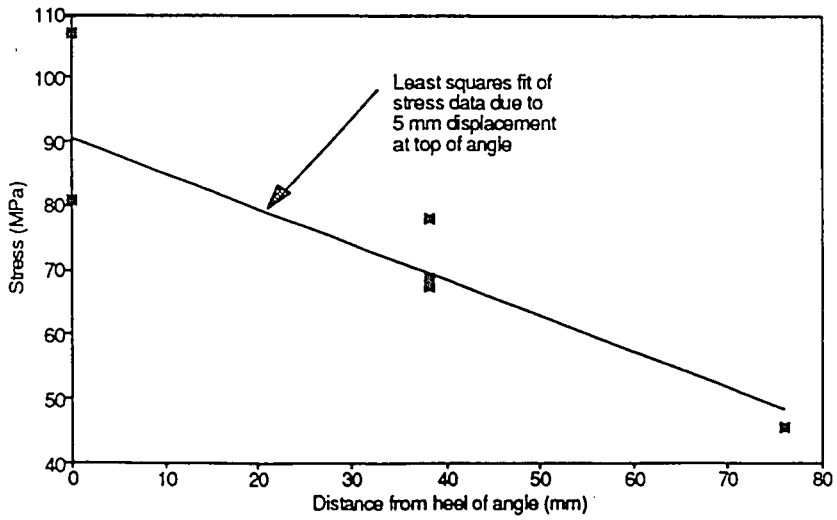

Figure 4.30 Stress gradient along angle leg parallel to web plate resulting from a bending load. This gradient indicates that the stress at the heel is on average 1.25 times that at the centerline of the leg.

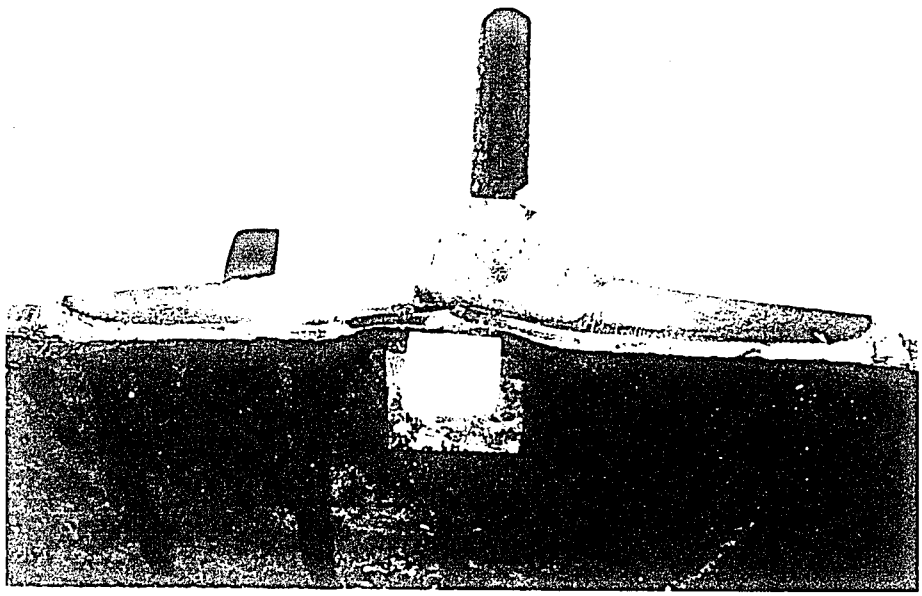

Figure 4.29 Typical crack surface of crack at toe of transverse leg of the Primary configuration subject to bending

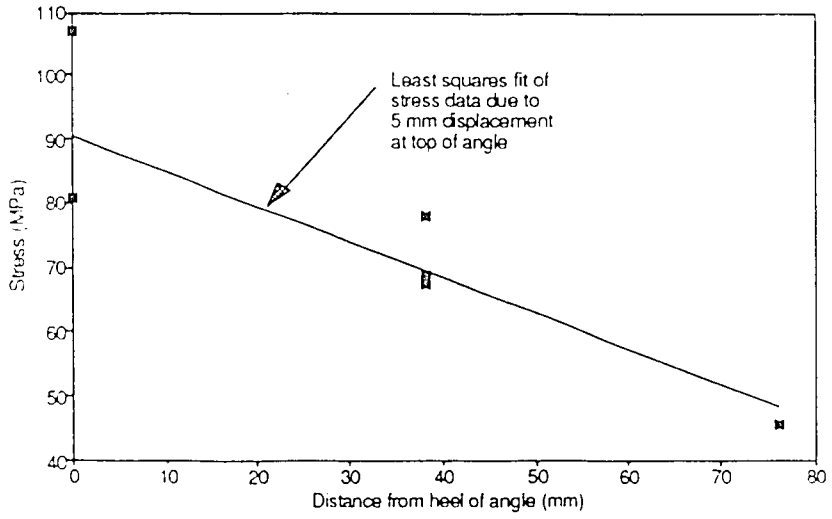

Figure 4.30 Stress gradient along angle leg parallel to web plate resulting from a bending load. This gradient indicates that the stress at the heel is on average 1.25 times that at the centerline of the leg.

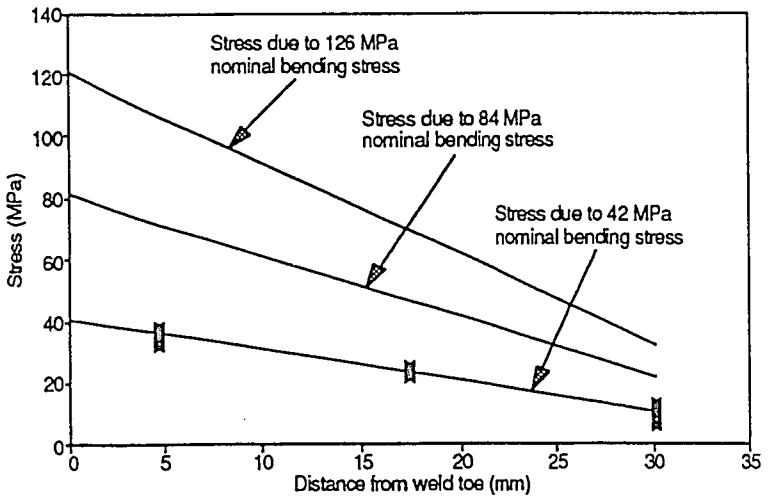

Figure 4.31 Stress gradient (due to bending) perpendicular to the weld toe at the centerline of the angle leg parallel to the web plate. Solid lines are results of a linear regression of data of several details with data points shown for 2.5 mm displ. to indicate degree of scatter.

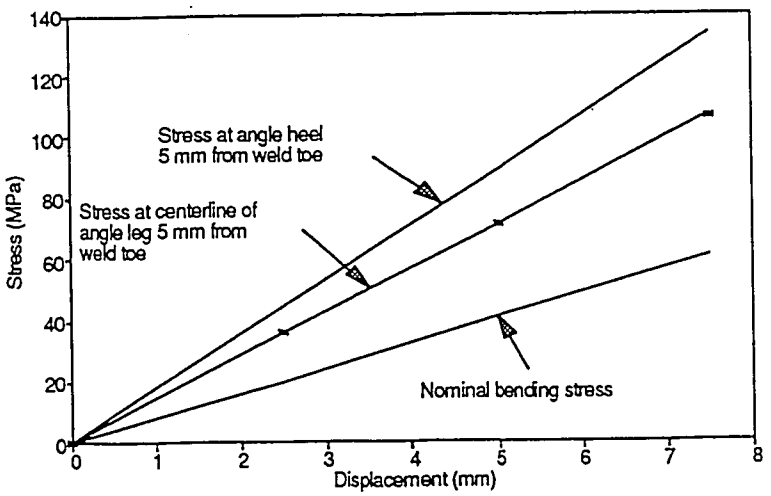

Figure 4.32 Hot-spot stress at angle heel as a function of lateral displacement.

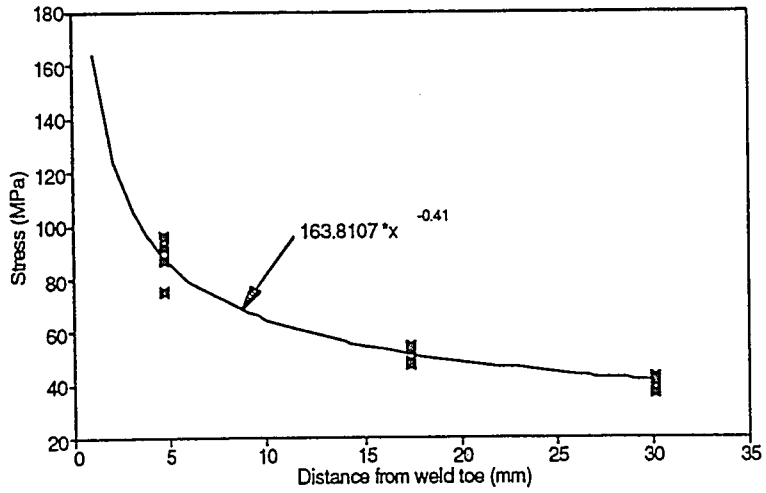

Figure 4.33 Stress gradient leading to the weld toe at the toe of the transverse leg of the Primary configuration subject to bending.

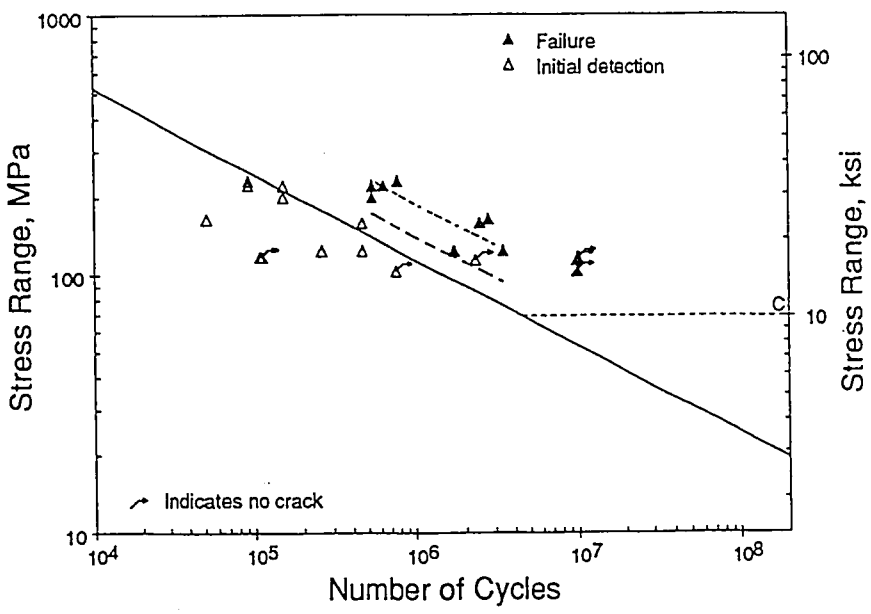

Figure 4.34 S-N plot with respect to the AASHTO C curve of all bending data using the 5 mm hot-spot stress range definition. Regression is of failure data

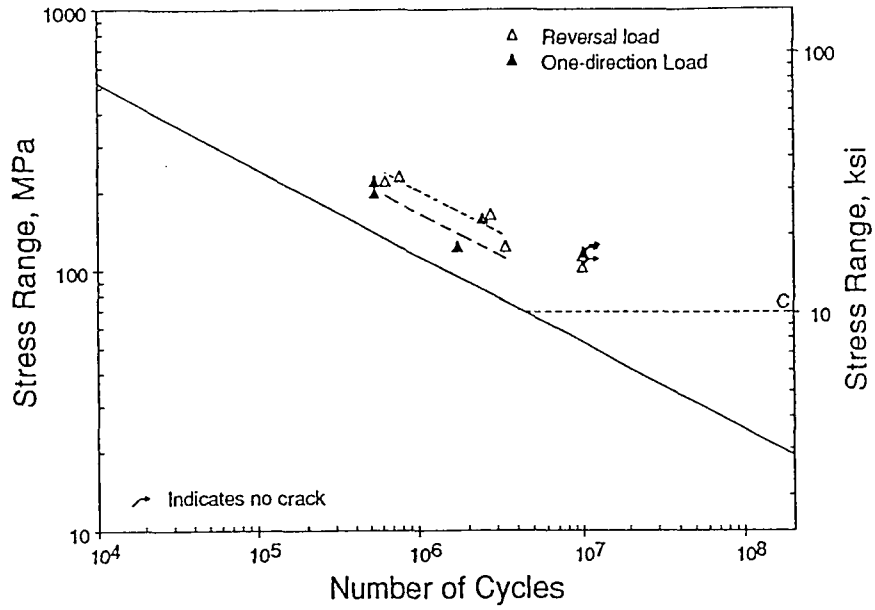

Figure 4.35 S-N plot of one-direction and reversal loaded bending tests with regression of reversal data shown.

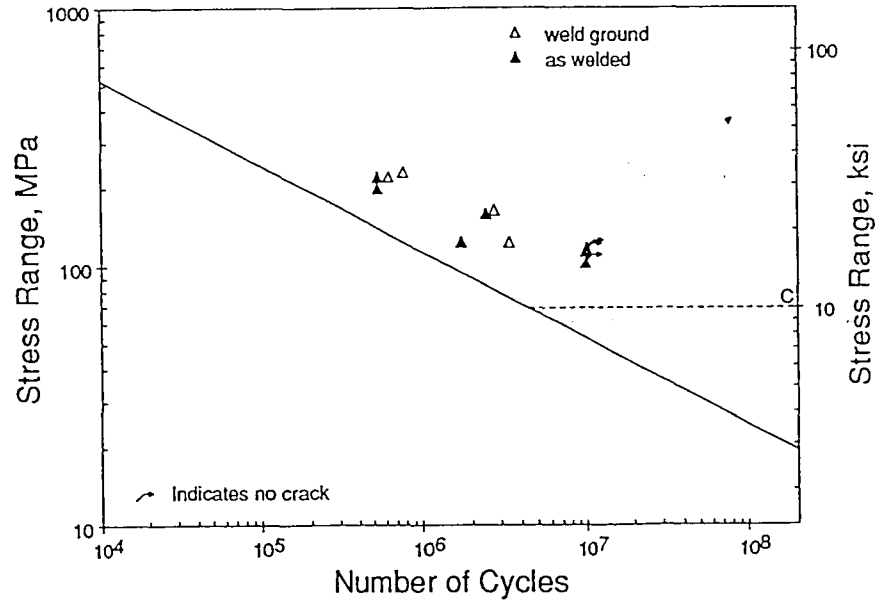

Figure 4.36 Comparison of ground and as-welded details subject to bending load including one-direction and reversal loaded tests

Figure 4.37 Typical crack along longitudinal leg of the Primary configuration subject to biaxial loading

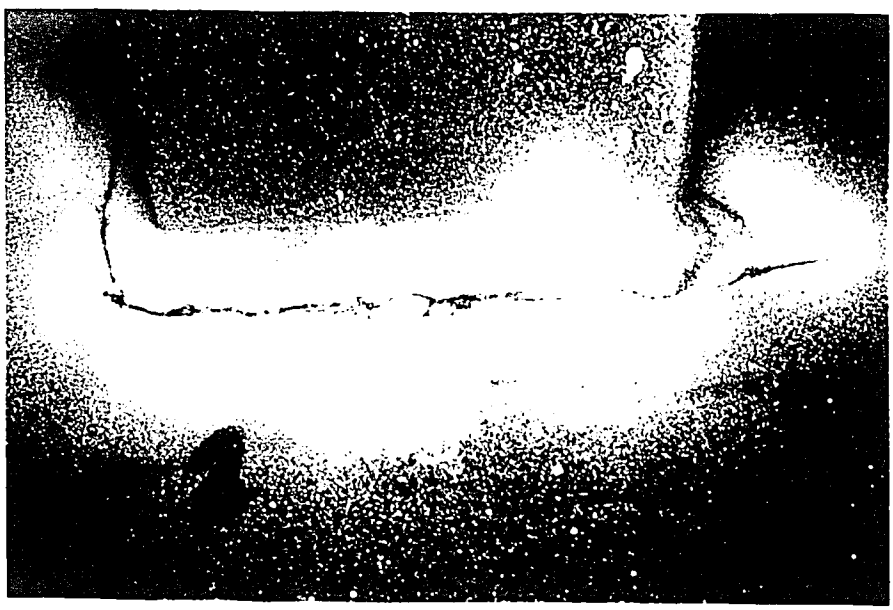

Figure 4.38 Typical crack following weld toe along longitudinal and transverse leg of the Primary configuration subject to biaxial load

Figure 4.37 Typical crack along longitudinal leg of the Primary configuration subject to biaxial loading

Figure 4.38 Typical crack following weld toe along longitudinal and transverse leg of the Primary configuration subject to biaxial load

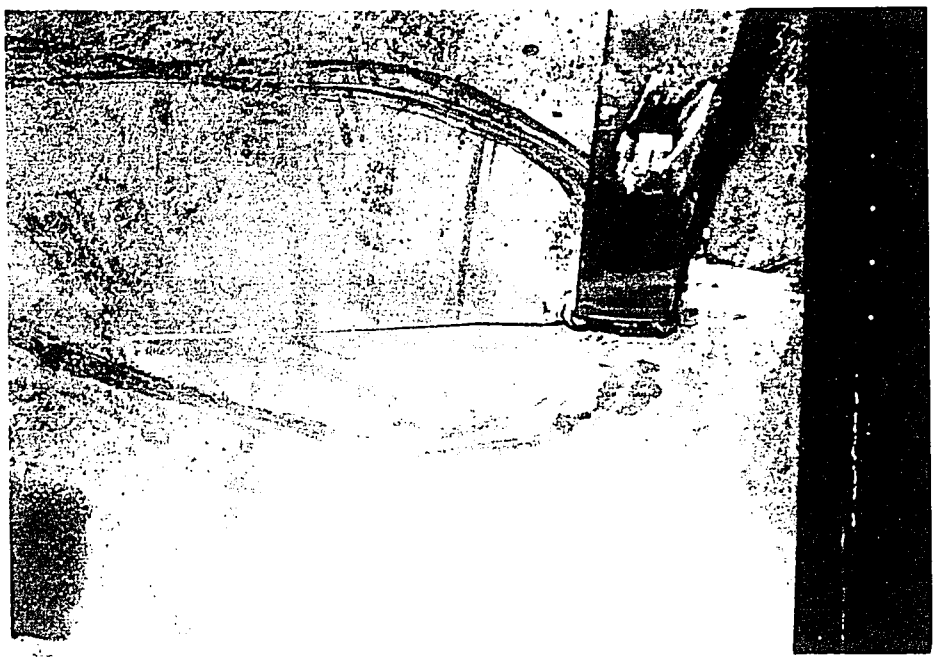

Figure 4.39 Large transverse crack resulting from biaxial loading.

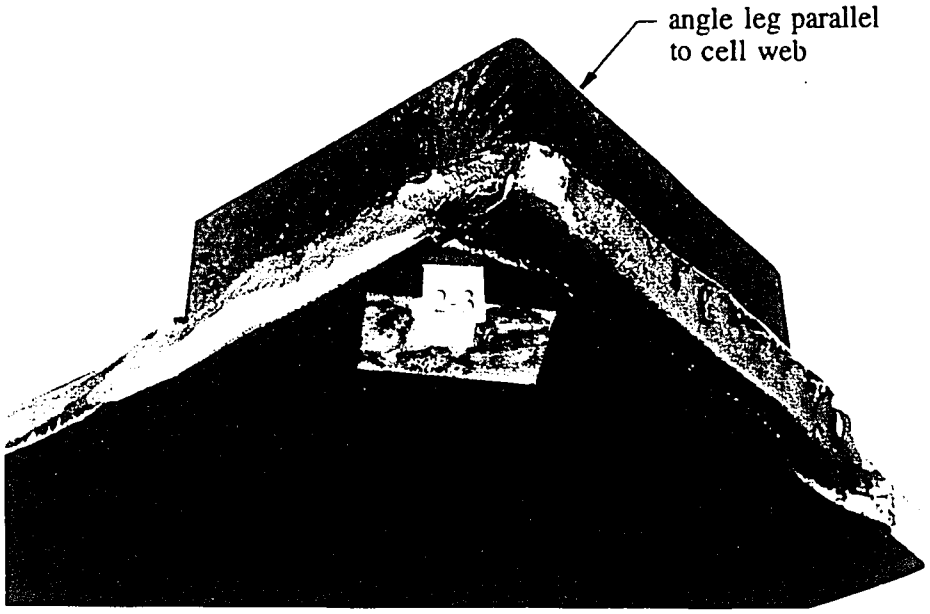

Figure 4.40 Crack surface of weld that followed the weld toe of both legs of the angle subject to biaxial loading.

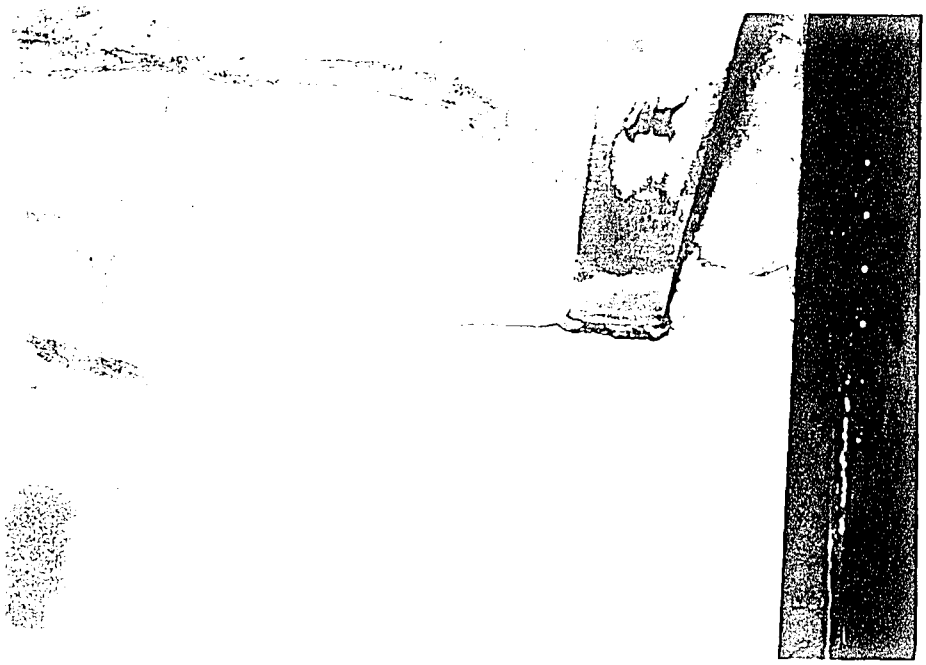

Figure 4.39 Large transverse crack resulting from biaxial loading.

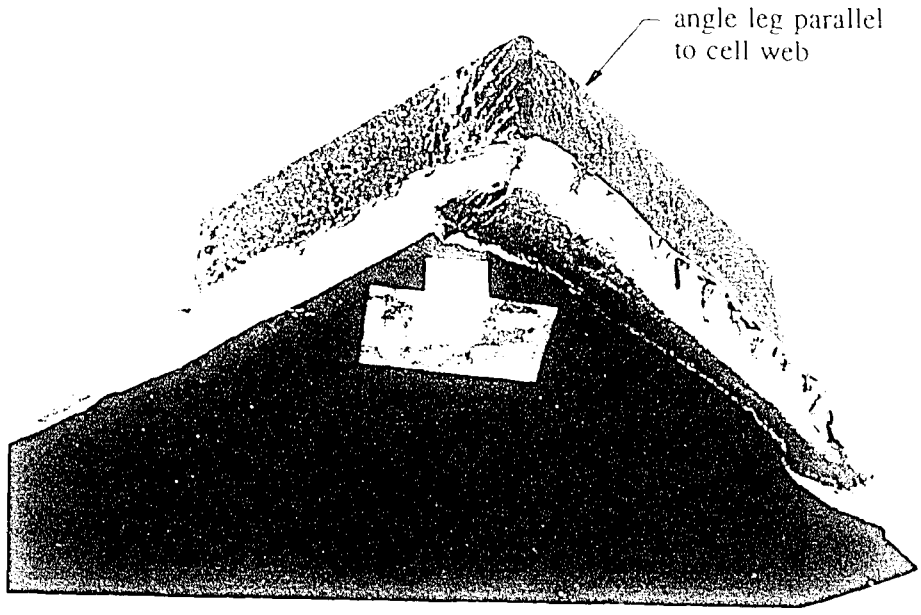

Figure 4.40 Crack surface of weld that followed the weld toe of both legs of the angle subject to biaxial loading.

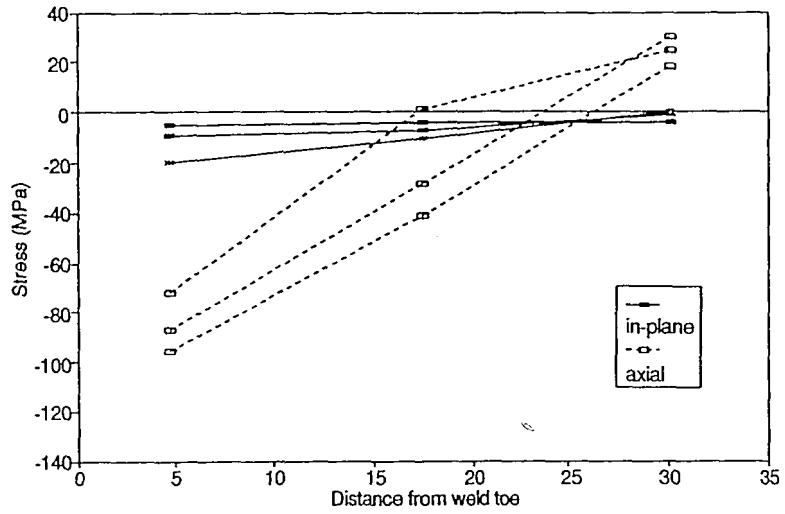

Figure 4.41 Stress gradient of three different details at centerline of leg parallel to web for an axial only stress of 8 MPa and an in-plane only stress of 19 MPa.

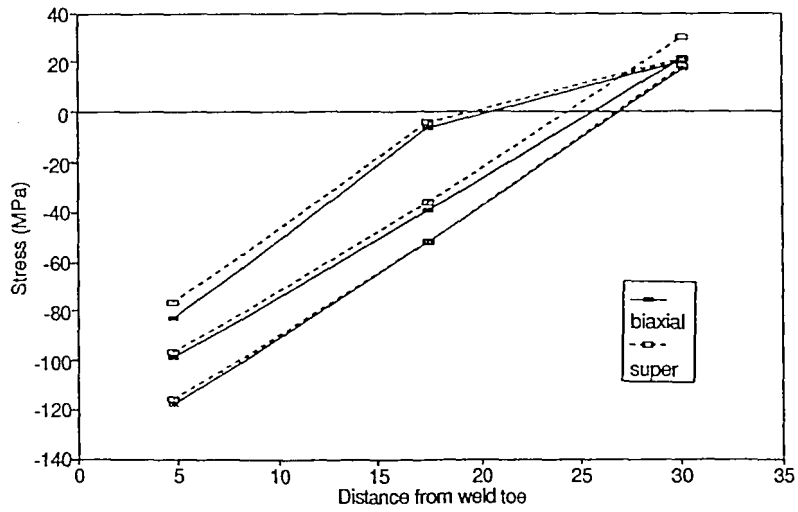

Figure 4.42 Comparison of measured stress gradient of three different details under biaxial load and the result of superposition of axial and in-plane stress components.

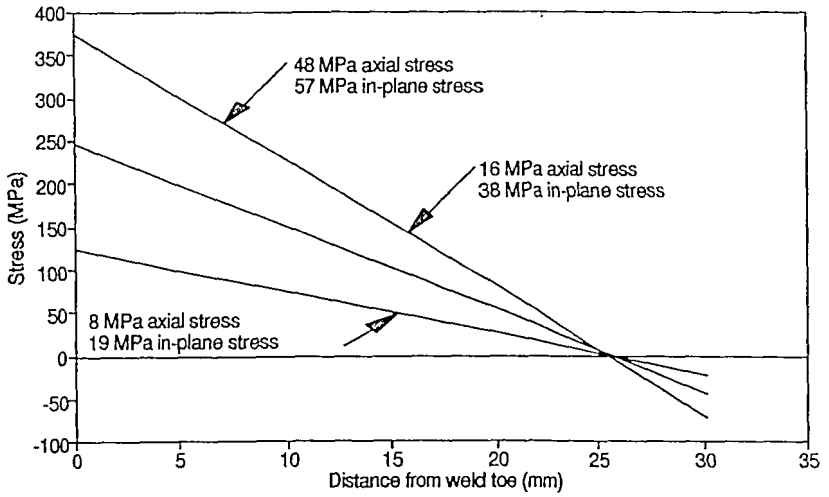

Figure 4.43 Stress gradient perpendicular to the weld toe at the centerline of the angle leg parallel to the web plate. Solid lines are results of linear regression at varying in-plane and axial loads of several details.

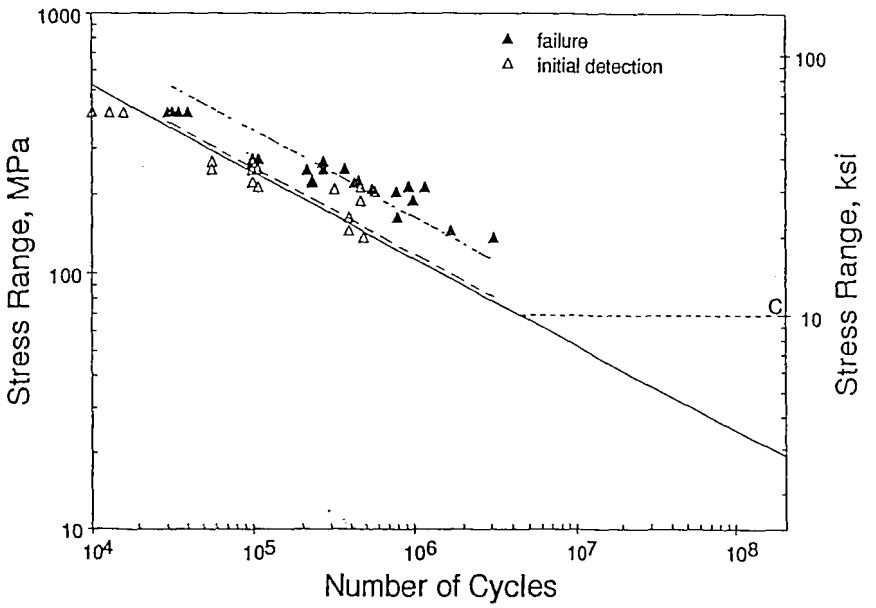

Figure 4.44 Biaxial test data plotted with respect to the AASHTO C curve using the 5 mm definition for the hot-spot stress range. Regression is of failure data.

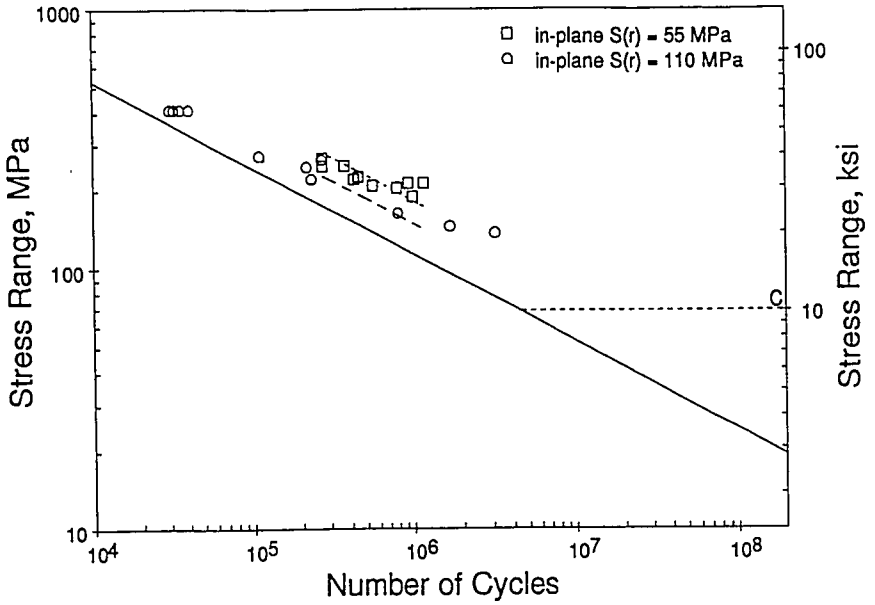

Figure 4.45 Comparison of the biaxial failure data for in-plane stress ranges of 55 MPa and 110 MPa. Regression of 55 MPa data is shown.

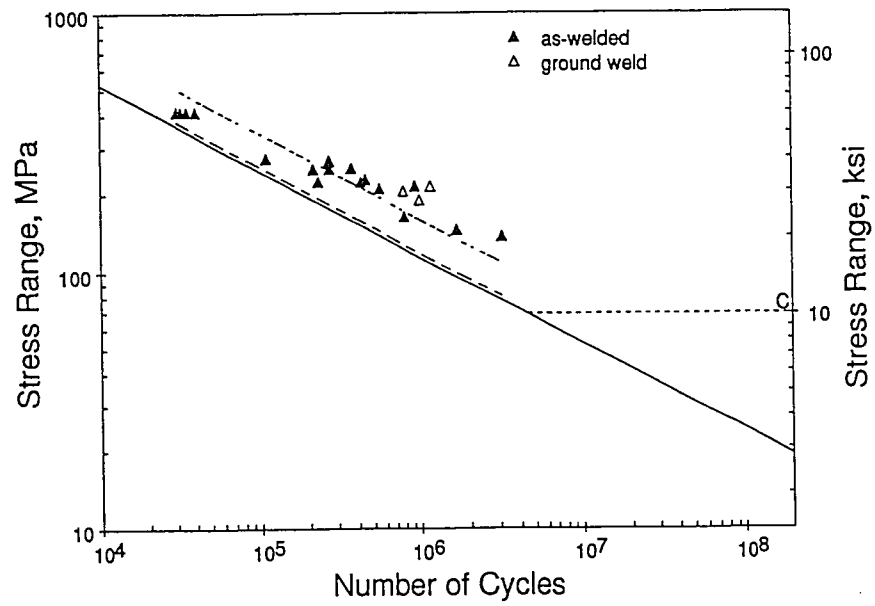

Figure 4.46 S-N plot of Biaxial data comparing ground and as-welded details Regression of as-welded data is shown.

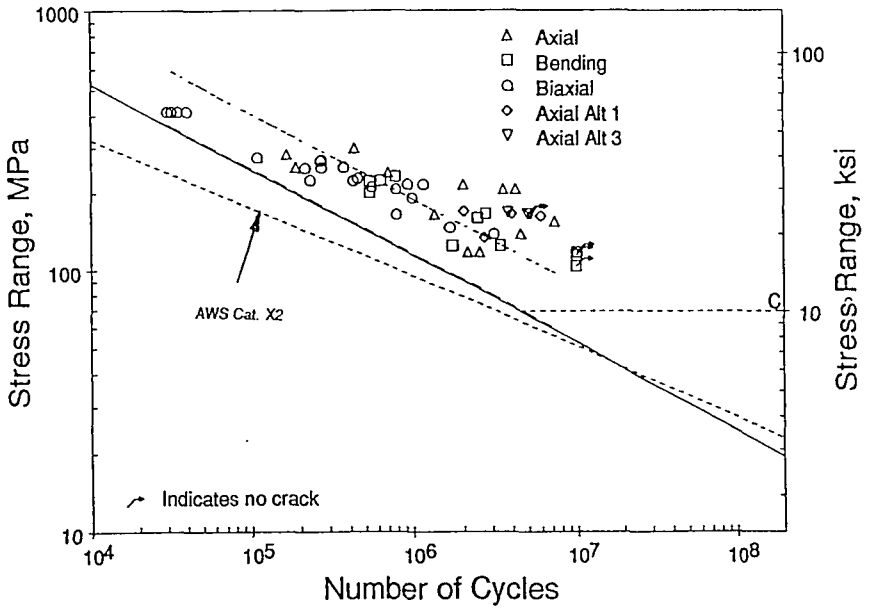

Figure 4.47 Compilation of all data plotted with respect to the AASHTO C curve (excluding Alternate 2 data). Also shown is the AWS Category X2 design curve.

5.0 SUMMARY & CONCLUSIONS

A total of 57 full-scale foundation attachment details of various configurations were fatigue tested with a variety of loading directions. The local hot-spot stress in the vicinity of the crack initiation site was measured as well as the loads and the nominal stresses. The number of cycles to initiation and to propagation as a through-thickness crack were recorded.

A number of suggested definitions of the hot-spot stress were evaluated. It was found that the most suitable definition was the stress at a point about 5 mm from the weld toe. All of the details with large eccentricity (greater than six times the thickness of the plate) can be safely designed by computing a hot-spot stress range and comparing to the AASHTO Category C fatigue design curve. The stress concentration factor (SCF) was defined as this hot-spot stress at 5 mm from the weld toe divided by the nominal axial stress in the angle. In bending, the SCF is the ratio of this hot-spot stress to the nominal bending stress at the weld.

With regard to the SCF defined in this manner, it was found that:

1. The experimentally determined SCF varied up to 25 percent between individual replicate details.

2. For axial loaded angles with a one thickness eccentricity, the SCF was 2.7 which is in agreement with a well known simple formula. This simple formula for the SCF does not work for six thickness eccentricity or greater.

3. The addition of a pad under the angle reduced the SCF significantly for a given eccentricity.

4. The SCF for loads in the angles were reduced slightly when tension was applied in the plane of the hull plate in addition to an axial load.

5. The maximum hot-spot stress range for loading in tension and in bending, or from multiaxial loading, can be determined by superposition, i.e. by summation of the individual SCF times the nominal stresses in each mode or direction.

When plotted in terms of the local hot-spot stress (measured with a strain gage centered 5 mm from the weld toe at the point of highest stress) and the cycles to through-thickness cracking, it was found that:

6. For eccentricity of six times the thickness or more, all the cracking originates at the weld toe at one end of the legs of the attachment angle or at the heel of the angle. For these weld toe cracks, greater than half the life remains after first detection of the crack until propagation through the thickness.

7. For these weld toe cracks (i.e. for 60 mm or six thickness eccentricity or greater), the AASHTO Category C design S-N curve is less than or equal to the 97.5 percent survival lower bound for all of the data considered as one group, or to any subset of the data.

8. When the eccentricity between the web plate and the outer face of the attachment angle is less than six times the thickness, the axial stress in the attachment begins to increase relative to the bending stress in the surface of the hull plate adjacent to the weld toe. Consequently, for smaller eccentricities, cracking at the weld root will eventually dominate the fatigue strength rather than cracking at the weld toe. The fatigue strength of the partial penetration welds in the attachments with eccentricity of one thickness was adequately predicted using the Frank and Fisher equation for the reduced fatigue strength in combination with the hot-spot stress.

9. Nominal membrane stress ranges of 55 and 110 MPa were applied in the hull plate in-phase with the axial loading and a trend of decreasing fatigue strength with increasing in-plane stress could be observed. However, the effect on the fatigue strength was insignificant with respect to the overall variability and the fatigue strength was still conservatively represented by Category C. Thus for secondary nominal stress ranges up to 110 MPa, the detail can be designed in terms of the hot-spot stress range in the direction of the primary stress only, i.e. in the direction perpendicular to the plane

of the initial crack. This primary hot-spot stress range should be compared to the Category C S-N curve for design.

10. The bending tests, as well as axial tests which were performed in reversal loading, exhibited slightly greater apparent fatigue strength. Several of the bending tests exhibited crack arrest after the development of a large part-through surface crack at the weld toe. However, in view of: 1) the few data involved in these comparisons, 2) the uncertainty in the loading and, 3) the desire to keep the design rules simplified, it is considered prudent to ignore these apparent increases in fatigue strength.

11. In the tests at one-thickness eccentricity where the cracks initiated at the weld root, initiation could not be observed. In all the other tests except the bending tests, the cycles to failure were above or only slightly below the Category C line. In the bending tests, the initiation occurred as early as 20 percent of the Category C design life. However, the life to propagation of a full-thickness crack was longer than typical so the early initiation is of no practical consequence.

12. Because the weld toe cracks exhibit consistent fatigue strength when plotted in terms of the hot spot stress, the relative fatigue performance of the various details can be ranked in terms of the SCF. This may allow the relative fatigue performance of various details to be evaluated from stress analysis such as the finite-element method.

6.0 RECOMMENDED RESEARCH

This investigation has demonstrated that the hot-spot stress concept can be a valuable tool for characterizing the fatigue strength of several ship details. The full-scale test database should be broadened further by testing a greater variety of details, for example the intersection between longitudinal girders and transverse ring frames.

Further investigation of the following issues is also recommended:

1. the effect of plate thickness,

2. the advantage of pad details,

3. the range of eccentricities between one and six thicknesses where the transition from weld root cracking to weld toe cracking occurs,

4. the interaction of multiaxial loads, including: loads in two or more axes that are almost equal in magnitude, loads that are out-of-phase or at different frequencies,

5. the effect of variable amplitude loading, particularly in view of recent evidence that Miner's rule can be unconservative for wideband frequency loading,

6. the apparent crack arrest that often occurs in reversal loading for the detail with the greatest eccentricity and bending loading.

REFERENCES

1. Shock Criteria for Surface Ships, NAVSEA report 0900-LP-000-3010, Sect 100,

2. Beach, J.E., "Advanced Surface Ship Hull Technology - Cluster B", Destroyer, Cruiser and Frigate Technology, pp. 89-112, ASNE Symposium -1990

3. Okamoto, T., Hori, T., Tateishi, M., Rashed, S.M.H., Miwa, S., "Strength Evaluation of Novel Unidirectional-girder-system Product Oil Carrier by Reliability Analysis," Paper No. 2, Annual Meeting of the Society of Naval Architects and M a r i n e Engineers, November 13-16, 1985.

4. Paik, J.K., Kim, D.H., Bong, H.S., Kim, M.S., and Han, S.K., "Deterministic and Probabilistic Safety Evaluation for a New Double-Hull Tanker with Transverseless System," Paper No. 6, Annual Meeting of the Society of Naval Architects and Marine Engineers, October 28-31, 1992.

5. Fisher, J.W., Jin, J., Wagner, D.C. and Yen, B.T., "Distortion-Induced Fatigue Cracking in Steel Bridges", NCHRP Report 336, 1990

6. Marshall, P.W., Design of Welded Tubular Connections, Elsevier, New York, NY 1992.

7. Radaj, D., Design and Analysis of Fatigue Resistant Welded Structures, Halsted Press, New York, NY 1990.

8. Rodabaugh, E.C., "Review of Data Relevant to the Design of Tubular Joints for Use in Fixed Offshore Platforms", Welding Research Bulletin 256, Welding Research Council, New York, NY 1980

9. Marshall, P.W., "Tubular Joint Design", contributing chapter to Planning and Design of Fixed Offshore Platforms, Edited by B. McClelland and M. reifel, Van Nostrand, Reinhold, New York, NY 1986.

10. AWS, Structural Welding Code. AWS D1.1-92, 13th edition, American Welding Society, 1992

11. American Petroleum Institute, Recommended Practice for Planning , Designing, and Constructing Fixed Offshore Platforms, API RP2A, , 18th edition, 1989

12. European Convention for Constructional Steelwork, Recommendations for the Fatigue Design of Steel Structures, ECCS, Technical Committee 6 - Fatigue, 1985

13. UK Health & Safety Executive (formerly the UK Dept of Energy), Fatigue Design Guidance for Steel Welded Joints in Offshore Structures, H.M.S.O., London, 1984

14. Yagi, J., Machida, S., Tomita, Y., Matoba, M., Kawasaki, T., "Definition of Hot-Spot Stress in Welded Plate Type Structure for Fatigue Assessment," International Institute of Welding, IIW-XIII-1414-91, 1991

15. AASHTO, Standard Specifications for Highway Bridges, American Association of State Highway Transportation Officials, 14th edition 1989

16. Niemi, E., "Recommendations Concerning Stress Calculation for Fatigue Analysis of Welded Components," International Institute of Welding, IIW-XIII-1426-91, 1991

17. Fisher, J.W., Frank, K.H., Hirt, M.A., and McNamee, B.M., "Effect of Weldments on the Fatigue Strength of Steel Beams," NCHRP Report 102, 1970

18. Fisher, J.W., Albrecht, P.A., Yen, B.T., Klingerman, D.J., and MacNamee, B.M., "Fatigue Strength of Steel Beams with Welded Stiffeners and Attachments," NCHRP Report 147, 1974

19. Munse, W.H., Wilbur, T.W., Tellalian, M.L., Nicoll, K., and Wilson, K., Fatigue Characterization of Fabricated Ship Details for Design, SSC-318, Ship Structures Committee, Washington D.C., 1982.

20. AISC, Manual for Steel Construction, LRFD 1st ed. or ASD 9th ed., The American Institute of Steel Construction, Chicago, IL, 1991

21. Fisher, J.W., et al, Structural Failure Modes for Advanced Double Hull, Fatigue and Fracture Failure Modes", TDL 91-01, vol 3a, Lehigh University, Bethlehem, PA, 1992

22. Gurney, T.R., and Maddox, S.J., "A Re-analysis of Fatigue Data for Welded Joints in Steel," Welding Research International, Vol 3, No.4, pp 1-54, 1973.

23. Petershagen, H., and Zwick, W., "Fatigue Strength of Butt Welds Made by Differenct Welding Processes," International Institute of Welding, IIW-XIII-1048-82, 1982

24. Keating, P.B. and Fisher, J.W., "Evaluation of Fatigue Tests and Design Criteria on Welded Detail", NCHRP Report 286, 1986

25 American Bureau of Shipbuilding, Guide for Fatigue Assessment of Tankers, ABS, New York, NY, June 1992

26. Stambaugh, K.A., et al., "Reduction of S-N Curves for Ship Structural Details," Draft Report SR-1336, Ships Structure Committee, Washington D.C. 199227.

27. Yagi, J., et al., "Definition of Hot Spot Stress in Welded Plate Type Structure for Fatigue Assessment," International Institute of Welding, IIW -XIII-1414-91, 1991

28. Puthli, R.S., et al., Numerical and Experimental Determination of Strain (Stress) Concentration Factors of Welded Joints between Square Hollow Sections, Heron, Vol. 33, 1988

29. Hugill, P.N. and Sumpter, J.D.G., "Fatigue Life Prediction at a Ship Deck/Superstructure Intersection", Strain, August 1990

30. Albrecht, P.A. and Simon, S., "Fatigue Notch Factors for Structural Details", Journal of the Stuctural Division, ASCE, Vol 107, No. ST7, July, 1981.

31. Boller, C. and Seeger, T., Materials Data for Cyclic Loading, Materials Science Monographs, Elsevier, 1987

32. UK Health & Safety Executive, Background to New Fatigue Design Guidance for Steel Welded Joints in Offshore Structures, HMSO, London, U.K., 1987

33. Underwater Engineering Group, "Design of Tubular Joints for Offshore Structures," Report UR33, London, U.K., 1985

34. Dr. John W. Fisher personal communication

35. Siljander, A., Kurath, P., Lawrence, F.V., Jr., "Nonproportional Fatigue of Welded Structures," Advances in Fatigue Lifetime Predictive Techniques

36. Ship Structure Committee, "Fatigue Performance Under Multiaxial Loading," SSC-356, December 1990

37. Gurney, T.R., and Maddox, S.J., "A re-analysis of fatigue data for welded joints in steel," Welding Research International, Vol 3, No.4, pp 1-54, 1973

38. Munse, W.H. and Stallmeyer, J.E., "Influence of Weld Details on Fatigue of Welded Beams and Girders," Symposium on Fatigue of Welded Structures, Cambridge University, 1960

39. Producibility: Foundation Integration with Double Hull, Executive Summary, Lehigh University/Vibtech, Inc., Bethlehem, PA, 1993

John E. Tarquinio was born in Pittsburgh, PA on March 26, 1962 to Eileen and Gino Tarquinio. After graduating from Sto-Rox High School, he attended Triangle Institute of Technology. After receiving an Associates Degree in Drafting and Construction, he accepted a position as a designer with Newport News Shipbuilding in Newport News, Virginia.

While at Newport News Shipyard, he returned to school and received his Bachelor of Science Degree of Civil Engineering from Old Dominion University in May 1991. In September 1991, he began graduate studies at Lehigh University. This education was made possible by the award of Advanced Technology for Large Structural Systems (ATLSS) scholarship. As an ATLSS scholar, he worked as a research assistant on various projects.

END

OF

TITLE